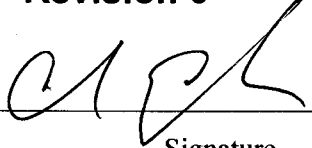


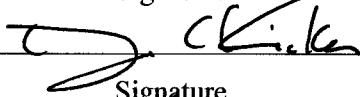
560252

SANDIA NATIONAL LABORATORIES
WASTE ISOLATION PILOT PLANT


Summary Report for the 2014 WIPP Compliance Recertification
Application Performance Assessment

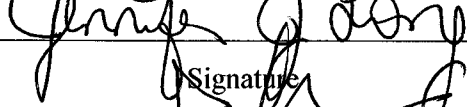
Revision 0

Author: R. Chris Camphouse  01/13/2013
Print Signature Date

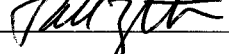
Author: Dwayne C. Kicker  6/13/2013
Print Signature Date

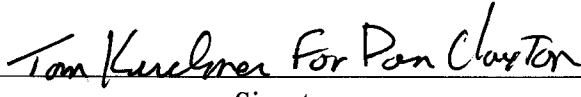
Author: Sungtae Kim  (For) 6/13/13
Print Signature Date


Author: Thomas B. Kirchner  6/13/13
Print Signature Date


Author: Jennifer J. Long  6/13/13
Print Signature Date

Author: Bwalya Malama  06/13/13
Print Signature Date

Author: Todd R. Zeitler  6/13/2013
Print Signature Date

Technical
Review: Daniel Clayton  For Dan Clayton 6/13/13
Print Signature Date

QA
Review: Shelly Nielsen  6-13-13
Print Signature Date

Management
Review: Sean Dunagan  6/13/13
Print Signature Date

WIPP:1.2.5:PA:QA-L:559199

Information Only

Table of Contents

Executive Summary	7
1 Introduction	8
2 Changes since the PABC-2009	9
2.1 Replacement of Option D with ROMPCS	9
2.2 Inclusion of Additional Mined Volume in the Experimental Region	16
2.3 Refinement to the Probability of Encountering Pressurized Brine	16
2.4 Refinement to the Corrosion Rate of Steel	17
2.5 Refinement to the Effective Shear Strength of WIPP Waste	17
2.6 Updates to Drilling Rate and Plugging Pattern Parameters	18
2.7 Updates to WIPP Waste Inventory Parameters	19
2.8 Implementation of Variable Brine Volume in the Calculation of Radionuclide Concentration ..	21
2.9 Updates to Radionuclide Solubilities and their Associated Uncertainty	22
2.10 Refinement to Repository Water Balance	24
2.11 Updated Colloid Parameters	27
2.12 Parameter Correction	27
3 FEPs Assessment	28
4 Methodology	29
5 Run Control	30
6 Results	30
6.1 Inventory Comparison	30
6.2 Radionuclide Mobilized Concentrations	32
6.3 Salado Flow Results	37
6.3.1 Results for an Undisturbed Repository (Scenario S1-BF)	41
6.3.2 Results for an E1 Intrusion at 350 Years (Scenario S2-BF)	52
6.3.3 Results for an E2 Intrusion at 350 Years (Scenario S4-BF)	56
6.3.4 Results for an E2 Intrusion at 1000 Years Followed by a E1 Intrusion at 2000 Years (Scenario S6-BF)	60
6.4 Radionuclide Transport Results	61
6.5 Direct Brine Release Results	65
6.6 Spallings Release Results	71
6.7 Cuttings and Cavings Results	73

6.8 Normalized Releases..... 75

6.9.1 Cuttings and Cavings Normalized Releases 75

6.9.2 Spallings Normalized Releases 76

6.9.3 Normalized Direct Brine Releases 76

6.9.4 Normalized Culebra Transport Releases..... 77

6.9.5 Total Normalized Releases 78

7 Summary 82

8 References 83

List of Figures

Figure 2-1: Schematic Diagram of the ROMPCS.....	10
Figure 6-1: WIPP CH- and RH-TRU Waste EPA Units from Closure to 10,000 Years	31
Figure 6-2: Dominant WIPP CH- and RH-TRU Waste Isotopes from Closure to 10,000 Years	32
Figure 6-3: CRA-2014 PA Total Mobilized Concentrations in Salado Brine, Replicate 1, BV1	34
Figure 6-4: CRA-2014 PA Total Mobilized Concentrations in Salado Brine, Replicate 1, BV5	34
Figure 6-5: CRA-2014 PA Total Mobilized Concentrations in Castile Brine, Replicate 1, BV1	35
Figure 6-6: CRA-2014 PA Total Mobilized Concentrations in Castile Brine, Replicate 1, BV5	35
Figure 6-7: PABC-2009 Total Mobilized Concentrations in Salado Brine, Replicate 1	36
Figure 6-8: PABC-2009 Total Mobilized Concentrations in Castile Brine, Replicate 1	36
Figure 6-9: PABC-2009 BRAGFLO Grid and Material Map for an E1 Intrusion (Δx , Δy , and Δz dimensions in meters).	39
Figure 6-10: CRA-2014 PA BRAGFLO Grid and Material Map for an E1 Intrusion (Δx , Δy , and Δz dimensions in meters).	40
Figure 6-11: Overall Means of Waste Panel Pressure, Scenario S1-BF	45
Figure 6-12: Overall Means of SRoR Pressure, Scenario S1-BF	45
Figure 6-13: Overall Means of NRoR Pressure, Scenario S1-BF.....	46
Figure 6-14: Overall Means of Experimental Region Pressure, Scenario S1-BF.....	46
Figure 6-15: Replicate 1 Means of Molar Gas Generation, Scenario S1-BF of the PABC-2009.....	47
Figure 6-16: Overall Means of Molar Gas Generation, Scenario S1-BF of the CRA-2014 PA.	47
Figure 6-17: Overall Means of Cumulative Brine Inflow to the Waste Panel, Scenario S1-BF.....	48
Figure 6-18: Overall Means of Cumulative Brine Inflow to the SRoR, Scenario S1-BF.....	48
Figure 6-19: Overall Means of Cumulative Brine Inflow to the NRoR, Scenario S1-BF.	49
Figure 6-20: Overall Means of Cumulative Brine Inflow to the Repository, Scenario S1-BF.....	49
Figure 6-21: Overall Means of Brine Flow up the Shaft, Scenario S1-BF.	50
Figure 6-22: Overall Means of Waste Panel Brine Saturation, Scenario S1-BF.	50
Figure 6-23: Overall Means of SRoR Saturation, Scenario S1-BF.	51
Figure 6-24: Overall Means of NRoR Saturation, Scenario S1-BF.....	51
Figure 6-25: Overall Means of Waste Panel Porosity, Scenario S1-BF.	52
Figure 6-26: Overall Means of Waste Panel Pressure, Scenario S2-BF	54
Figure 6-27: Overall Means of Cumulative Brine Inflow to the Waste Panel, Scenario S2-BF.....	54
Figure 6-28: Overall Means of Cumulative Brine Inflow to the Repository, Scenario S2-BF.....	55
Figure 6-29: Overall Means of Brine Flow up the Borehole, Scenario S2-BF.....	55
Figure 6-30: Overall Means of Waste Panel Brine Saturation, Scenario S2-BF.	56
Figure 6-31: Overall Means of Waste Panel Pressure, Scenario S4-BF	58
Figure 6-32: Overall Means of Cumulative Brine Inflow to the Waste Panel, Scenario S4-BF.....	58
Figure 6-33: Overall Means of Cumulative Brine Inflow to the Repository, Scenario S4-BF.....	59
Figure 6-34: Overall Means of Brine Flow up the Borehole, Scenario S4-BF.....	59
Figure 6-35: Overall Means of Waste Panel Brine Saturation, Scenario S4-BF.	60
Figure 6-36: Overall Means of Brine Flow up the Borehole, Scenario S6-BF.....	61
Figure 6-37: CRA-2014 PA Cumulative Transport Release to the Culebra, Scenario S2-BF.....	62
Figure 6-38: CRA-2014 PA Cumulative Transport Release to the Culebra, Scenario S3-BF.....	63
Figure 6-39: CRA-2014 PA Cumulative Transport Release to the Culebra, Scenario S4-BF.....	63

Figure 6-40: CRA-2014 PA Cumulative Transport Release to the Culebra, Scenario S5-BF..... 64
Figure 6-41: CRA-2014 PA Cumulative Transport Release to the Culebra, Scenario S6-BF..... 64
Figure 6-42: CRA-2014 PA DBR Computational Grid and Material Map (logical grid). 67
Figure 6-43: PABC-2009 DBR Computational Grid and Material Map (logical grid). 68
Figure 6-44: DBR Volume vs. Pressure, Scenario S2-DBR, Replicate 1, Lower Intrusion, CRA-2014 PA
..... 70
Figure 6-45: Frequency of Cavings Area in the CRA-2014 PA and the PABC-2009..... 74
Figure 6-46: CRA-2014 PA Cuttings and Cavings Areas as a Function of Shear Strength 74
Figure 6-47: CRA-2014 PA and CRA-2009 PABC Overall Mean CCDFs for Normalized Cuttings and
Cavings Releases 75
Figure 6-48: CRA-2014 PA and CRA-2009 PABC Overall Mean CCDFs for Normalized Spallings
Releases 76
Figure 6-49: CRA-2014 PA and CRA-2009 PABC Overall Mean CCDFs for Normalized Direct Brine
Releases 77
Figure 6-50: CRA-2014 PA and CRA-2009 PABC Overall Mean CCDFs for Normalized Culebra
Transport Releases 78
Figure 6-51: CRA-2014 PA Total Normalized Release CCDFs for Replicates 1, 2, and 3..... 80
Figure 6-52: CRA-2014 PA Confidence Limits on Overall Mean for Total Normalized Releases..... 80
Figure 6-53: Comparison of Overall Means for Release Components of the CRA-2014 PA 81
Figure 6-54: CRA-2014 PA and CRA-2009 PABC Overall Mean CCDFs for Total Normalized Releases
..... 81

List of Tables

Table 2-1: Sampled ROMPCS Parameters for the CRA-2014 PA	12
Table 2-2: Constant Panel Closure Parameters for the CRA-2014 PA.....	14
Table 2-3: DRZ_1 and DRZ_PCS Porosities and Permeabilities	15
Table 2-4: GLOBAL:PBRINE Distribution for the CRA-2014 PA	17
Table 2-5: STEEL:CORRMCO2 Distribution in the CRA-2014 PA	17
Table 2-6: BOREHOLE:TAUFAIL Distribution for the CRA-2014 PA	18
Table 2-7: Drilling Rate and Plugging Pattern Parameters for the CRA-2014 PA.....	19
Table 2-8: WIPP Waste Inventory Parameters for the CRA-2014 PA	19
Table 2-9: Oxidation State III Baseline Actinide Solubilities for the CRA-2014 PA	23
Table 2-10: Oxidation State IV Baseline Actinide Solubilities for the CRA-2014 PA	23
Table 2-11: Oxidation State V Baseline Actinide Solubilities for the CRA-2014 PA	24
Table 2-12: Solubility Uncertainties for the CRA-2014 PA.....	24
Table 2-13: Constant Parameters in the CRA-2014 PA Water Balance Implementation.....	25
Table 2-14: Sampled Parameters in the CRA-2014 PA Water Balance Implementation	26
Table 2-15: Updated Colloid Parameters Used in the CRA-2014 PA.....	27
Table 2-16: DRZ_PCS:RELP_MOD Distribution for the CRA-2014 PA	28
Table 6-1: BRAGFLO Modeling Scenarios	37
Table 6-2: Summary Statistics for Scenario S1-BF.....	44
Table 6-3: Summary Statistics for Scenario S2-BF.....	53
Table 6-4: Summary Statistics for Scenario S4-BF.....	57
Table 6-5: Summary Statistics for Scenario S6-BF.....	60
Table 6-6: PA Intrusion Scenarios Used in Calculating Direct Brine Releases.....	65
Table 6-7: DBR Summary Statistics for the CRA-2014 PA and PABC-2009 DBR Calculations	69
Table 6-8: CRA-2014 PA Summary Spallings Results by Intrusion Scenario	72
Table 6-9: CRA-2014 PA Summary Spallings Results by Intrusion Location.....	72
Table 6-10: Cavings Area Statistics for the PABC-2009 and the CRA-2014 PA	73
Table 6-11: CRA-2014 PA and CRA-2009 PABC Statistics on the Overall Mean for Total Normalized Releases in EPA Units at Probabilities of 0.1 and 0.001	79

EXECUTIVE SUMMARY

The Waste Isolation Pilot Plant (WIPP), located in southeastern New Mexico, has been developed by the U.S. Department of Energy (DOE) for the geologic (deep underground) disposal of transuranic (TRU) waste. Containment of TRU waste at the WIPP is regulated by the U.S. Environmental Protection Agency (EPA) according to the regulations set forth in Title 40 of the Code of Federal Regulations (CFR), Part 191. The DOE demonstrates compliance with the containment requirements according to the Certification Criteria in Title 40 CFR Part 194 by means of performance assessment (PA) calculations performed by Sandia National Laboratories (SNL). WIPP PA calculations estimate the probability and consequence of potential radionuclide releases from the repository to the accessible environment for a regulatory period of 10,000 years after facility closure. WIPP PA models are used to support the repository recertification process that occurs at five-year intervals following the receipt of the first waste shipment at the site in 1999. The current regulatory baseline was established by the 2009 Performance Assessment Baseline Calculation (PABC-2009).

The 2014 Compliance Recertification Application (CRA-2014) is the third WIPP recertification application submitted by the DOE for EPA approval. Several changes are incorporated into the CRA-2014 PA relative to the PABC-2009. These modifications are comprised of planned repository changes, parameter updates, refinements to PA implementation, and include the following:

- Replacement of the “Option D” WIPP panel closure with a newly designed Run-of-Mine Panel Closure System (ROMPCS).
- Inclusion of additional mined volume in the repository north end.
- An update to the probability that a drilling intrusion into a repository excavated region will result in a pressurized brine encounter.
- Refinement to the corrosion rate of steel.
- Refinement to the effective shear strength of WIPP waste.
- Updates to drilling rate and plugging pattern parameters.
- Updates to WIPP waste inventory parameters.
- Calculation of radionuclide concentration in brine as a function of the actual brine volume present in the waste panel.
- Updates to radionuclide solubilities and their associated uncertainty.
- Implementation of a more detailed repository water balance that includes MgO hydration.
- Updated colloid parameters.
- Parameter corrections.

Total normalized releases obtained in the CRA-2014 PA are lower than those in the PABC-2009, and continue to remain below regulatory limits. As a result, the CRA-2014 PA demonstrates that the WIPP remains in compliance with the containment requirements of 40 CFR Part 191.

Cuttings and cavings releases and DBRs were the two primary release components contributing to total releases in the PABC-2009, and continue to be so in the CRA-2014 PA. Reductions are seen in the contributing mechanisms to total releases in the CRA-2014 PA as compared to the PABC-2009.

1 INTRODUCTION

The Waste Isolation Pilot Plant (WIPP), located in southeastern New Mexico, has been developed by the U.S. Department of Energy (DOE) for the geologic (deep underground) disposal of transuranic (TRU) waste. Containment of TRU waste at the WIPP is regulated by the U.S. Environmental Protection Agency (EPA) according to the regulations set forth in Title 40 of the Code of Federal Regulations (CFR), Part 191. The DOE demonstrates compliance with the containment requirements according to the Certification Criteria in Title 40 CFR Part 194 by means of performance assessment (PA) calculations performed by Sandia National Laboratories (SNL). WIPP PA calculations estimate the probability and consequence of potential radionuclide releases from the repository to the accessible environment for a regulatory period of 10,000 years after facility closure. The models used in PA are maintained and updated with new information as part of an ongoing process. Improved information regarding important WIPP features, events, and processes typically results in refinements and modifications to PA models and the parameters used in them. Planned changes to the repository and/or the components therein also result in updates to WIPP PA models. WIPP PA models are used to support the repository recertification process that occurs at five-year intervals following the receipt of the first waste shipment at the site in 1999.

PA calculations were included in the 1996 Compliance Certification Application (CCA) (U.S. DOE 1996), and in a subsequent Performance Assessment Verification Test (PAVT) (MacKinnon and Freeze 1997a, 1997b and 1997c). Based in part on the CCA and PAVT PA calculations, the EPA certified that the WIPP met the regulatory containment criteria. The facility was approved for disposal of transuranic waste in May 1998 (U.S. EPA 1998). PA calculations were an integral part of the 2004 Compliance Recertification Application (CRA-2004) (U.S. DOE 2004). During their review of the CRA-2004, the EPA requested an additional PA calculation, referred to as the CRA-2004 Performance Assessment Baseline Calculation (PABC) (Leigh et al. 2005), be conducted with modified assumptions and parameter values (Cotsworth 2005). Following review of the CRA-2004 and the CRA-2004 PABC, the EPA recertified the WIPP in March 2006 (U.S. EPA 2006).

PA calculations were completed for the second WIPP recertification and documented in the 2009 Compliance Recertification Application (CRA-2009). The CRA-2009 PA resulted from continued review of the CRA-2004 PABC, including a number of technical changes and corrections, as well as updates to parameters and improvements to the PA computer codes (Clayton et al. 2008). To incorporate additional information which was received after the CRA-2009 PA was completed, but before the submittal of the CRA-2009, the EPA requested an additional PA calculation, referred to as the 2009 Compliance Recertification Application Performance Assessment Baseline Calculation (PABC-2009) (Clayton et al. 2010), be undertaken which included updated information (Cotsworth 2009). Following the completion and submission of the PABC-2009, the WIPP was recertified in 2010 (U.S. EPA 2010a).

The Land Withdrawal Act (U.S. Congress 1992) requires that the DOE apply for WIPP recertification every five years following the initial 1999 waste shipment. The 2014 Compliance Recertification Application (CRA-2014) is the third WIPP recertification application submitted

by the DOE for EPA approval. The PA executed by SNL in support of the CRA-2014 is detailed in AP-164 (Camphouse 2013a). The CRA-2014 PA includes a number of technical changes and parameter refinements, as well as a redesigned WIPP panel closure system. Results found in the CRA-2014 PA are compared to those obtained in the PABC-2009 in order to assess repository performance in terms of the current regulatory baseline. This document comprises the summary report of the CRA-2014 PA analysis.

2 CHANGES SINCE THE PABC-2009

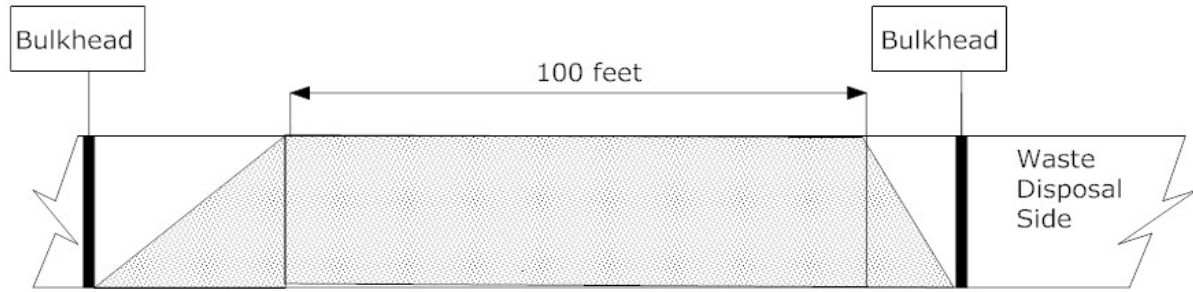
Several changes are incorporated into the CRA-2014 PA relative to the PABC-2009. The modifications included in the CRA-2014 PA include planned repository changes, parameter updates, and refinements to PA implementation. More specifically, changes included in the CRA-2014 PA include the following:

- Replacement of the “Option D” WIPP panel closure with a newly designed Run-of-Mine Panel Closure System (ROMPCS).
- Inclusion of additional mined volume in the repository north end.
- An update to the probability that a drilling intrusion into a repository excavated region will result in a pressurized brine encounter.
- Refinement to the corrosion rate of steel.
- Refinement to the effective shear strength of WIPP waste.
- Updates to drilling rate and plugging pattern parameters.
- Updates to WIPP waste inventory parameters.
- Calculation of radionuclide concentration in brine as a function of the actual brine volume present in the waste panel.
- Updates to radionuclide solubilities and their associated uncertainty.
- Implementation of a more detailed repository water balance that includes MgO hydration.
- Updated colloid parameters.
- Parameter corrections.

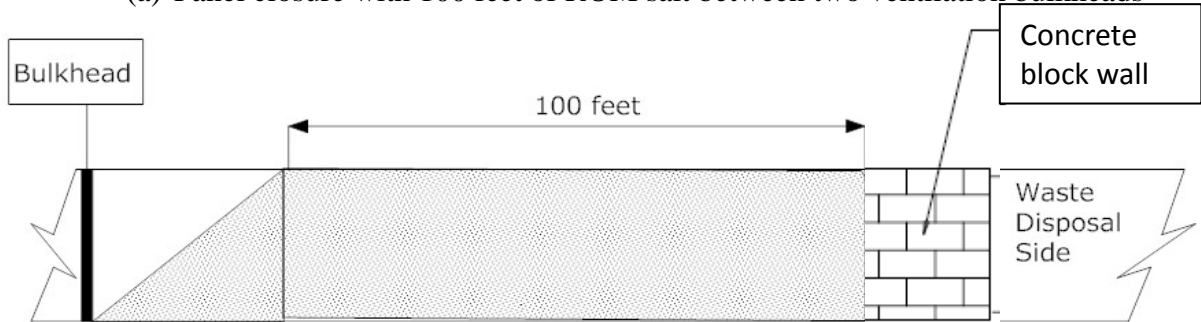
These changes are discussed in more detail in the sections that follow

2.1 Replacement of Option D with ROMPCS

Among the changes included in the CRA-2014 PA is the replacement of the Option D WIPP panel closure system (PCS) with the ROMPCS. The DOE has submitted a planned change request (PCR) to the EPA requesting that EPA modify Condition 1 of the Final Certification Rulemaking for 40 CFR Part 194 (U. S. EPA, 1998) for the WIPP, and that the ROMPCS be approved for use in all waste panels (U.S. DOE, 2011a). Regulatory compliance impacts associated with the implementation of the ROMPCS in the WIPP were assessed in a PA named PCS-2012. Results of the PCS-2012 PA are documented in Camphouse et al. (2012a). Total normalized releases calculated in the PCS-2012 PA remained below their regulatory limits. The WIPP remains in compliance with the containment requirements of 40 CFR Part 191 with the Option D panel closure replaced by the ROMPCS design.



(a) Panel closure with 100 feet of ROM salt between two ventilation bulkheads



(b) Panel closure with 100 feet of ROM salt between a ventilation bulkhead & explosion wall

Figure 2-1: Schematic Diagram of the ROMPCS

The ROMPCS design (Figure 2-1) is comprised of 100 feet of run-of-mine (ROM) salt with barriers at each end. The ROM salt is generated from ongoing mining operations at the WIPP while the barriers consist of ventilation bulkheads, similar to those currently used in the panels as room closures. The ROM salt comprising the ROMPCS is represented by three materials, denoted as PCS_T1 for the first 100 years after facility closure, PCS_T2 from 100 to 200 years, and PCS_T3 for 200 to 10,000 years. For the first 200 years post-closure, the disturbed rock zone (DRZ) above and below the ROMPCS maintains the same properties as specified to the DRZ surrounding the disposal rooms (PA material DRZ_1). After 200 years, the DRZ above and below the ROMPCS is modeled as having healed, and is represented by material DRZ_PCS.

In the PCS-2012 PA, the permeabilities of material PCS_T1 were assigned a uniform distribution having a minimum value of $1 \times 10^{-21} \text{ m}^2$. The permeability for material PCS_T2 was calculated as a function of its sampled porosity value. The lowest obtainable calculated value for the permeability of PCS_T2 in the X, Y, and Z directions was $1.44 \times 10^{-21} \text{ m}^2$, which is slightly greater than the minimum possible sampled value during the first 100 years. A lower ROMPCS permeability could be obtained during the first 100 years than was feasible for years 100 to 200, depending on the sampled PCS_T1 permeability value. As creep closure reconsolidates the ROMPCS over time, the expectation is that ROMPCS permeability will not increase as time increases. As a result, the permeability distribution of ROMPCS material PCS_T1 is modified slightly in the CRA-2014 PA (as compared to the PCS-2012 PA), and is assigned a uniform

distribution with a minimum value of $1 \times 10^{-20.84} \text{ m}^2$ and the same maximum value as in the PCS-2012 PA. This parameter change is cosmetic in nature, and is implemented to improve consistency between the modeled ROMPCS temporal evolution and the mechanics of ROM salt reconsolidation. As was done in the PCS-2012 PA (Camphouse et al. 2012a), a conditional relationship is enforced in the CRA-2014 PA so that the permeability of material PCS_T2 is never greater than the permeability of material PCS_T1. Likewise, the permeability of material PCS_T3 is never greater than the permeability of material PCS_T2.

For similar reasons, the permeability of material DRZ_PCS is modified slightly in the CRA-2014 PA as compared to the PCS-2012 PA and the PABC-2009. It is expected that healing of the DRZ region above and below the PCS will not yield an increase in permeability when compared to the damaged DRZ. A relationship is implemented in the CRA-2014 PA to enforce that the permeability of material DRZ_PCS is never greater than the permeability of material DRZ_1. Using the MATERIAL:PROPERTY parameter naming convention used in WIPP PA, the constraint placed on the permeability for DRZ_PCS is that $\text{DRZ_PCS:PRMX} \leq \text{DRZ_1:PRMX}$, and likewise in the y and z directions. If the sampled permeability for DRZ_PCS is greater than that obtained for DRZ_1, then DRZ_PCS retains the DRZ_1 permeability. The uncertainty distributions specified for the permeabilities of materials DRZ_1 and DRZ_PCS in the CRA-2014 PA are identical to those used in the PCS-2012 PA and the PABC-2009.

Finally, in the CRA-2014 PA, the initial brine saturation of the ROMPCS is set equal to the sampled residual brine saturation value for material PCS_T1 in each vector. This modification ensures that the initial brine saturation of the PCS is never lower than the PCS residual brine saturation in a given vector. The full set of sampled and constant parameters used to represent the ROMPCS in the CRA-2014 PA is shown in Table 2-1 and Table 2-2. Select parameters associated with the damaged and healed DRZ are shown in Table 2-3.

Table 2-1: Sampled ROMPCS Parameters for the CRA-2014 PA

Parameter	Units	Description	Distribution Type	Distribution Parameters	Default Value	Source
PCS_T1:POROSITY	none	Porosity of run-of-mine panel closure, years 0 to 100	Uniform	Min = 0.066 Max = 0.187 Mean = 0.1265	0.1265	Camphouse et al. (2012b) Table 2 and page 15
PCS_T2:POROSITY ¹	none	Porosity of run-of-mine panel closure, years 100 to 200	Uniform	Min = 0.025 Max = 0.075 Mean = 0.05	0.05	Camphouse et al. (2012b) Table 2 and page 15
PCS_T3:POROSITY ²	none	Porosity of run-of-mine panel closure, years 200 to 10,000	Uniform	Min = 0.001 Max = 0.0519 Mean = 0.0265	0.0265	Camphouse et al. (2012b) Table 2 and page 15
PCS_T1:PRMX_LOG ³ PCS_T1:PRMY_LOG PCS_T1:PRMZ_LOG	log(m ²)	log ₁₀ of intrinsic permeability, X, Y, and Z directions.	Uniform	Min = -20.84 Max = -12.0 Mean = -16.42	-16.42	Camphouse (2013a) Table 2-1
PCS_T2:POR2PERM ⁴ PCS_T3:POR2PERM	none	Distribution used to calculate permeability from sampled porosity values	Normal	Min = -1.72 Max = 1.72 Mean = 0.0 SD = 0.86	0.0	Camphouse et al. (2012b) Page 15 (sampled α value)
PCS_T1:SAT_RBRN ⁵ PCS_T2:SAT_RBRN PCS_T3:SAT_RBRN	none	Residual Brine Saturation	Cumulative	(Prob, Value): (0,0) (0.5,0.2) (1.0,0.6)	0.2	Camphouse et al. (2012b) Table 6

¹ PCS_T2:POROSITY is constrained such that PCS_T2:POROSITY ≤ PCS_T1:POROSITY for a given vector in order to avoid non-physical instantaneous increases in ROMPCS porosity at 100 years.

² PCS_T3:POROSITY is constrained such that PCS_T3:POROSITY ≤ PCS_T2:POROSITY for a given vector in order to avoid non-physical instantaneous increases in ROMPCS porosity at 200 years.

³ Parameter values are sampled for PCS_T1:PRMX_LOG. PCS_T1:PRMY_LOG and PCS_T1:PRMZ_LOG inherit the sampled value obtained for PCS_T1:PRMX_LOG for each vector.

⁴ Parameter values are sampled for PCS_T2:POR2PERM. PCS_T3:POR2PERM inherits the sampled value obtained for PCS_T2:POR2PERM for each vector.

⁵ Parameter values are sampled for PCS_T1:SAT_RBRN. PCS_T2: SAT_RBRN and PCS_T3: SAT_RBRN inherit the sampled value obtained for PCS_T1:SAT_RBRN for each vector.

Table 2-1 (cont): Sampled Panel Closure Parameters for the CRA-2014 PA

PCS_T1:SAT_RGAS ⁶ PCS_T2:SAT_RGAS PCS_T3:SAT_RGAS	none	Residual Gas Saturation	Uniform	Min = 0.0 Max = 0.4 Mean = 0.2	0.2	Camphouse et al. (2012b) Table 6
PCS_T1:PORE_DIS ⁷ PCS_T2:PORE_DIS PCS_T3:PORE_DIS	none	Brooks-Corey pore distribution parameter	Cumulative	(Prob,Value): (0,0.11) (0.5,0.94) (1.0,8.1)	0.94	Camphouse et al. (2012b) Table 8

⁶ Parameter values are sampled for PCS_T1:SAT_RGAS. PCS_T2: SAT_RGAS and PCS_T3: SAT_RGAS inherit the sampled value obtained for PCS_T1:SAT_RGAS for each vector.

⁷ Parameter values are sampled for PCS_T1:PORE_DIS. PCS_T2: PORE_DIS and PCS_T3: PORE_DIS inherit the sampled value obtained for PCS_T1: PORE_DIS for each vector.

Table 2-2: Constant Panel Closure Parameters for the CRA-2014 PA

Parameter	Units	Description	Value	Source
PCS_T2:PRMX_LOG ⁸ PCS_T2:PRMY_LOG PCS_T2:PRMZ_LOG	log(m ²)	log ₁₀ of intrinsic permeability, X, Y, and Z directions.	-18.6	See Footnote
PCS_T3:PRMX_LOG ⁹ PCS_T3:PRMY_LOG PCS_T3:PRMZ_LOG	log(m ²)	log ₁₀ of intrinsic permeability, X, Y, and Z directions.	-19.1	See Footnote
PCS_T1:RELP_MOD PCS_T2:RELP_MOD PCS_T3:RELP_MOD	none	Relative Permeability Model Number	4	Camphouse et al. (2012a) Table 7
PCS_T1:CAP_MOD PCS_T2:CAP_MOD PCS_T3:CAP_MOD	none	Capillary Pressure Model Number	1	Camphouse (2012a) Camphouse (2012b)
PCS_T1:KPT PCS_T2:KPT PCS_T3:KPT	none	Flag to Enable Dynamic Updating of Threshold Capillary Pressure as a Function of Permeability	0.0	Camphouse et al. (2012b) Table 8
PCS_T1:PCT_A PCS_T2:PCT_A PCS_T3:PCT_A	Pa	Threshold Capillary Pressure Linear Parameter	0.0	Camphouse (2012a) Camphouse (2012b)
PCS_T1:PCT_EXP PCS_T2:PCT_EXP PCS_T3:PCT_EXP	none	Threshold Capillary Pressure Exponential Parameter	0.0	Camphouse (2012a) Camphouse (2012b)
PCS_T1:PC_MAX PCS_T2:PC_MAX PCS_T3:PC_MAX	Pa	Maximum Allowable Capillary Pressure	1 x 10 ⁸	Camphouse et al. (2012b) Table 8

⁸ Permeabilities of PCS_T2 in the X, Y, and Z directions are calculated from the sampled PCS_T2:POROSITY values as described in Camphouse et al. (2012a). A constant default log-permeability is specified, however, to allow for parameter traceability in CRA-2014 PA input files as compared to those used in the PABC-2009. The specified default value is the average of the minimum and maximum values listed in Table 5 of Camphouse et al. (2012a).

⁹ Permeabilities of PCS_T3 in the X, Y, and Z directions are calculated from the sampled PCS_T3:POROSITY values as described in Camphouse et al. (2012a). The specified constant default value is the average of the minimum and maximum values listed in Table 5 of Camphouse et al. (2012a).

Table 2-2 (cont): Constant Panel Closure Parameters for the CRA-2014 PA

PCS_T1:P0_MIN PCS_T2:P0_MIN PCS_T3:P0_MIN	Pa	Minimum Brine Pressure for Capillary Model 3 (CAP_MOD = 3 has never been used in PA)	1.01325×10^5	Camphouse et al. (2012b) Table 8
PCS_T1:COMP_RCK PCS_T2:COMP_RCK PCS_T3:COMP_RCK	Pa ⁻¹	Bulk Compressibility	8.0×10^{-11}	Camphouse et al. (2012b) Table 8

Table 2-3: DRZ_1 and DRZ_PCS Porosities and Permeabilities

Parameter	Units	Description	Distribution Type	Distribution Parameters	Default Value	Source
DRZ_1:POROSITY	none	Porosity of the DRZ after facility closure	Cumulative	Min = 0.0039 Median = 0.0129 Max = 0.0548	0.0129	Ismail (2007a)
DRZ_1:PRMX_LOG DRZ_1:PRMY_LOG DRZ_1:PRMZ_LOG	log(m ²)	log ₁₀ of intrinsic permeability, X, Y, and Z directions	Uniform	Min = -19.4 Mean = -16.0 Max = -12.5	-16.0	Hansen (2002)
DRZ_PCS:POROSITY	none	Porosity of the healed DRZ above and below the PCS	Cumulative	Min = 0.0039 Median = 0.0129 Max = 0.0548	0.0129	Ismail (2007b)
DRZ_PCS:PRMX_LOG ¹⁰ DRZ_PCS:PRMY_LOG DRZ_PCS:PRMZ_LOG	log(m ²)	log ₁₀ of intrinsic permeability, X, Y, and Z directions	Triangular	Min = -20.699 Mode = -18.7496 Max = -17.0	-18.7496	Stein (2002)

¹⁰In the CRA-2014 PA, the sampled permeability value of material DRZ_PCS is compared to the sampled permeability value for DRZ_1. If the sampled value for DRZ_PCS is greater than that sampled for DRZ_1, then DRZ_PCS retains the sampled DRZ_1 value.

2.2 Inclusion of Additional Mined Volume in the Experimental Region

Following the recertification of the WIPP in November of 2010 (U.S. EPA 2010a), the DOE submitted a planned change notice (PCN) to the EPA that justified additional excavation in the WIPP experimental area (U.S. DOE, 2011b). A PA was undertaken to determine the impact of the additional excavation on the long-term performance of the facility, and is documented in Camphouse et al. (2011). Total normalized releases remained below regulatory release limits when the additional excavated volume was added to the repository. Moreover, total normalized releases calculated with the additional excavation were indistinguishable from those obtained in the PABC-2009. The WIPP remains in compliance with the containment requirements of 40 CFR Part 191 with additional excavated volume added to the experimental area.

The same approach used in Camphouse et al. (2011) is used in the CRA-2014 PA to include the additional mined volume in the WIPP experimental area. The volume of the experimental region implemented in the PABC-2009 was 87,675 m³. The added volume that results from additional excavation in the experimental area is 60,335 m³. As a result, the target volume of the experimental region implemented in the CRA-2014 PA is 87,675 m³ + 60,335 m³ = 148,010 m³. To achieve this value, the experimental region in the CRA-2014 PA is modified as in Camphouse et al. (2011) to yield an experimental region with a volume of 148,011 m³, one cubic meter greater than the target value.

2.3 Refinement to the Probability of Encountering Pressurized Brine

Penetration into a region of pressurized brine during a WIPP drilling intrusion can have significant consequences with respect to releases. WIPP PA parameter GLOBAL:PBRINE (hereafter PBRINE) is used to specify the probability that a drilling intrusion into the excavated region of the repository encounters a region of pressurized brine below the repository. In the current regulatory baseline established by the PABC-2009, a uniform distribution between 0.01 and 0.60 with a mean value of 0.305 is assigned to this parameter. Initial development of this distribution was the result of an analysis of TDEM data (Rechard et al. 1991, Peake 1998). A framework that provides a quantitative argument for refinement of parameter PBRINE has been developed since the PABC-2009 (Kirchner et al. 2012). The refinement of PBRINE results from a re-examination of the TDEM data while also including a greatly expanded set of drilling data for locations adjacent to the WIPP site than were available when the original analysis was performed in 1998. A sub-region exhibiting a high-density cluster of drilling intrusions was used to provide a conservative estimate of the probability of brine pocket intrusion based solely on the drilling data and to estimate a probability of encountering a brine pocket given that a well is drilled into a TDEM-identified region. The resulting distribution for PBRINE is shown in Table 2-4, and is used in the CRA-2014 PA.

Table 2-4: GLOBAL:PBRINE Distribution for the CRA-2014 PA

Parameter	Units	Description	Distribution Type	Distribution Parameters	Default Value
GLOBAL:PBRINE	(none)	Probability that a Drilling Intrusion in Excavated Area Encounters Pressurized Brine	Normal	Mean = 0.127 SD = 0.0272	0.127

As shown in Kirchner et al. (2012), the distribution shown in Table 2-4 yields simulated frequencies of brine intrusions that cover the same range as that produced using the former uniform distribution, but with a greater degree of positive skewness, resulting in a mode that is shifted to the left.

2.4 Refinement to the Corrosion Rate of Steel

WIPP PA parameter STEEL:CORRMCO2 represents the anoxic steel corrosion rate for brine-inundated steel in the absence of microbially produced CO₂. This parameter was represented with a uniform distribution having a minimum of 0.0 and a maximum of 3.17e-14 in the PABC-2009, with units of m/s. A series of steel and lead corrosion experiments have recently been conducted under Test Plan TP 06-02, *Iron and Lead Corrosion in WIPP-Relevant Conditions* (Wall and Enos, 2006). The object of these experiments has been to directly determine steel and lead corrosion rates under WIPP-relevant conditions. A description of the new experiments and the use of their results to determine an updated steel corrosion rate are presented in Roselle (2013a). Based on the newly obtained experimental corrosion data and its subsequent analysis, Roselle (2013a) recommends that both the distribution type and values for parameter STEEL:CORRMCO2 be changed. The revised steel corrosion parameter is shown in Table 2-5, and is used in the CRA-2014 PA.

Table 2-5: STEEL:CORRMCO2 Distribution in the CRA-2014 PA

Parameter	Units	Description	Distribution Type	Distribution Parameters	Default Value
STEEL:CORRMCO2	m/s	Inundated corrosion rate for steel in the absence of CO ₂	Student-t (n = 64)	Min=3.287e-16 Mean = 6.059e-15 Max=1.835e-14	6.059e-15

2.5 Refinement to the Effective Shear Strength of WIPP Waste

WIPP PA includes scenarios in which human intrusion results in a borehole intersecting the repository. During the intrusion, drilling mud flowing up the borehole will apply a hydrodynamic shear stress on the borehole wall. Erosion of the wall material can occur if this stress is high enough, resulting in a release of radionuclides being carried up the borehole with

the drilling mud. In this intrusion event, the drill bit would penetrate repository waste, and the drilling mud would flow up the borehole in a predominately vertical direction. In order to experimentally simulate these conditions, a flume was designed and constructed. In the flume experimental apparatus, eroding fluid enters a vertical channel from the bottom and flows past a specimen of surrogate WIPP waste. Experiments were conducted to determine the erosive impact on surrogate waste materials that were developed to represent degraded WIPP waste. A description of the vertical flume, the experiments conducted in it, and conclusions to be drawn from those experiments are discussed in Herrick et al. (2012). WIPP PA parameter BOREHOLE:TAUFAIL is used to represent the effective shear strength for erosion of WIPP waste. This parameter was represented in the PABC-2009 by a loguniform distribution having a minimum of 0.05 and a maximum of 77, with units of Pa. Based on experimental results that realistically simulate the effect of a drilling intrusion on an accepted surrogate waste material, as well as analyses of existing data, Herrick (2013) recommends a refinement to parameter BOREHOLE:TAUFAIL. The refinement of this parameter is shown in Table 2-6, and is used in the CRA-2014 PA.

Table 2-6: BOREHOLE:TAUFAIL Distribution for the CRA-2014 PA

Parameter	Units	Description	Distribution Type	Distribution Parameters	Default Value
BOREHOLE:TAUFAIL	Pa	Effective shear strength for erosion of waste.	Uniform	Max = 77.0 Mean = 39.61 Min = 2.22	39.61

2.6 Updates to Drilling Rate and Plugging Pattern Parameters

WIPP regulations require that current drilling practices are assumed for future inadvertent intrusions. The DOE continues to survey drilling activity in the Delaware Basin in accordance with the criteria established in 40 CFR 194.33. Local well operators are surveyed annually to provide the WIPP project with information on drilling practices, Castile brine encounters, etc. Results for the year 2012 are documented in the 2012 Delaware Basin Monitoring Annual Report (U.S. DOE 2012). The 2012 summary report shows that drilling practices have not changed since the summary report used for the PABC-2009.

Drilling parameters are updated in the CRA-2014 PA to reflect information contained in U.S. DOE (2012). These parameter updates are developed in Camphouse (2013a), and are summarized in Table 2-7. In that table, values used for these parameters in the PABC-2009 are listed in parenthesis below their CRA-2014 PA values.

Table 2-7: Drilling Rate and Plugging Pattern Parameters for the CRA-2014 PA

Parameter	Units	Description	Distribution Type	Value (PABC-2009)
GLOBAL: LAMBDA	km ⁻² yr ⁻¹	Drilling rate per unit area	Constant	6.73 x 10 ⁻³ (5.98 x 10 ⁻³)
GLOBAL: ONEPLG	(none)	Probability of having Plug Pattern 1	Constant	0.04 (0.022)
GLOBAL: TWOPLG	(none)	Probability of having Plug Pattern 2	Constant	0.594 (0.652)
GLOBAL: THREEPLG	(none)	Probability of having Plug Pattern 3	Constant	0.366 (0.326)

2.7 Updates to WIPP Waste Inventory Parameters

The Performance Assessment Inventory Report (PAIR) – 2012 (Van Soest 2012) was released on November 29, 2012. The PAIR – 2012 contains updated estimates to the radionuclide content and waste material parameters, scaled to a full repository, based on inventory information collected up through December 31, 2011. Parameters for the initial radionuclides, chemical components, and waste material inventories are updated in the CRA-2014 PA to reflect information in the PAIR-2012. In addition, parameters which are calculated based on the initial radionuclide inventories, such as the Waste Unit Factor (WUF) and the initial lumped radionuclide inventories are updated as well. Waste inventory parameter updates used in the CRA-2014 PA are documented in Kicker and Zeitler (2013b), and are listed in Table 2-8.

Table 2-8: WIPP Waste Inventory Parameters for the CRA-2014 PA

Material	Property	Value	Units	Description	Source
BOREHOLE	WUF	2.06 (PABC-2009: 2.60)	none	Waste Unit Factor	Kicker and Zeitler (2013b), Table C-1
AM241	INVCHD	6.97E+05	curies	Radionuclide Parameters	Kicker and Zeitler (2013b), Table C-2
AM241	INVRHD	8.06E+03			
AM243	INVCHD	2.18E+01			
AM243	INVRHD	2.95E+01			
CF252	INVCHD	7.62E-01			
CF252	INVRHD	9.26E-04			
CM243	INVCHD	2.16E+02			
CM243	INVRHD	1.81E+01			
CM244	INVCHD	5.24E+03			
CM244	INVRHD	4.73E+03			
CM245	INVCHD	3.70E-01			
CM245	INVRHD	8.55E-01			
CM248	INVCHD	1.03E-01			
CM248	INVRHD	1.62E-02			
CS137	INVCHD	2.31E+03			
CS137	INVRHD	2.33E+05			
NP237	INVCHD	2.04E+01			
NP237	INVRHD	2.84E+00			

Table 2-8 (continued)					
Material	Property	Value	Units	Description	Source
PA231	INVCHD	5.88E-01	curies	Radionuclide Parameters	Kicker and Zeitler (2013b), Table C-2
PA231	INVRHD	4.92E-02			
PB210	INVCHD	4.53E-01			
PB210	INVRHD	1.38E+01			
PM147	INVCHD	1.00E-01			
PM147	INVRHD	4.53E-01			
PU238	INVCHD	5.95E+05			
PU238	INVRHD	5.80E+03			
PU239	INVCHD	5.67E+05			
PU239	INVRHD	7.27E+03			
PU240	INVCHD	1.67E+05			
PU240	INVRHD	7.94E+03			
PU241	INVCHD	6.48E+05			
PU241	INVRHD	1.49E+04			
PU242	INVCHD	1.66E+03			
PU242	INVRHD	6.44E+03			
PU244	INVCHD	1.01E-02			
PU244	INVRHD	7.38E-06			
RA226	INVCHD	6.19E-01			
RA226	INVRHD	1.65E+01			
RA228	INVCHD	1.45E+00			
RA228	INVRHD	1.76E-02			
SR90	INVCHD	2.31E+03			
SR90	INVRHD	2.07E+05			
TH229	INVCHD	4.19E-01			
TH229	INVRHD	9.81E-01			
TH230	INVCHD	4.13E+00			
TH230	INVRHD	1.02E-02			
TH232	INVCHD	1.48E+00			
TH232	INVRHD	1.46E-02			
U233	INVCHD	9.82E+01			
U233	INVRHD	4.04E+01			
U234	INVCHD	2.10E+02			
U234	INVRHD	3.23E+01			
U235	INVCHD	8.66E+00			
U235	INVRHD	6.77E+01			
U236	INVCHD	5.08E+00			
U236	INVRHD	3.65E-01			
U238	INVCHD	3.51E+01			
U238	INVRHD	2.97E+01			
AM241L	INVCHD	7.18E+05	curies	Lumped Radionuclide Parameters	Kicker and Zeitler (2013b), Table C-3
AM241L	INVRHD	8.56E+03			
TH230L	INVCHD	4.54E+00			
TH230L	INVRHD	9.91E-01			
PU238L	INVCHD	5.95E+05			
PU238L	INVRHD	5.80E+03			
U234L	INVCHD	3.08E+02			
U234L	INVRHD	7.28E+01			
PU239L	INVCHD	7.60E+05			

Table 2-8 (continued)					
Material	Property	Value	Units	Description	Source
PU239L	INVRHD	1.15E+05	curies	Lumped Radionuclide Parameters	Kicker and Zeitler (2013b), Table C-3
WAS_AREA	IRONCHW	1.09E+07	kg	Waste Material Parameters	Kicker and Zeitler (2013b), Table C-4
WAS_AREA	IRONRHW	1.35E+06			
WAS_AREA	IRNCCHW	3.00E+07			
WAS_AREA	IRNCRHW	6.86E+06			
WAS_AREA	CELLCHW	3.55E+06			
WAS_AREA	CELLRHW	1.18E+05			
WAS_AREA	CELCCHW	7.23E+05			
WAS_AREA	CELCRHW	0.00E+00			
WAS_AREA	CELECHW	2.60E+05			
WAS_AREA	CELERHW	0.00E+00			
WAS_AREA	PLASCHW	5.20E+06			
WAS_AREA	PLASRHW	2.93E+05			
WAS_AREA	PLSCCHW	2.47E+06			
WAS_AREA	PLSCRHW	3.01E+05			
WAS_AREA	PLSECHW	1.25E+06			
WAS_AREA	PLSERHW	0.00E+00			
WAS_AREA	RUBBCHW	1.09E+06			
WAS_AREA	RUBBRHW	8.80E+04			
WAS_AREA	RUBCCHW	6.91E+04			
WAS_AREA	RUBCRHW	4.18E+03			
WAS_AREA	RUBECHW	0.00E+00			
WAS_AREA	RUBERHW	0.00E+00			
NITRATE	QINIT	2.74E+07	moles	Oxyanion Parameters	Kicker and Zeitler (2013b), Table C-5
SULFATE	QINIT	4.91E+06			

2.8 Implementation of Variable Brine Volume in the Calculation of Radionuclide Concentration

In the PABC-2009, the minimum necessary brine volume in the repository for a direct brine release (DBR) to occur was established as 17,400 m³ (Clayton 2008). This value is also used in the CRA-2014 PA as no changes warranting an update to it have occurred since the PABC-2009.

To date, the minimum brine volume necessary for a DBR has been used as an input to the radionuclide solubility calculation. The entire organic ligand waste inventory was assumed to be dissolved in the minimum necessary DBR brine volume, and the resulting organic ligand concentrations were then used in the calculation of radionuclide solubilities. The WIPP organic ligand inventory has increased over time, resulting in mass-balance issues when determining radionuclide concentrations from only the minimum brine volume necessary for a DBR. As a result, the calculation of radionuclide solubilities is extended in the CRA-2014 PA so that organic ligand concentrations used in their calculation are dependent on the actual volume of brine present in the repository.

Using results from previous PA calculations, waste region brine volumes that result in a DBR are between the minimum necessary for a DBR and five times the minimum necessary volume. As a result, brine volumes of 1x, 2x, 3x, 4x, and 5x the minimum necessary volume are used in the calculation of radionuclide solubilities in the CRA-2014 PA. The organic ligand inventory is dissolved in each of these multiples of the minimum necessary brine volume. The resulting organic ligand concentrations, now dependent on a range of brine volumes, are then used to calculate radionuclide solubilities. This approach keeps radionuclide mass constant over realized brine volumes, rather than keeping radionuclide concentration constant over realized brine volumes. The use of five multiples of the minimum necessary DBR volume provides a sufficient range with which to calculate solubilities while keeping the additional solubility calculation workload at a feasible level. WIPP PA codes PRECCDFGF v2.0 and CCDFGF v6.0 have been developed and qualified for this revised implementation of radionuclide concentration as a function of brine volume, and are used in the CRA-2014 PA.

2.9 Updates to Radionuclide Solubilities and their Associated Uncertainty

The solubilities of actinide elements are influenced by the chemical components of the waste. With the release of the PAIR - 2012 (Van Soest 2012), updated information on the amount of various chemical components in the waste is available. To incorporate this updated information, parameters used to represent actinide solubilities are updated in the CRA-2014 PA. Solubilities are calculated in the CRA-2014 PA using multiples of the minimum brine volume (17,400 m³) necessary for a DBR to occur. Brine volumes of 1x, 2x, 3x, 4x, and 5x this minimum necessary brine volume are used in the calculation of baseline radionuclide solubilities. The use of five multiples of the minimum necessary DBR volume provides a sufficient range with which to calculate solubilities while keeping the additional solubility calculation workload at a feasible level. Additional experimental results have been published in the literature since the PABC-2009, and this new information is used to enhance the uncertainty ranges and probability distributions for actinide solubilities in the CRA-2014 PA. The developments of baseline solubilities and their uncertainty distributions in the CRA-2014 PA are given in Brush (2013) and Brush and Domski (2013). These parameters are listed in Table 2-9 to Table 2-12. In Table 2-9 to Table 2-11, the numerical suffix indicates the minimum brine volume multiple used to calculate the solubility. For example, SOLCOH2 is calculated using 2x the minimum necessary brine volume, SOLCOH3 is calculated using 3x the minimum necessary brine volume, etc.

Table 2-9: Oxidation State III Baseline Actinide Solubilities for the CRA-2014 PA

Material	Property	Value	Units	Description	Source
SOLMOD3	SOLSOH	2.59×10^{-6}	M (mol/L)	Oxidation state III model, solubility in the minimum volume of Salado brine	Brush (2013), Table 1
	SOLSOH2	1.38×10^{-6}		Oxidation state III model, solubility in 2 × the minimum volume of Salado brine	
	SOLSOH3	9.74×10^{-7}		Oxidation state III model, solubility in 3 × the minimum volume of Salado brine	
	SOLSOH4	7.69×10^{-7}		Oxidation state III model, solubility in 4 × the minimum volume of Salado brine	
	SOLSOH5	6.47×10^{-7}		Oxidation state III model, solubility in 5 × the minimum volume of Salado brine	
	SOLCOH	1.48×10^{-6}		Oxidation state III model, solubility in the minimum volume of Castile brine	
	SOLCOH2	8.59×10^{-7}		Oxidation state III model, solubility in 2 × the minimum volume of Castile brine	
	SOLCOH3	5.99×10^{-7}		Oxidation state III model, solubility in 3 × the minimum volume of Castile brine	
	SOLCOH4	4.69×10^{-7}		Oxidation state III model, solubility in 4 × the minimum volume of Castile brine	
	SOLCOH5	3.92×10^{-7}		Oxidation state III model, solubility in 5 × the minimum volume of Castile brine	

Table 2-10: Oxidation State IV Baseline Actinide Solubilities for the CRA-2014 PA

Material	Property	Value	Units	Description	Source
SOLMOD4	SOLSOH	6.05×10^{-8}	M (mol/L)	Oxidation state IV model, solubility in the minimum volume of Salado brine	Brush (2013), Table 1
	SOLSOH2	6.06×10^{-8}		Oxidation state IV model, solubility in 2 × the minimum volume of Salado brine	
	SOLSOH3	6.07×10^{-8}		Oxidation state IV model, solubility in 3 × the minimum volume of Salado brine	
	SOLSOH4	6.07×10^{-8}		Oxidation state IV model, solubility in 4 × the minimum volume of Salado brine	
	SOLSOH5	6.07×10^{-8}		Oxidation state IV model, solubility in 5 × the minimum volume of Salado brine	
	SOLCOH	7.02×10^{-8}		Oxidation state IV model, solubility in the minimum volume of Castile brine	
	SOLCOH2	7.14×10^{-8}		Oxidation state IV model, solubility in 2 × the minimum volume of Castile brine	
	SOLCOH3	7.17×10^{-8}		Oxidation state IV model, solubility in 3 × the minimum volume of Castile brine	
	SOLCOH4	7.19×10^{-8}		Oxidation state IV model, solubility in 4 × the minimum volume of Castile brine	
	SOLCOH5	7.20×10^{-8}		Oxidation state IV model, solubility in 5 × the minimum volume of Castile brine	

Table 2-11: Oxidation State V Baseline Actinide Solubilities for the CRA-2014 PA

Material	Property	Value	Units	Description	Source
SOLMOD5	SOLSOH	2.77×10^{-7}	M (mol/L)	Oxidation state V model, solubility in the minimum volume of Salado brine	Brush (2013), Table 1
	SOLSOH2	2.18×10^{-7}		Oxidation state V model, solubility in 2 × the minimum volume of Salado brine	
	SOLSOH3	1.98×10^{-7}		Oxidation state V model, solubility in 3 × the minimum volume of Salado brine	
	SOLSOH4	1.88×10^{-7}		Oxidation state V model, solubility in 4 × the minimum volume of Salado brine	
	SOLSOH5	1.82×10^{-7}		Oxidation state V model, solubility in 5 × the minimum volume of Salado brine	
	SOLCOH	8.76×10^{-7}		Oxidation state V model, solubility in the minimum volume of Castile brine	
	SOLCOH2	7.39×10^{-7}		Oxidation state V model, solubility in 2 × the minimum volume of Castile brine	
	SOLCOH3	6.86×10^{-7}		Oxidation state V model, solubility in 3 × the minimum volume of Castile brine	
	SOLCOH4	6.60×10^{-7}		Oxidation state V model, solubility in 4 × the minimum volume of Castile brine	
	SOLCOH5	6.44×10^{-7}		Oxidation state V model, solubility in 5 × the minimum volume of Castile brine	

Table 2-12: Solubility Uncertainties for the CRA-2014 PA

Material	Property	Distribution/ Statistics	Units	Description	Source
SOLMOD3	SOLVAR	Cumulative/ Min = -3.55 Mean = -0.68 Max = 2.97 Default Value = -0.68	(none)	Oxidation State III Solubility Multiplier	Brush and Domski (2013), Table 8
SOLMOD4	SOLVAR	Cumulative/ Min = -1.52 Mean = 0.66 Max = 3.19 Default Value = 0.66	(none)	Oxidation State IV Solubility Multiplier	Brush and Domski (2013), Table 5

2.10 Refinement to Repository Water Balance

The saturation and pressure history of the repository are used throughout PA. Along with flow in and out of the repository, the saturation and pressure are influenced by the reaction of materials placed in the repository with the surrounding environment. As part of the review of the CRA-2009, EPA noted several issues for possible additional investigation, including the potential implementation of a more detailed repository water balance (U.S. EPA 2010b). The repository water balance implementation is refined in the CRA-2014 PA in order to include the

major gas and brine producing and consuming reactions in the existing conceptual model. The development of parameters used in the refined water budget implementation is given in Clayton (2013). WIPP PA code BRAGFLO Version 6.02 was developed to utilize the additional water balance parameters, and was used in the CRA-2014 PA. Parameters associated with the water balance refinement implemented in the CRA-2014 PA are listed in Table 2-13 and Table 2-14.

Table 2-13: Constant Parameters in the CRA-2014 PA Water Balance Implementation

Material	Property	Value	Units	Description	Source
REFCON	STCO_10	0	(none)	Fe Corrosion: Hydromagnesite Stoichiometric Coefficient	Clayton (2013), Table 3
	STCO_20	0		Microbial Gas Generation: Hydromagnesite Stoichiometric Coefficient	
	STCO_30	0		FeOH2 Sulfidation: Hydromagnesite Stoichiometric Coefficient	
	STCO_40	0		Metallic Fe Sulfidation: Hydromagnesite Stoichiometric Coefficient	
	STCO_50	0		MgO Hydration: Hydromagnesite Stoichiometric Coefficient	
	STCO_60	0.25		MgOH2 Carbonation: Hydromagnesite Stoichiometric Coefficient	
	STCO_70	0		MgO Carbonation: Hydromagnesite Stoichiometric Coefficient	
	STCO_81	0		Hydromagnesite Conversion: H2 Stoichiometric Coefficient	
	STCO_82	4		Hydromagnesite Conversion: H2O Stoichiometric Coefficient	
	STCO_83	0		Hydromagnesite Conversion: Fe Stoichiometric Coefficient	
	STCO_84	0		Hydromagnesite Conversion: Cellulosics Stoichiometric Coefficient	
	STCO_85	0		Hydromagnesite Conversion: FeOH2 Stoichiometric Coefficient	
	STCO_86	0		Hydromagnesite Conversion: FeS Stoichiometric Coefficient	
	STCO_87	0		Hydromagnesite Conversion: MgO Stoichiometric Coefficient	
	STCO_88	1		Hydromagnesite Conversion: MgOH2 Stoichiometric Coefficient	
	STCO_89	4		Hydromagnesite Conversion: MgCO3 Stoichiometric Coefficient	
	STCO_80	-1		Hydromagnesite Conversion: Hydromagnesite Stoichiometric Coefficient	
	STCO_62	0		MgOH2 Carbonation: H2O Stoichiometric Coefficient	Clayton (2013), Table 4
	STCO_68	-1.25		MgOH2 Carbonation: MgOH2 Stoichiometric Coefficient	
	STCO_69	0		MgOH2 Carbonation: MgCO3 Stoichiometric Coefficient	

Table 2-13 (continued)					
Material	Property	Value	Units	Description	Source
	DN_HYDRO	2300	(kg/m ³)	Density of Hydromagnesite	Clayton (2013), Table 5
	MW_HYDRO	467.636 x 10 ⁻³	(kg/mol)	Molecular Weight of Hydromagnesite	

Table 2-14: Sampled Parameters in the CRA-2014 PA Water Balance Implementation

Material	Property	Distribution/ Statistics	Units	Description	Source
WAS_AREA	HYMAGCON	Uniform/ Max = 6.8e-10 Min = 6.8e-12 Mean = 3.4e-10 S.D. = 1.9e-10 Default Value = 3.4e-10	mol/(kg*s)	Rate of conversion of hydromagnesite to magnesite	Clayton (2013), Table 6
	BRUCITEC	Normal/ Mean = 5.2e-8 S.E. = 1.9e-9 Max = 5.64e-8 Min = 4.76e-8 Default Value = 5.2e-8		MgO inundated hydration rate in ERDA- 6 brine	Clayton (2013), Table 8
	BRUCITES	Normal/ Mean = 5.2e-8 S.E. = 4.0e-9 Max = 6.13e-8 Min = 4.27e-8 Default Value = 5.2e-8		MgO inundated hydration rate in GWB brine	
	BRUCITEH	Normal/ Mean = 2.0e-8 S.E. = 8.2e-10 Max = 2.19e-8 Min = 1.81e-8 Default Value = 2.0e-8		MgO humid hydration rate	

2.11 Updated Colloid Parameters

Colloid parameters are updated in the CRA-2014 PA to incorporate recently available data. Discussions of this data and the development of WIPP PA parameters from it are given in Reed et al. (2013) and Roselle (2013b). Updated colloid parameters used in the CRA-2014 PA are listed in Table 2-15.

Table 2-15: Updated Colloid Parameters Used in the CRA-2014 PA

Material	Property	Value	Units	Description	Source
AM	CONCINT	4×10^{-9}	moles/liter	Americium Colloid Parameters	Roselle (2013b), Table 1
	PROPMIC	0.32	(none)		Roselle (2013b), Table 2
	CAPMIC	3.1×10^{-8}	moles/liter		Roselle (2013b), Table 3
NP	CONCINT	2×10^{-8}	moles/liter	Neptunium Colloid Parameters	Roselle (2013b), Table 1
	PROPMIC	1.76	(none)		Roselle (2013b), Table 2
	CAPMIC	2.3×10^{-6}	moles/liter		Roselle (2013b), Table 3
PU	CONCINT	2×10^{-8}	moles/liter	Plutonium Colloid Parameters	Roselle (2013b), Table 1
	PROPMIC	1.76	(none)		Roselle (2013b), Table 2
	CAPMIC	2.3×10^{-6}	moles/liter		Roselle (2013b), Table 3
TH	CONCINT	2×10^{-8}	moles/liter	Thorium Colloid Parameters	Roselle (2013b), Table 1
	PROPMIC	1.76	(none)		Roselle (2013b), Table 2
	CAPMIC	2.3×10^{-6}	moles/liter		Roselle (2013b), Table 3
U	CONCINT	3×10^{-8}	moles/liter	Uranium Colloid Parameters	Roselle (2013b), Table 1
	PROPMIC	1.76	(none)		Roselle (2013b), Table 2
	CAPMIC	2.3×10^{-6}	moles/liter		Roselle (2013b), Table 3

2.12 Parameter Correction

PA material DRZ_PCS was developed in 2002 to represent healed portions of the DRZ above a panel closure (Stein 2002). As developed in 2002, it was intended that property values assigned to material DRZ_PCS be exactly the same as those used for material DRZ_1, with the exception of log-permeabilities in the X, Y, and Z directions. Parameter DRZ_1:RELP_MOD is assigned a Delta distribution having a minimum of 1, a maximum of 4, with the mean, median, and default value all assigned a value of 4. Conversely, the Delta distribution entered into the PA parameter database for parameter DRZ_PCS:RELP_MOD has a minimum of 1, a maximum of 4, but a mean, median, and default value of 0. To bring parameter DRZ_PCS:RELP_MOD into agreement with the justification used in its original 2002 development, it is updated in the CRA-2014 PA so that it is identical to parameter DRZ_1:RELP_MOD. The revised distribution for parameter DRZ_PCS:RELP_MOD is shown in Table 2-16.

Table 2-16: DRZ_PCS:RELP_MOD Distribution for the CRA-2014 PA

Material	Property	Distribution/ Statistics	Units	Description	Source
DRZ_PCS	RELP_MOD	Delta/ Max = 4 Mean = 4 Median = 4 Min = 1 Default Value = 4 (Prob., Value) Pairs: (0.33,1) (0,2) (0,3) (0.67,4)	(none)	Model number, relative permeability number	Camphouse (2013a), Table 2-10

Note that this refinement to parameter DRZ_PCS:RELP_MOD will have no impact on computed PA results. Values of DRZ_PCS:RELP_MOD are inherited from those prescribed to parameter DRZ_1:RELP_MOD in the Algebra1 input file to BRAGFLO, and have been since the TBM PA. The refinement of parameter DRZ_PCS:RELP_MOD is cosmetic in nature, and is being done to enhance agreement between the historical development of this parameter and the values entered into the PA parameter database.

3 FEPS ASSESSMENT

The CRA-2014 PA began with an assessment that identified and evaluated the features, events, and processes (FEPs) that are related to the changes introduced in the PA. The purpose of the FEPs evaluation was to determine if the current FEPs baseline (currently the PABC-2009 FEPs baseline) is suitable for the CRA-2014 PA, or if changes to FEPs descriptions, screening arguments, or decisions are necessary. The results of this assessment concluded that no changes are needed to the FEPs baseline (Kirkes 2013). It should be pointed out that the FEPs analysis only determines that the WIPP design features are appropriately identified, described, and screened according to established FEPs screening methods. WIPP FEPs W109 Panel Closure Geometry and W110, Panel Closure Properties, are directly related to changes included in the CRA-2014 PA, and are included in the FEPs assessment. These two FEPs have been screened in (represented) as part of previous performance assessments in all scenarios, and continue to be so in the CRA-2014 PA.

4 METHODOLOGY

The PA methodology accommodates both aleatory (i.e. stochastic) and epistemic (i.e. subjective) uncertainty in its constituent models. Aleatory uncertainty pertains to unknowable future events such as intrusion times and locations that may affect repository performance. It is accounted for by the generation of random sequences of future events. Epistemic uncertainty concerns parameter values that are assumed to be constants and the constants' true values are uncertain due to a lack of knowledge about the system. An example of a parameter with epistemic uncertainty is the permeability of a material. Epistemic uncertainty is accounted for by sampling of parameter values from assigned distributions. One set of sampled values required to run a WIPP PA calculation is termed a vector. In the CRA-2014 PA, models were executed for three replicates of 100 vectors. Parameter sampling performed in the CRA-2014 PA is documented in Kirchner (2013a), and the sensitivities of variable output to sampled parameters are documented in Kirchner (2013b). A sample size of 10,000 possible sequences of future events is used in PA calculations to address aleatory uncertainty. The releases for each of 10,000 possible sequences of future events are tabulated for each of the 300 vectors, totaling 3,000,000 possible sequences.

For a random variable, the complementary cumulative distribution function (CCDF) provides the probability of the variable being greater than a particular value. By regulation, PA results are presented as a distribution of CCDFs of releases (U.S. EPA 1996). Each individual CCDF summarizes the likelihood of releases across all futures for one vector of parameter values. The uncertainty in parameter values results in a distribution of CCDFs.

Releases are quantified in terms of "EPA units". Releases in EPA units result from a normalization by radionuclide and the total inventory. For each radionuclide, the ratio of its 10,000 year cumulative release (in curies) to its release limit is calculated. The sum of these ratios is calculated across the set of radionuclides and normalized by the transuranic inventory (in curies) of α -emitters with half-lives greater than 20 years. Mathematically, the formula used to calculate releases in terms of EPA units is of the form

$$R = \frac{1 \times 10^6 \text{ curies}}{C} \sum_i \frac{Q_i}{L_i}$$

where R is the normalized release in EPA units. Quantity Q_i is the 10,000 year cumulative release (in curies) of radionuclide i . Quantity L_i is the release limit for radionuclide i , and C is the total transuranic inventory (in curies) of α -emitters with half-lives greater than 20 years.

The CRA-2014 PA was developed so that the structure of calculations performed therein is as similar as possible to that used in the PABC-2009. As seen in Section 2, a number of planned repository changes, implementation changes, and parameter changes are included in the CRA-2014 PA as compared to the PABC-2009. The approach taken in the CRA-2014 PA is to reasonably isolate impacts associated with these changes, and then to assess the combined impact when all are included in the PA (Camphouse 2013a). This report provides a summary of results obtained when the comprehensive set of changes described in Section 2 are included in the PA. The impact of individual changes (or combined changes where appropriate) is more fully discussed in the individual analysis packages produced as part of the CRA-2014 PA. Citations

for this additional documentation are included in the references section of this summary report, and are indicated in the list below.

- Unit Loading Calculation (Kicker and Zeitler 2013a)
- Inventory Screening Analysis (Kicker and Zeitler 2013b)
- Parameter Sampling (Kirchner 2013a)
- Salado Flow (Camphouse 2013b)
- Direct Brine Release Volumes (Malama 2013)
- Cuttings, Cavings, and Spallings (Kicker 2013)
- Actinide Mobilization (Kim 2013a)
- Radionuclide Transport (Kim 2013b)
- CCDF Normalized Releases (Zeitler 2013)
- Sensitivity Analysis (Kirchner 2013b)
- Run Control (Long 2013)

5 RUN CONTROL

Run control documentation of codes executed in the CRA-2014 PA is provided in Long (2013). This documentation contains:

1. A description of the hardware platform and operating system used to perform the calculations.
2. A listing of the codes and versions used to perform the calculations.
3. A listing of the scripts used to run each calculation.
4. A listing of the input and output files for each calculation.
5. A listing of the library and class where each file is stored.
6. File naming conventions.

Outputs from WIPP PA codes DRSPALL and SECOTP2D are not impacted by the changes implemented in the CRA-2014 PA. Therefore, results obtained or used in the PABC-2009 for these codes are also used in the CRA-2014 PA. Documentation of run control for results calculated in the PABC-2009 is provided in Long (2010).

6 RESULTS

Summary results obtained in the CRA-2014 PA are broken out in sections below, and are compared to PABC-2009 results.

6.1 Inventory Comparison

The code EPAUNI calculates the time varying activity of the waste, accounting for radioactive decay, which is used in calculating direct solid releases during a drilling intrusion. Ten radionuclides are modeled for the solid release source term: ^{241}Am , ^{244}Cm , ^{137}Cs , ^{238}Pu , ^{239}Pu , ^{240}Pu , ^{241}Pu , ^{90}Sr , ^{233}U , and ^{234}U . Kicker and Zeitler (2013b) indicate that these 10 radionuclides account for 99.55% of the EPA units at the time of repository closure in the CRA-2014 PA inventory.

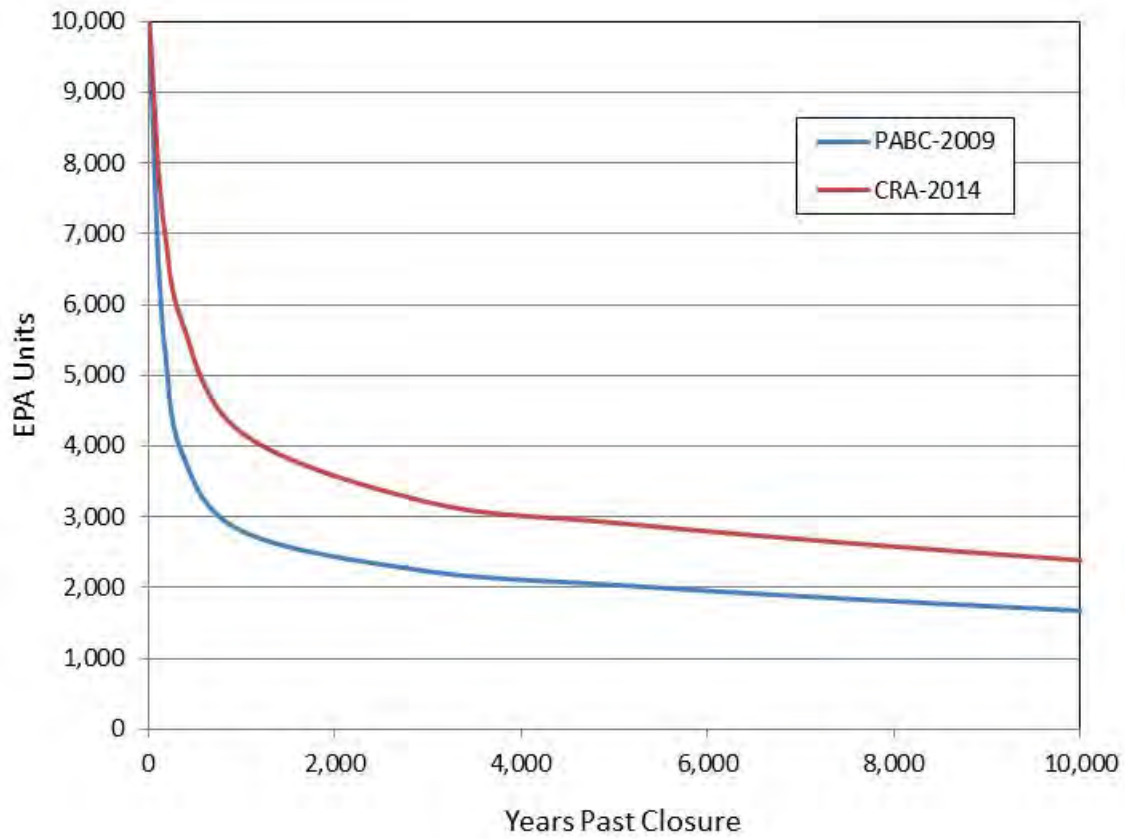


Figure 6-1: WIPP CH- and RH-TRU Waste EPA Units from Closure to 10,000 Years

The total number of EPA Units in the CRA-2014 PA waste inventory at the closure year of 2033 is 10,197 (Kicker and Zeitler 2013a). This number is slightly higher than the value of 10,080 EPA units corresponding to the PABC-2009 waste inventory at year 2033 (Fox and Clayton 2010). By 10,000 years post-closure, the total number of EPA Units in the CRA-2014 PA decreases to 2,388. The analogous number in the PABC-2009 was 1,680 EPA Units, indicating an increase in the CRA-2014 PA. A comparison of the total EPA Units as a function of time for the CRA-2014 PA waste inventory and the inventory used for the PABC-2009 PA is shown in Figure 6-1. As seen in that figure, the total EPA Units for both inventories start at similar levels, but the CRA-2014 PA inventory is higher after approximately 100 years and remains higher throughout the 10,000-year regulatory period. The increase seen in the CRA-2014 PA result is primarily due to an increase in ^{239}Pu inventory.

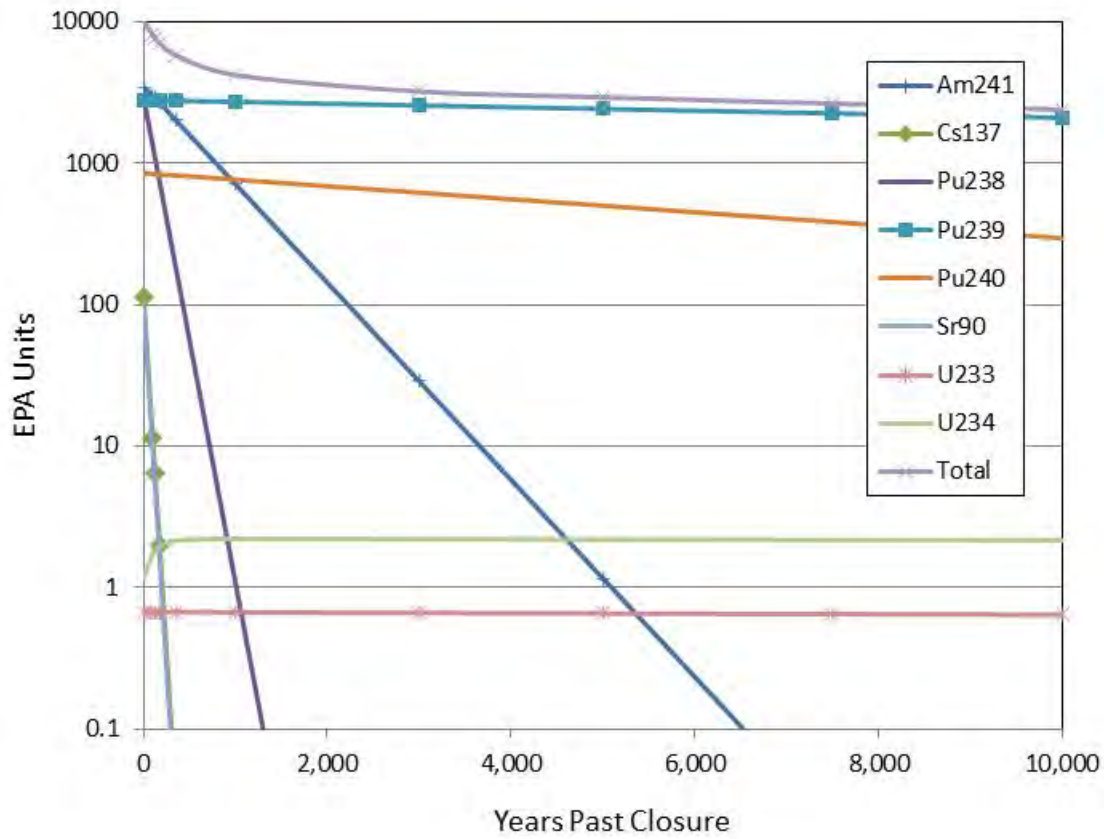


Figure 6-2: Dominant WIPP CH- and RH-TRU Waste Isotopes from Closure to 10,000 Years

Figure 6-2 shows the total EPA Units as a function of time for the CRA-2014 PA, along with the dominant radionuclides that contribute to the overall total. As seen in that figure, the initial normalized activity of the inventory is dominated by ^{241}Am , ^{238}Pu , ^{239}Pu and ^{240}Pu . The ^{241}Am and ^{238}Pu inventories decay rapidly and so the total normalized activity of the inventory is dominated at later times (> 2,000 years) by mainly ^{239}Pu with a smaller contribution from ^{240}Pu . The ^{137}Cs , ^{90}Sr , ^{233}U and ^{234}U do not appreciably contribute to the total normalized activity at any time throughout the 10,000-year regulatory period. These trends are consistent with those seen in the PABC-2009 (Fox and Clayton 2010).

6.2 Radionuclide Mobilized Concentrations

WIPP PA code PANEL calculates the time-varying concentration of radionuclides mobilized in brine, either as dissolved isotopes or as isotopes sorbed to mobile colloids. PANEL results obtained in the CRA-2014 PA are fully discussed in Kim (2013a), and are now summarized. Two different brines are considered by PANEL: the interstitial brine present in the Salado Formation called GWB, which is magnesium rich; and the brine in the Castile Formation called ERDA-6, which is sodium rich. As discussed in Section 2.9, baseline radionuclide solubilities in the CRA-2014 PA are calculated using multiples of the minimum brine volume (17,400 m³) necessary for a DBR to occur. Brine volumes of 1x, 2x, 3x, 4x, and 5x this minimum necessary brine volume are used in the calculation of baseline radionuclide solubilities in ERDA-6 and GWB brines, and these solubilities are listed in Table 2-9 to Table 2-11.

Figure 6-3 and Figure 6-4 show the concentration of radioactivity mobilized in Salado brine as a function of time for all vectors in replicate 1 of the CRA-2014 PA. Figure 6-3 shows results obtained using baseline solubilities corresponding to the minimum brine volume of 17,400 m³ (denoted as BV1 in that figure). Figure 6-4 shows results obtained using baseline solubilities corresponding to 5x the minimum brine volume (denoted as BV5 in that figure). Analogous results for Castile brine are shown in Figure 6-5 and Figure 6-6. Concentrations are expressed as EPA units/m³ to combine the radioactivity of different isotopes. At early times (before 2000 years), the total mobilized concentrations (in both Salado and Castile brines) have their highest values because of the contribution of americium. After about 4000 years, the contribution from americium decreases because of the decay of ²⁴¹Am. After about 4000 years, the total mobilized concentrations are dominated by plutonium, with concentrations of uranium and thorium being orders of magnitude lower.

For the sake of comparison, radionuclide mobilized concentrations obtained in the PABC-2009 for GWB and ERDA-6 brines are shown in Figure 6-7 and Figure 6-8, respectively. Results obtained in the PABC-2009 were obtained using a single brine volume of 17,400 m³. The CRA-2014 PA results for total mobilized concentrations show a similar variability to what was obtained in the PABC-2009. However, total mobilized concentrations obtained in the CRA-2014 PA decrease as the brine volume increases. This trend is expected to reduce releases associated with large DBR volumes in the CRA-2014 PA as compared to the PABC-2009.

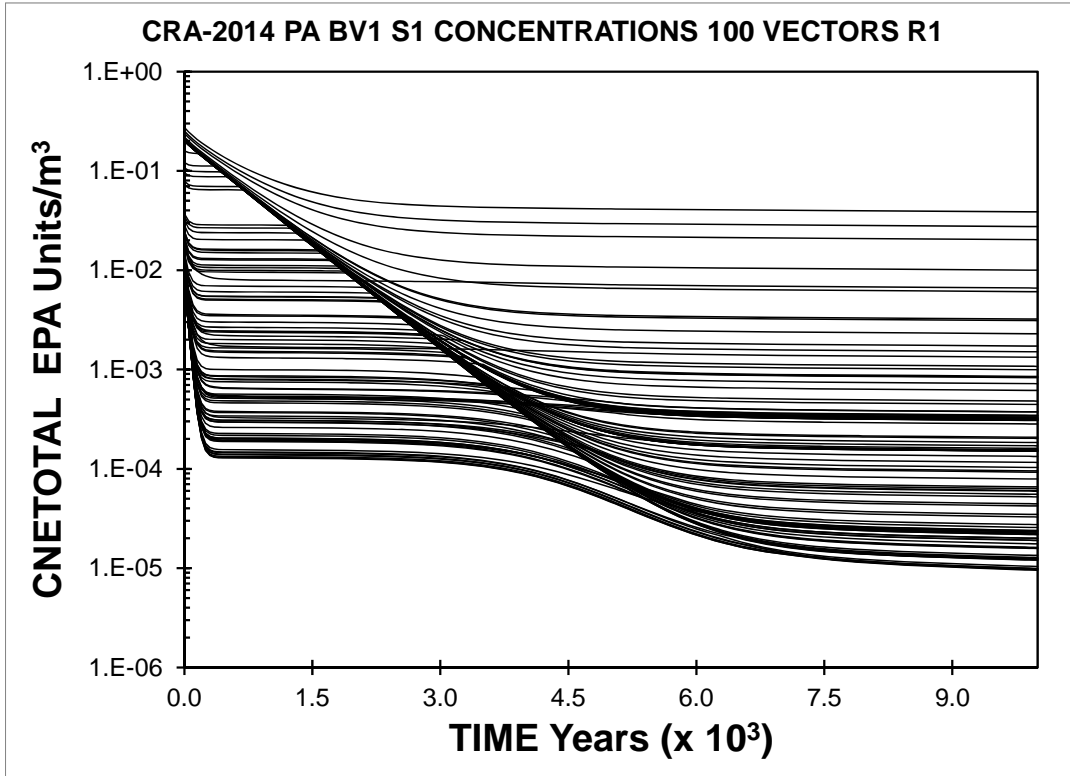


Figure 6-3: CRA-2014 PA Total Mobilized Concentrations in Salado Brine, Replicate 1, BV1

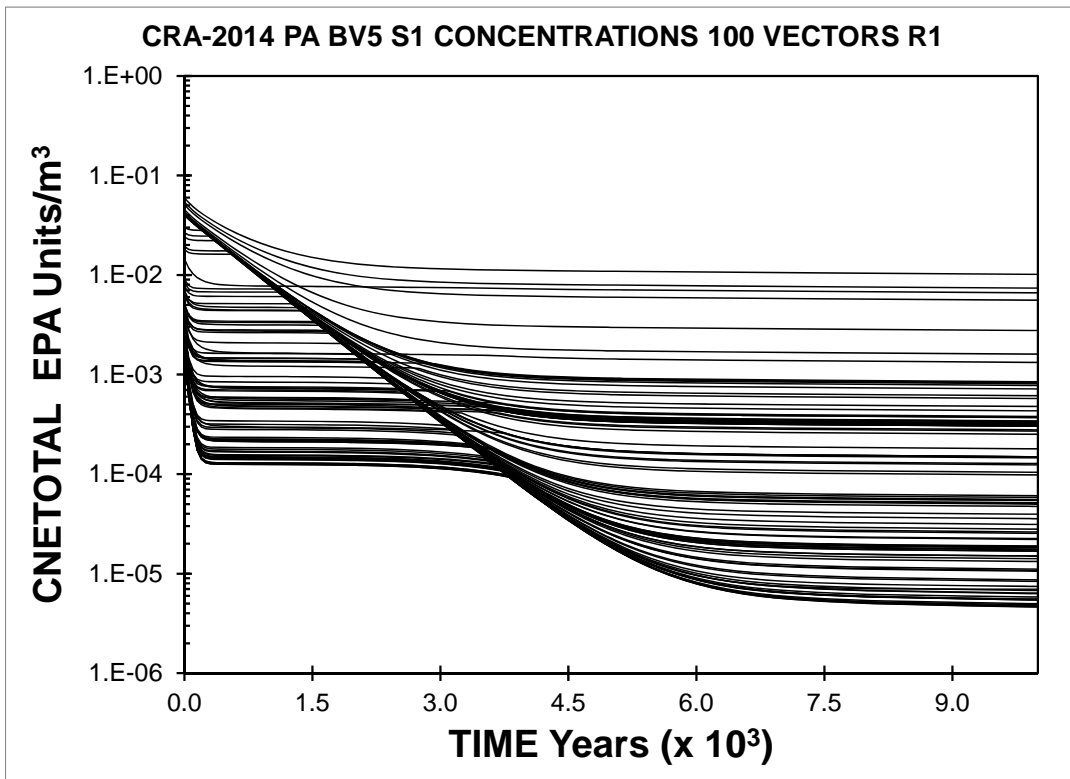


Figure 6-4: CRA-2014 PA Total Mobilized Concentrations in Salado Brine, Replicate 1, BV5

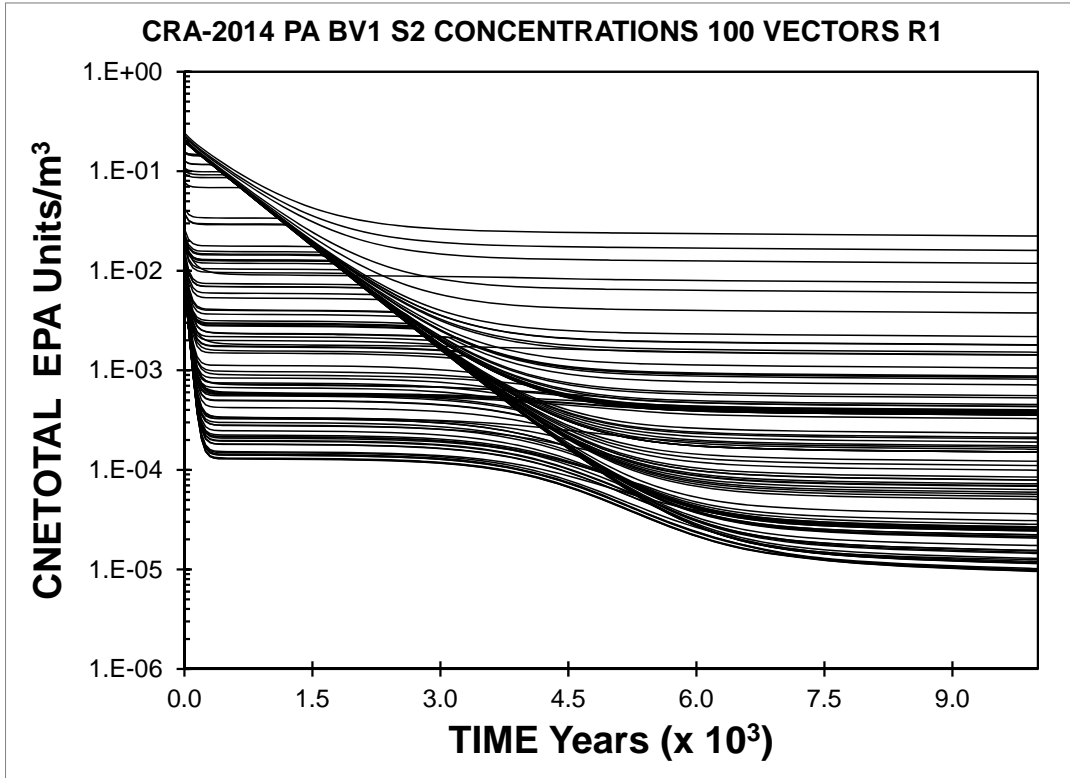


Figure 6-5: CRA-2014 PA Total Mobilized Concentrations in Castile Brine, Replicate 1, BV1

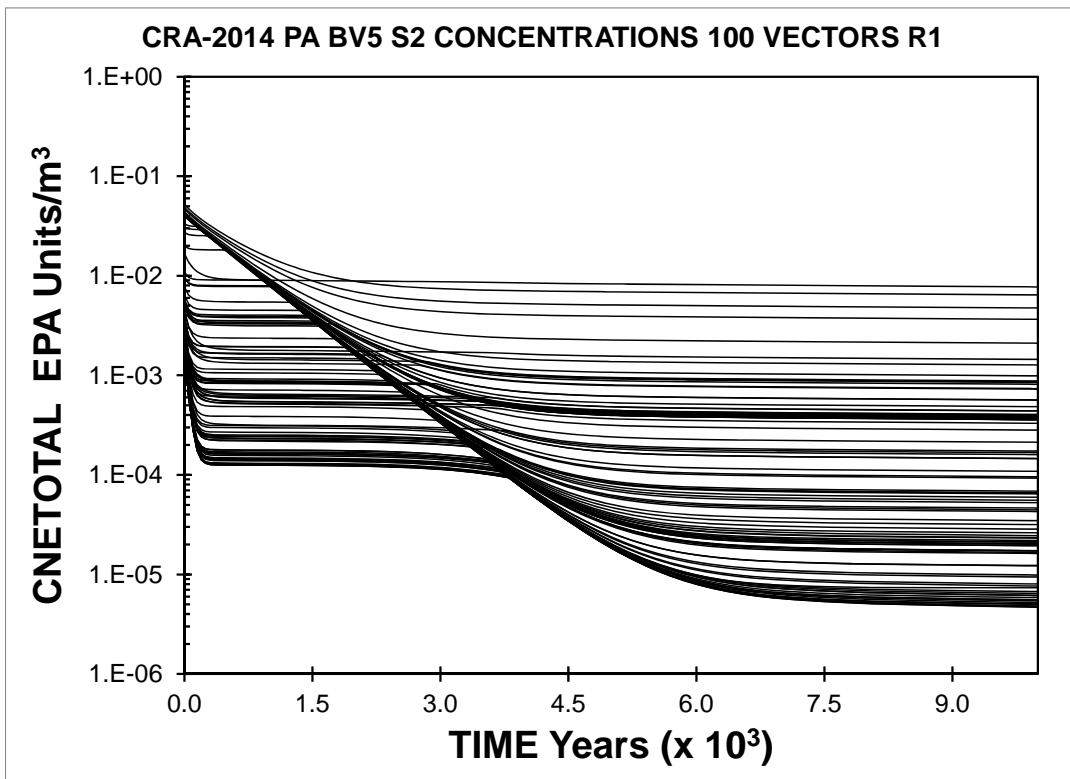


Figure 6-6: CRA-2014 PA Total Mobilized Concentrations in Castile Brine, Replicate 1, BV5

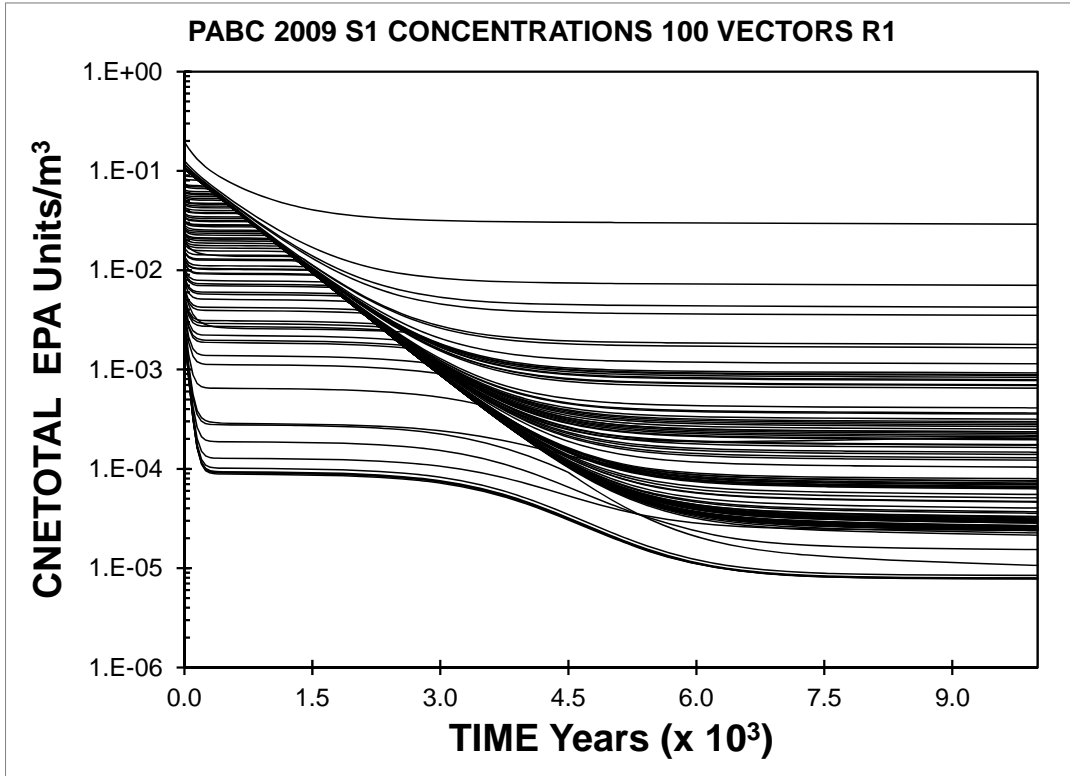


Figure 6-7: PABC-2009 Total Mobilized Concentrations in Salado Brine, Replicate 1

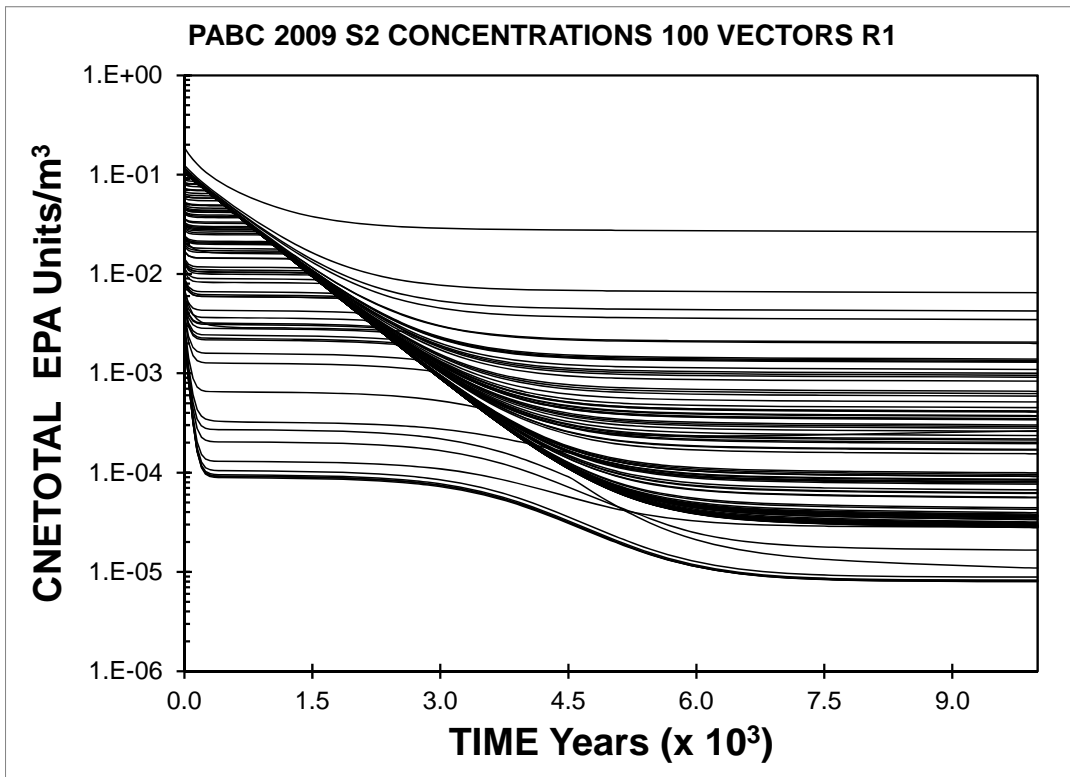


Figure 6-8: PABC-2009 Total Mobilized Concentrations in Castile Brine, Replicate 1

6.3 Salado Flow Results

PA code BRAGFLO calculates the flow of brine and gas in the vicinity of the WIPP repository over the 10,000-year regulatory compliance period. During BRAGFLO calculations, stochastic uncertainty is addressed by defining a set of six scenarios for which brine and gas flow is calculated for each of the vectors generated via parameter sampling. The total number of BRAGFLO simulations executed in the CRA-2014 PA is 1,800 (300 vectors times 6 scenarios).

The six scenarios used in the CRA-2014 PA are unchanged from those used for the PABC-2009. The scenarios include one undisturbed scenario (S1-BF), four scenarios that include a single inadvertent future drilling intrusion into the repository during the 10,000 year regulatory period (S2-BF to S5-BF), and one scenario investigating the effect of two intrusions into a single waste panel (S6-BF). Two types of intrusions, denoted as E1 and E2, are considered. An E1 intrusion assumes the borehole passes through a waste-filled panel and into a pressurized brine pocket that may exist under the repository in the Castile formation. An E2 intrusion assumes that the borehole passes through the repository but does not encounter a brine pocket. Scenarios S2-BF and S3-BF model the effect of an E1 intrusion occurring at 350 years and 1000 years, respectively, after the repository is closed. Scenarios S4-BF and S5-BF model the effect of an E2 intrusion at 350 and 1000 years. Scenario S6-BF models an E2 intrusion occurring at 1000 years, followed by an E1 intrusion into the same panel at 2000 years. Calculated brine flows up the intrusion borehole obtained in scenario S6-BF are used in PA code PANEL to determine the radionuclide source term to the Culebra. Table 6-1 summarizes the six scenarios used in this analysis.

Table 6-1: BRAGFLO Modeling Scenarios

Scenario	Description
S1-BF	Undisturbed Repository
S2-BF	E1 intrusion at 350 years
S3-BF	E1 intrusion at 1000 years
S4-BF	E2 intrusion at 350 years
S5-BF	E2 intrusion at 1000 years
S6-BF	E2 intrusion at 1000 years; E1 intrusion at 2000 years.

Summary Salado flow results are presented for the CRA-2014 PA and compared with those obtained in the PABC-2009. Results are discussed in terms of overall means. Overall means are obtained by forming the average of the 300 realizations calculated for a given quantity and scenario. Results are presented for undisturbed scenario S1-BF. Intruded results are presented for scenarios S2-BF and S4-BF, as these are representative of the intrusion types considered in scenarios S2-BF to S5-BF with the only differences being the timing of drilling intrusions. Results from scenario S6-BF are also briefly discussed. More detailed Salado flow results can be found in Camphouse (2013b).

Option D panel closures were implemented in the PABC-2009. The computational grid and material map used in the PABC-2009 Salado flow calculations are shown in Figure 6-9. A

minor error has been corrected in the material map schematic shown in Figure 6-9. That figure depicts an E1 intrusion into the repository. The BRAGFLO schematic included with the PABC-2009 Salado flow analysis package (Nemer 2010) depicts the lower borehole extending only to the bottom horizon of the lower DRZ. In actuality, the lower borehole extends to the floor of the intruded waste panel. The PABC-2009 BRAGFLO grid and material map shown in Figure 6-9 has been modified so that it represents the correct extent of the lower borehole in an E1 intrusion. The analogous CRA-2014 PA BRAGFLO computational grid and material map are shown in Figure 6-10. As that figure also depicts an E1 intrusion scenario, with 350 years post-closure being the first time instance at which an intrusion occurs, materials DRZ_PCS and ROMPCS material PCS_T3 are in place at the time of all intrusions in the Salado flow calculations. The development of the CRA-2014 PA BRAGFLO grid, as well as the representation of the temporal evolution of the ROMPCS in the BRAGFLO material map, is fully discussed in Camphouse (2013b).

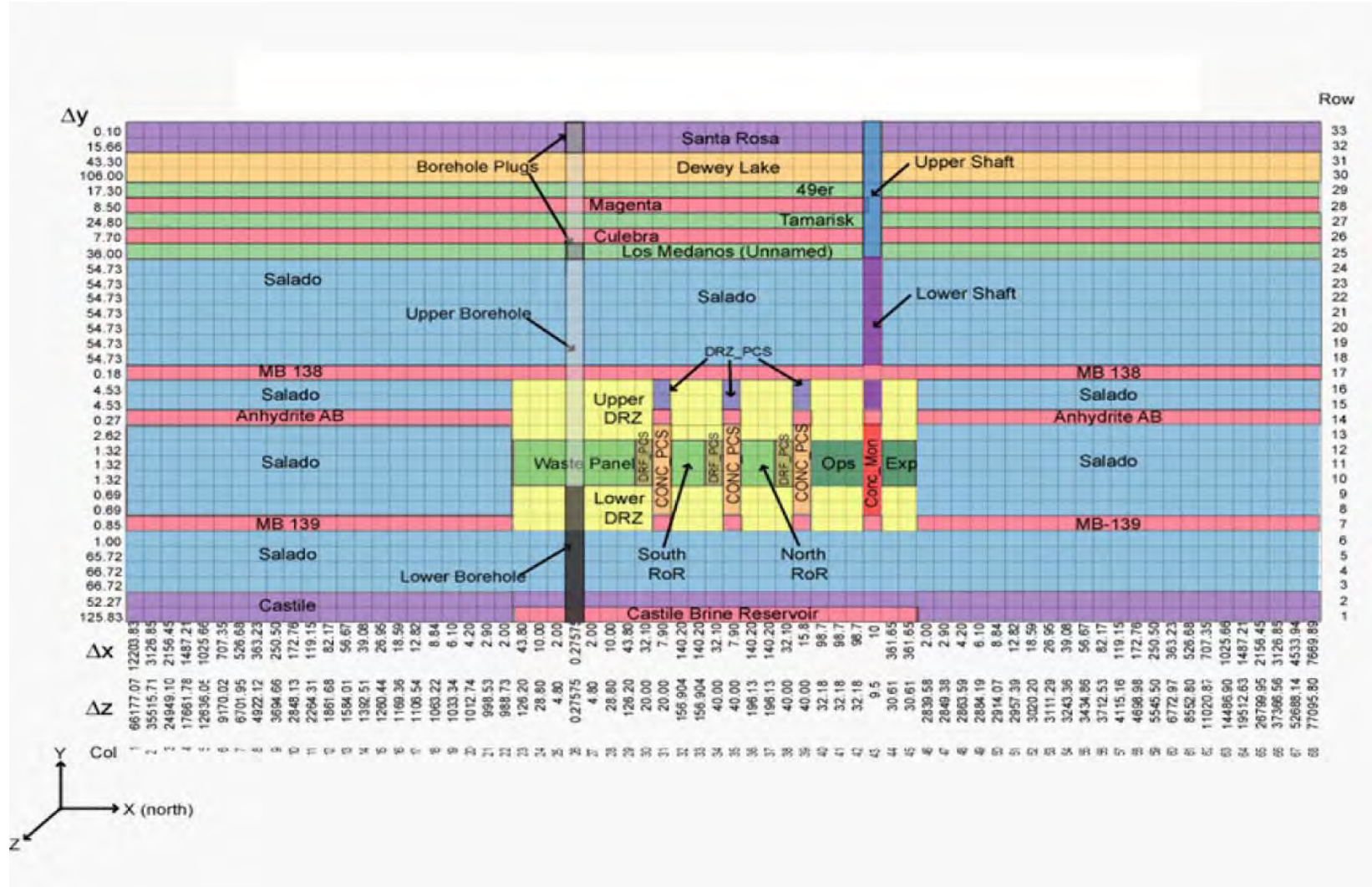


Figure 6-9: PABC-2009 BRAGFLO Grid and Material Map for an E1 Intrusion (Δx , Δy , and Δz dimensions in meters).

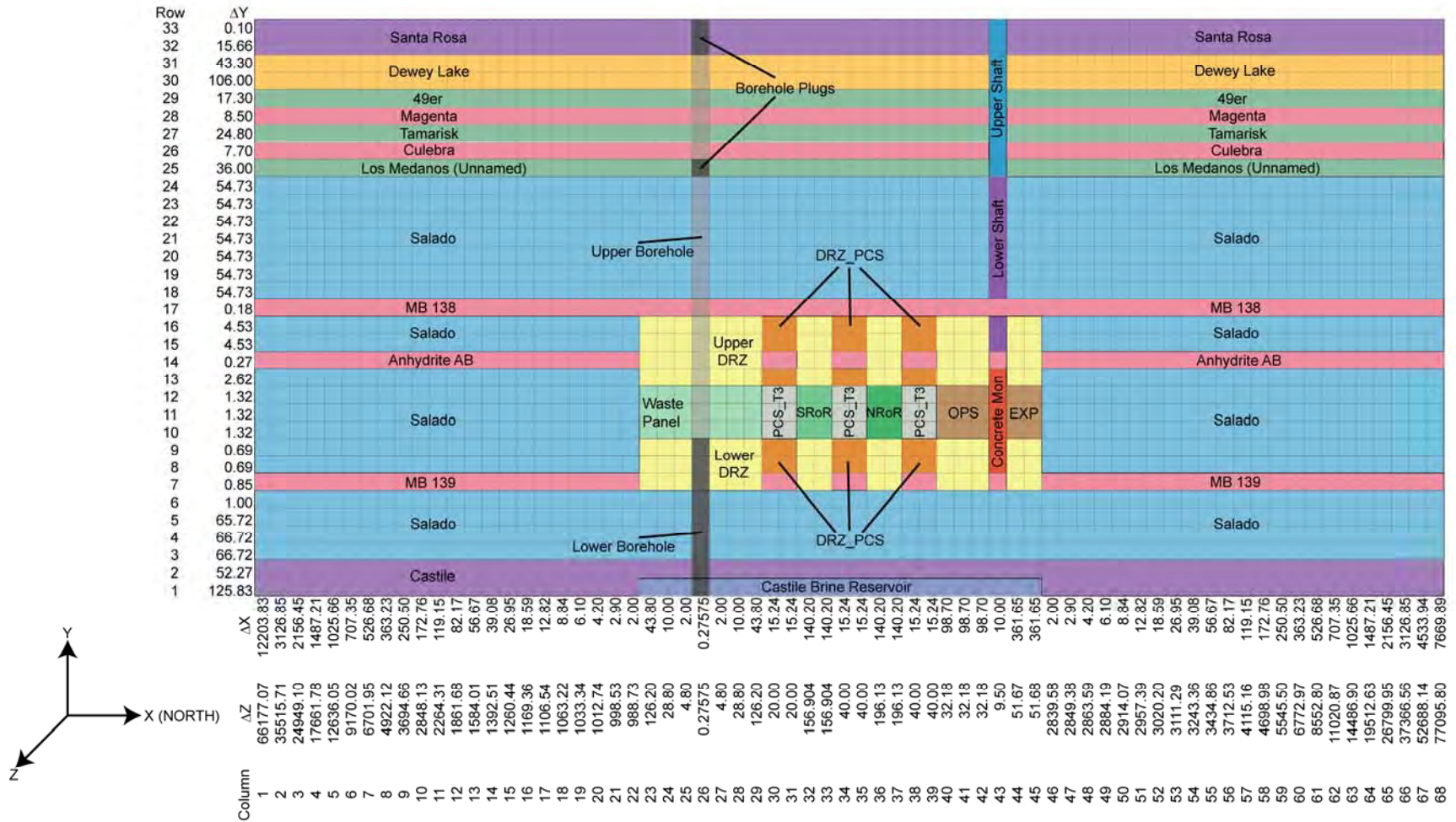


Figure 6-10: CRA-2014 PA BRAGFLO Grid and Material Map for an E1 Intrusion (Δx , Δy , and Δz dimensions in meters).

6.3.1 Results for an Undisturbed Repository (Scenario S1-BF)

Results are now presented for undisturbed scenario S1-BF. Results for each quantity are compared to those obtained in the PABC-2009. Results presented in this section are more fully discussed in Camphouse (2013b).

The overall means of volume-averaged waste panel pressure, quantity WAS_PRES, obtained in the CRA-2014 PA and the PABC-2009 are plotted together in Figure 6-11. By itself, the replacement of the Option D PCS with the ROMPCS results in a slightly higher mean pressure in the waste panel for undisturbed conditions (Camphouse 2012c). However, additional mined volume in the WIPP experimental area results in a slight reduction to the mean waste panel pressure. Decreases in the iron and CPR inventory in the CRA-2014 PA also likely contribute to a reduction in mean waste panel pressure. The revised steel corrosion rate and water balance implementation utilized in the CRA-2014 PA result in even further reduction to the mean waste panel pressure. The net effect of all changes included in the CRA-2014 PA is a reduction to the mean waste panel pressure as compared to the PABC-2009. Pressure trends seen in the waste panel are also evident in the South Rest-of-Repository (SRoR) and North Rest-of-Repository (NRoR) waste regions. Pressure in these regions is denoted by SRR_PRES and NRR_PRES, respectively, and results for these quantities are shown in Figure 6-12 and Figure 6-13. Similar pressure trends are also apparent in the repository experimental area (Figure 6-14).

The reduction in waste region mean pressure in the CRA-2014 PA is largely due to the revised iron corrosion rate. Replicate 1 means of cumulative gas generation (in moles) obtained in the PABC-2009 is shown in Figure 6-18 of Nemer (2010). That figure is also included as Figure 6-15 of this report for clarity in the discussion that follows. Shown in that figure are the Replicate 1 means of total cumulative gas generation in repository waste areas (quantity GAS_MOLE) as well as means of molar gas produced by iron corrosion (quantity FE_MOLE) and microbial activity (quantity CEL_MOLE). The majority of gas generated in repository waste regions in the PABC-2009 was due to iron corrosion (on average). The analogous plot, showing means calculated over all 300 vectors obtained in Scenario S1-BF of the CRA-2014 PA, is shown in Figure 6-16. (Note that quantities GAS_MOLE, FE_MOLE, and CEL_MOLE have been renamed as GASMOL_T, FEMOL_T, and CELMOL_T, respectively, in the CRA-2014 PA.) As is clear from Figure 6-16, gas generation due to iron corrosion is still the dominant gas production mechanism in the CRA-2014 PA. However, the moles of gas generated by iron corrosion in the CRA-2014 PA are significantly reduced (on average) as compared to the PABC-2009. The revised iron corrosion rate implemented in the CRA-2014 PA results in a slower rate of gas production (on average). The inclusion of MgO chemistry in the revised water balance implementation also contributes to the reduction in gas generation for the CRA-2014 PA. Gas production due to iron corrosion and CPR microbial degradation both require freely available brine in repository waste regions. The formation of brucite in the revised water balance implementation sequesters free water, making less available for gas production processes. The impact of the revised water balance implementation on gas production can be determined by comparing the mean curves for molar gas produced via microbial activity in Figure 6-15 and Figure 6-16. Moles of gas produced by microbial degradation of cellulose is slightly reduced (on average) in the CRA-2014 PA. The revised iron corrosion rate and water balance implementation both contribute to the reduction in mean total molar gas generation. Decreased iron and CPR inventories in the CRA-2014 PA also likely contribute to the reduction seen in the

CRA-2014 PA results. However, most of the gas generation reduction seen in the CRA-2014 PA is due to the reduction in gas generated via iron corrosion.

The trend toward waste panel pressure reduction in the CRA-2014 PA yields a corresponding increase (on average) in cumulative waste panel brine inflow, denoted by quantity BRNWASIC. The overall means of cumulative waste panel brine inflow, calculated over all 300 vector realizations, obtained in the PABC-2009 and the CRA-2014 PA are plotted together in Figure 6-17. As is clear from that figure, a reduction in the mean cumulative waste panel brine inflow is seen in the CRA-2014 PA results. Results obtained for the south and north rest-of-repository regions are similar to those seen for the waste panel. Cumulative brine inflows to these repository regions are denoted by BRNSRRIC and BRNNRRIC, respectively, and results for these quantities are shown in Figure 6-18 and Figure 6-19. As can be seen by comparing Figure 6-17, Figure 6-18, and Figure 6-19, the increase to the mean cumulative brine inflow relative to the PABC-2009 is more pronounced for panels at lower elevation. Mean brine inflow results obtained in the PABC-2009 and the CRA-2014 PA are quite similar for the NRoR (Figure 6-19), while the difference seen between the PABC-2009 and Case CRA14-0 result is more pronounced for the SRoR (Figure 6-18) and the southernmost (lowest elevation) waste panel (Figure 6-17). Trends seen in the waste panel for cumulative brine inflow are also apparent when investigated for the entire repository. Results obtained for cumulative brine inflow to the repository, denoted by quantity BRNREPIC, are shown in Figure 6-20.

The repository shaft is modeled in WIPP PA as being directly between the operations and experimental regions of the repository. Consequently, the pressure in these repository regions impacts the volume of brine moved up the shaft toward the ground surface (quantity BNSHUDRZ). The overall mean of quantity BNSHUDRZ obtained in the CRA-2014 PA is compared to the PABC-2009 result in Figure 6-21. As seen in that figure, the mean cumulative brine flow up the shaft is reduced in the CRA-2014 PA, with trends following those seen for mean pressure in the experimental region (Figure 6-14).

The changes in brine inflow to repository waste regions have a direct impact on the brine saturations calculated for those areas. The overall means of waste panel brine saturation (quantity WAS_SATB) obtained in the PABC-2009 and the CRA-2014 PA are plotted together in Figure 6-22. The increase in cumulative waste panel brine inflow seen in the CRA-2014 PA yields a corresponding increase in the waste panel brine saturation. The refined water budget implementation results in brine being sequestered at early times as brucite is formed, yielding a mean waste panel brine saturation curve that is lower than that seen in the PABC-2009 prior to roughly 750 years. As brucite is transformed to hydromagnesite and then magnesite, water is released to the repository, yielding a mean waste panel brine saturation curve with an upward trend as compared to the PABC-2009 result. As seen in the results already discussed, increased mean cumulative brine inflows are seen in the CRA-2014 PA for the SRoR and the NRoR as compared to the PABC-2009, but the increases are less pronounced than those seen in the waste panel due to its lower elevation. For the SRoR and NRoR, the refined water budget implementation results in mean brine saturation curves that remain below those calculated in the PABC-2009 for the duration of the regulatory period. As the SRoR and NRoR together represent nine of the ten repository waste panels, the sequestration of brine in the refined water budget implementation yields a repository that tends to be drier overall for undisturbed

conditions as compared to the PABC-2009. CRA-2014 PA results obtained for the SRoR and NRoR are shown in Figure 6-23 and Figure 6-24.

The trend toward lower mean pressure in repository waste areas in the CRA-2014 PA yields a corresponding trend toward reduced mean porosity in those areas. The overall means of waste panel porosity (quantity WAS_POR) obtained in the PABC-2009 and the CRA-2014 PA are plotted together in Figure 6-25. The lower mean waste panel pressure seen in the CRA-2014 PA translates to a lower mean waste panel porosity when compared to the PABC-2009. Porosity results for the SRoR and NRoR waste regions are virtually identical to those obtained for the waste panel.

Summary statistics for BRAGFLO scenario S1-BF are shown in Table 6-2. Results presented in that table are calculated over all 300 vector realizations (and all times) of the PABC-2009 and the CRA-2014 PA.

Table 6-2: Summary Statistics for Scenario S1-BF

Quantity (units)	Description	Mean Value		Maximum Value	
		PABC-2009	CRA14-0	PABC-2009	CRA14-0
WAS_PRES (MPa)	Volume-averaged pressure in the waste panel.	6.52	3.44	16.19	15.73
SRR_PRES (MPa)	Volume-averaged pressure in the SRoR.	6.37	2.93	16.17	15.85
NRR_PRES (MPa)	Volume-averaged pressure in the NRoR.	6.21	2.66	16.12	15.71
EXP_PRES (MPa)	Volume-averaged pressure in the experimental area.	4.46	1.79	15.65	14.27
GASMOL_T (x10 ⁶ moles)	Total moles of gas generated in repository waste areas.	231.35	84.44	1345.67	878.83
FEMOL_T (x10 ⁶ moles)	Total moles of gas generated by iron corrosion in repository waste areas.	189.20	67.60	920.94	796.25
CELMOL_T (x10 ⁶ moles)	Total moles of gas generated by microbial degradation of CPRs in repository waste areas.	42.15	16.85	494.01	404.80
BRNWASIC (x10 ³ m ³)	Cumulative brine inflow to the waste panel.	1.78	2.80	12.46	16.40
BRNSRRIC (x10 ³ m ³)	Cumulative brine inflow to the SRoR.	4.82	5.26	37.78	49.73
BRNNRRIC (x10 ³ m ³)	Cumulative brine inflow to the NRoR.	6.04	6.18	48.02	39.27
BRNREPIC (x10 ³ m ³)	Cumulative brine inflow to the entire repository.	17.83	21.68	118.86	140.04
WAS_SATB (none)	Brine saturation in the waste panel.	0.160	0.209	0.985	0.991
SRR_SATB (none)	Brine saturation in the SRoR.	0.120	0.085	0.938	0.936
NRR_SATB (none)	Brine saturation in the NRoR.	0.121	0.077	0.937	0.720
BNSHUDRZ (m ³)	Cumulative brine flow up the repository shaft.	2.74	0.61	34.76	24.66
WAS_POR (none)	Porosity in the waste panel.	0.17	0.13	0.85	0.85

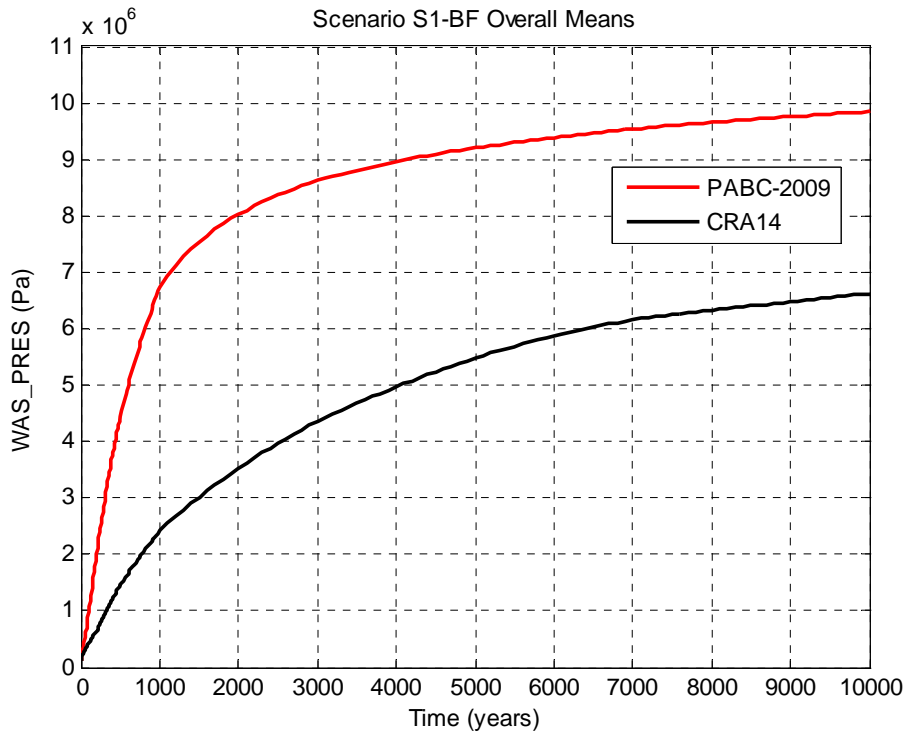


Figure 6-11: Overall Means of Waste Panel Pressure, Scenario S1-BF

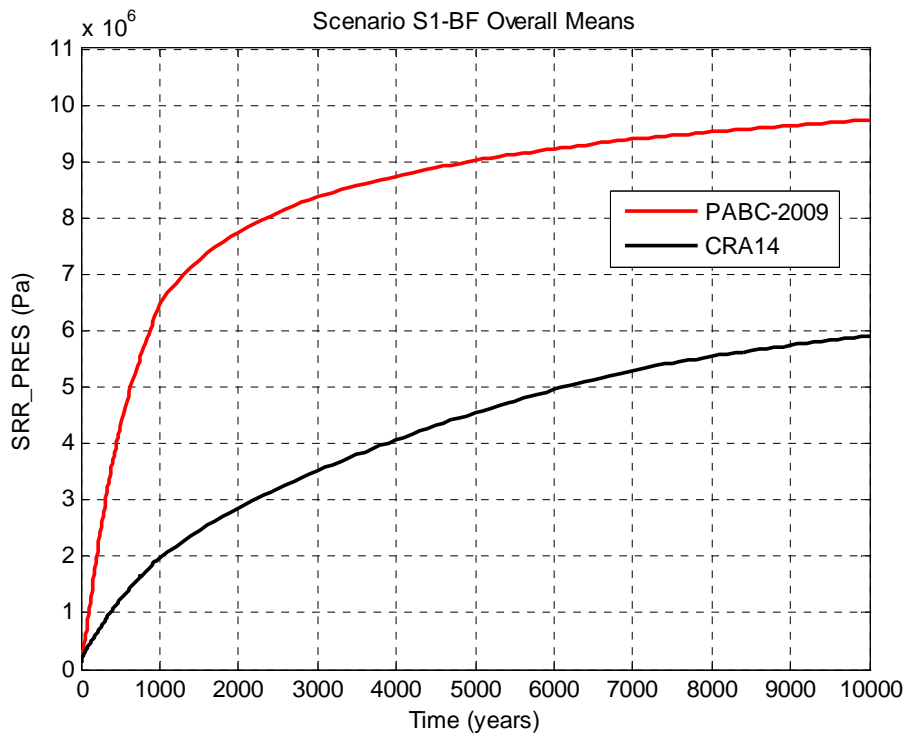


Figure 6-12: Overall Means of SRoR Pressure, Scenario S1-BF

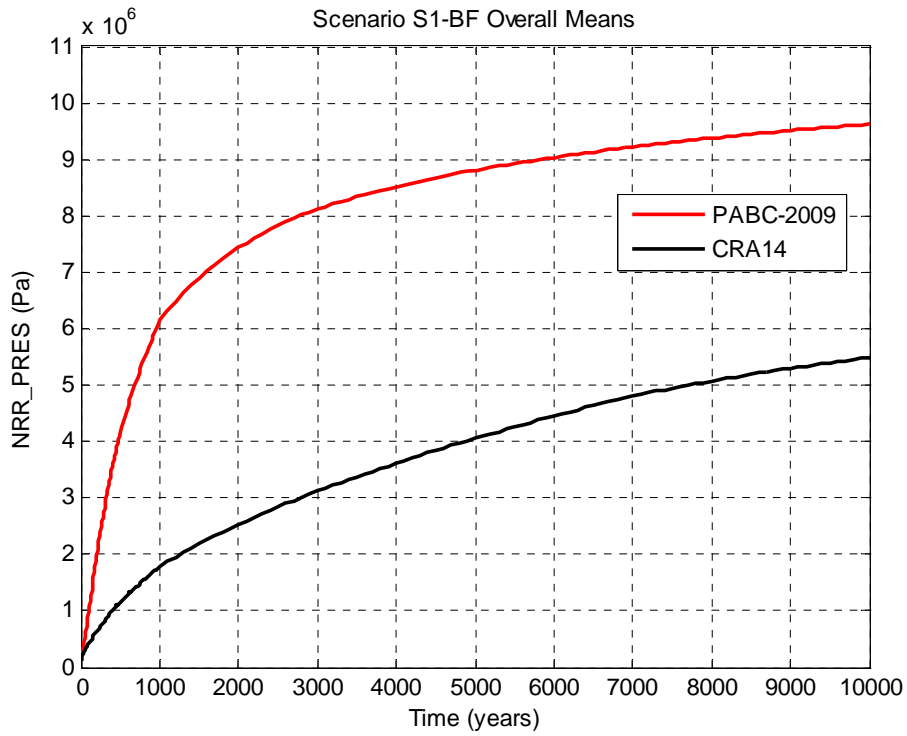


Figure 6-13: Overall Means of NRoR Pressure, Scenario S1-BF

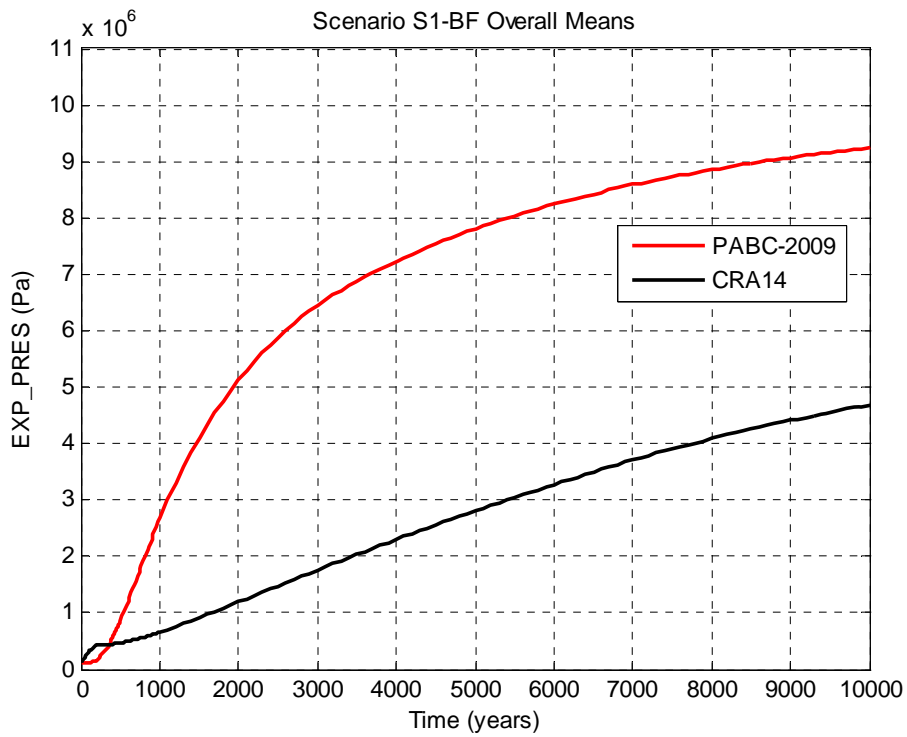


Figure 6-14: Overall Means of Experimental Region Pressure, Scenario S1-BF

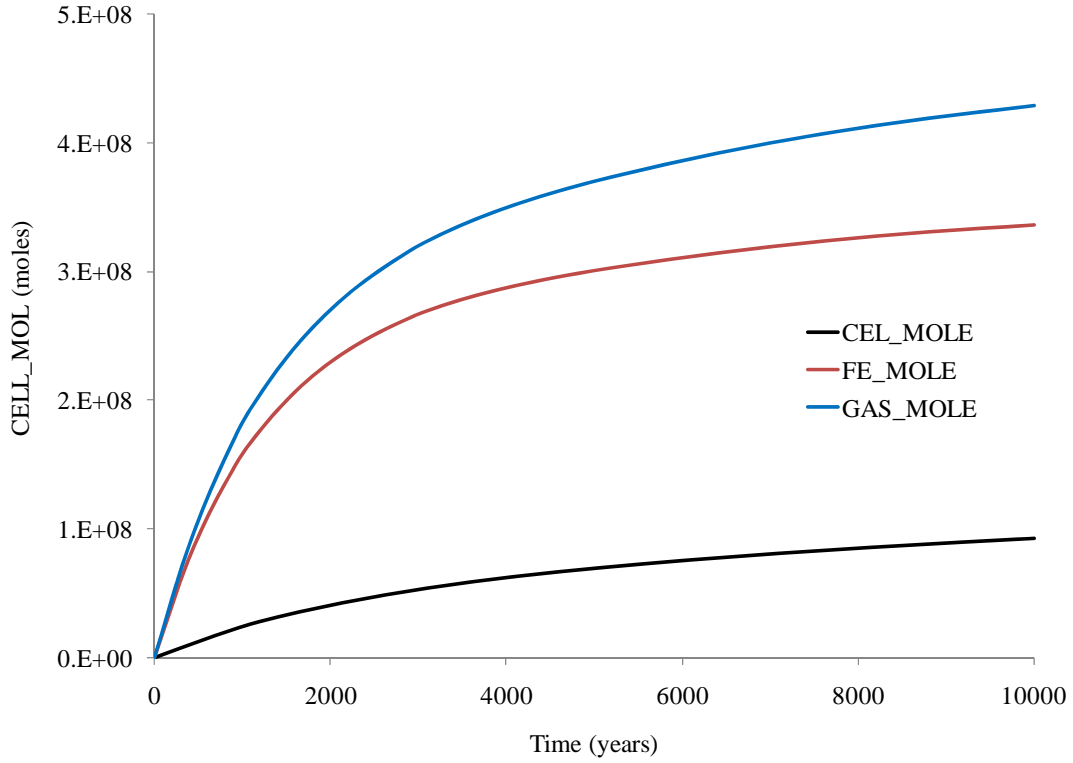


Figure 6-15: Replicate 1 Means of Molar Gas Generation, Scenario S1-BF of the PABC-2009.

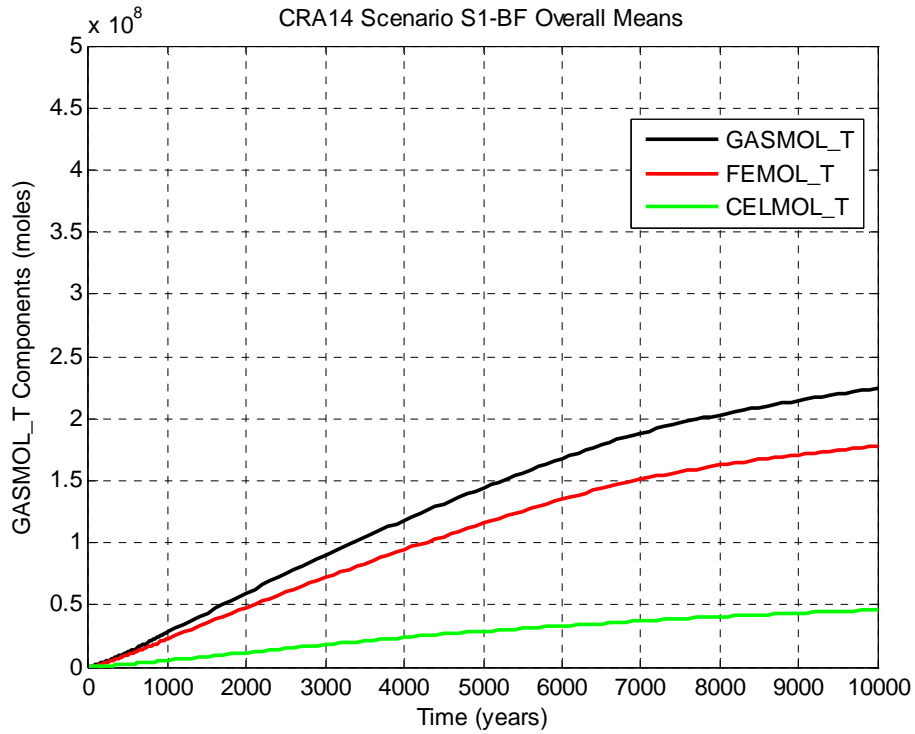


Figure 6-16: Overall Means of Molar Gas Generation, Scenario S1-BF of the CRA-2014 PA.

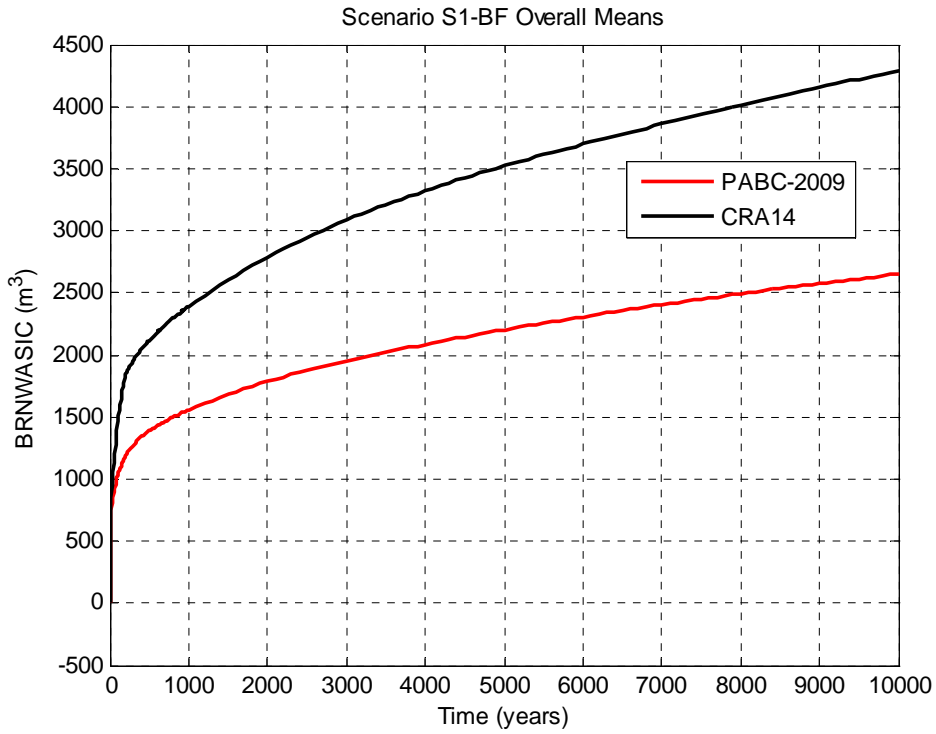


Figure 6-17: Overall Means of Cumulative Brine Inflow to the Waste Panel, Scenario S1-BF.

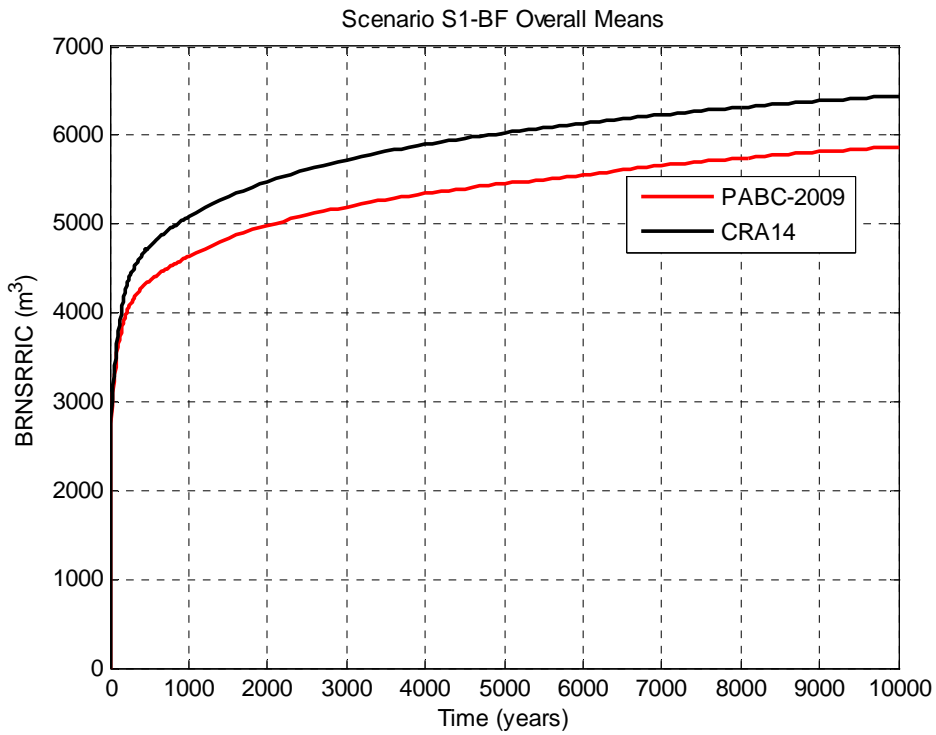


Figure 6-18: Overall Means of Cumulative Brine Inflow to the SRoR, Scenario S1-BF.

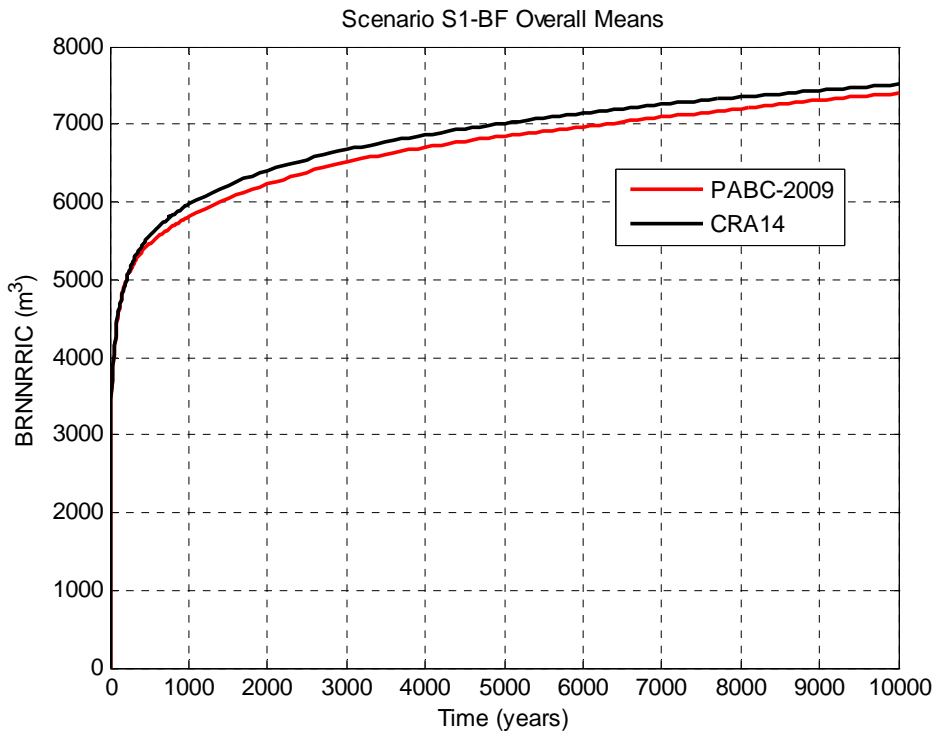


Figure 6-19: Overall Means of Cumulative Brine Inflow to the NRoR, Scenario S1-BF.

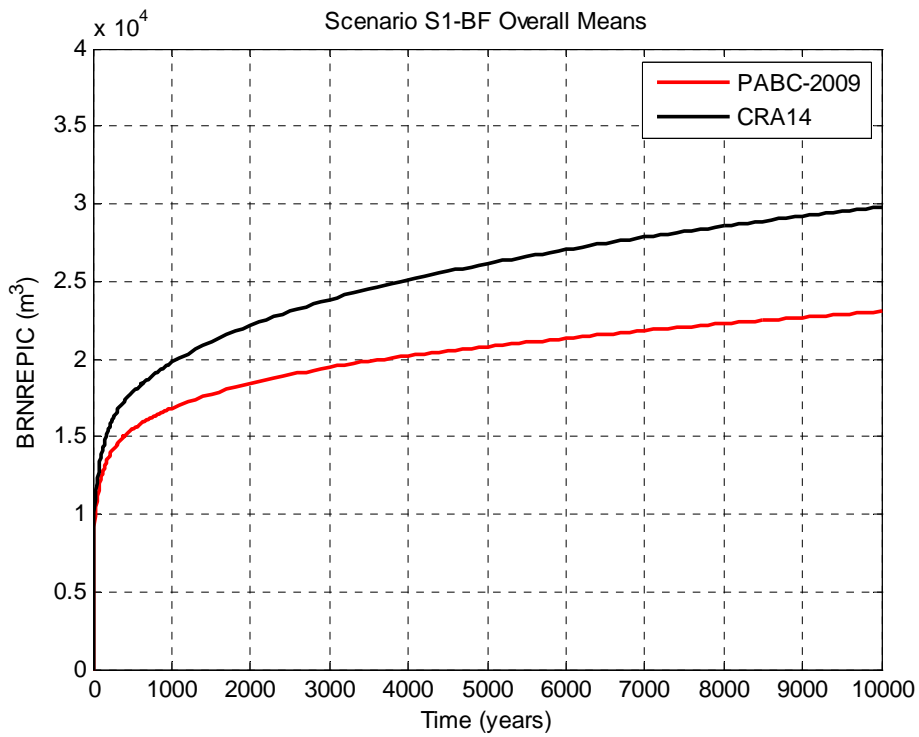


Figure 6-20: Overall Means of Cumulative Brine Inflow to the Repository, Scenario S1-BF.

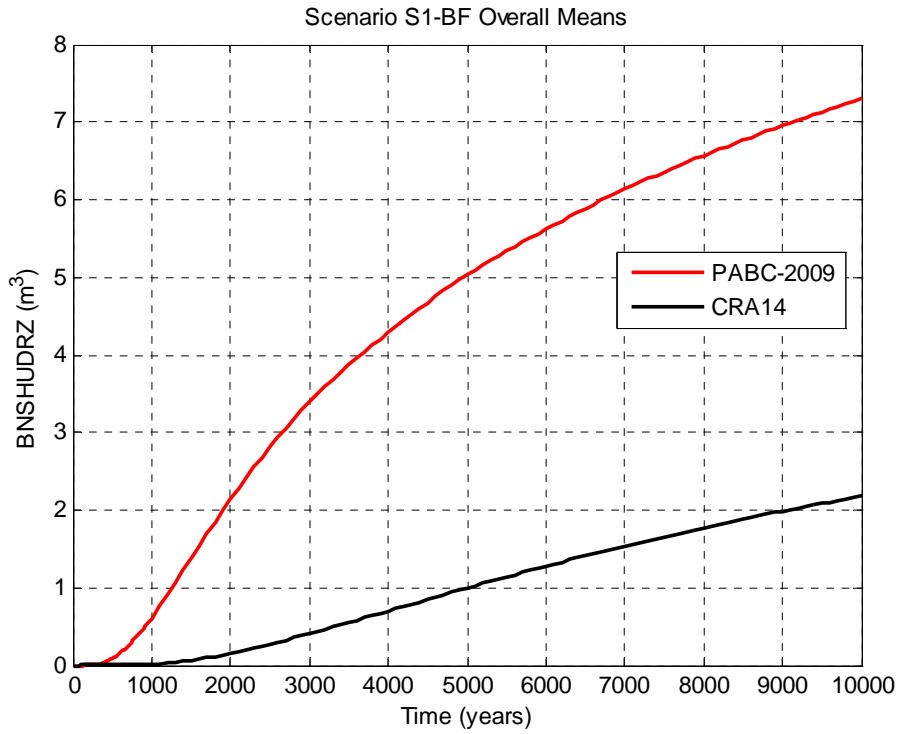


Figure 6-21: Overall Means of Brine Flow up the Shaft, Scenario S1-BF.

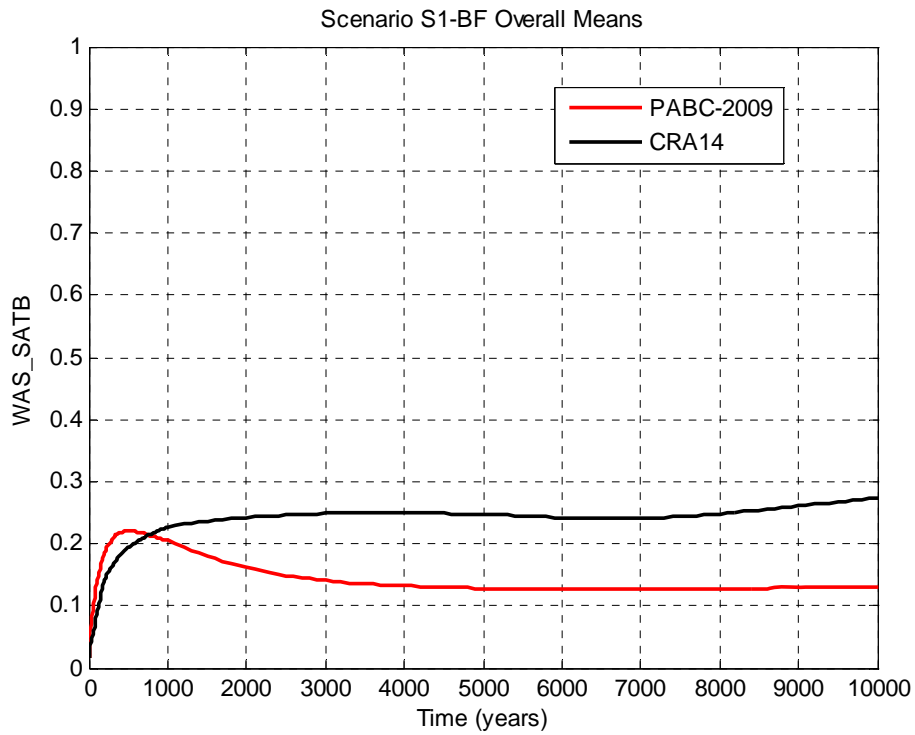


Figure 6-22: Overall Means of Waste Panel Brine Saturation, Scenario S1-BF.

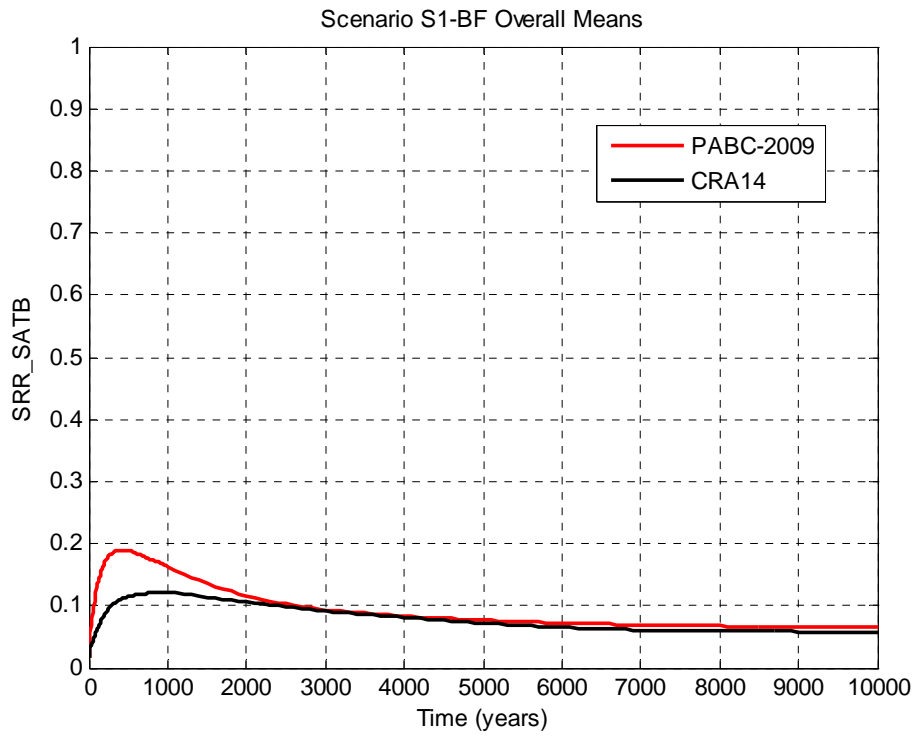


Figure 6-23: Overall Means of SRR Saturation, Scenario S1-BF.

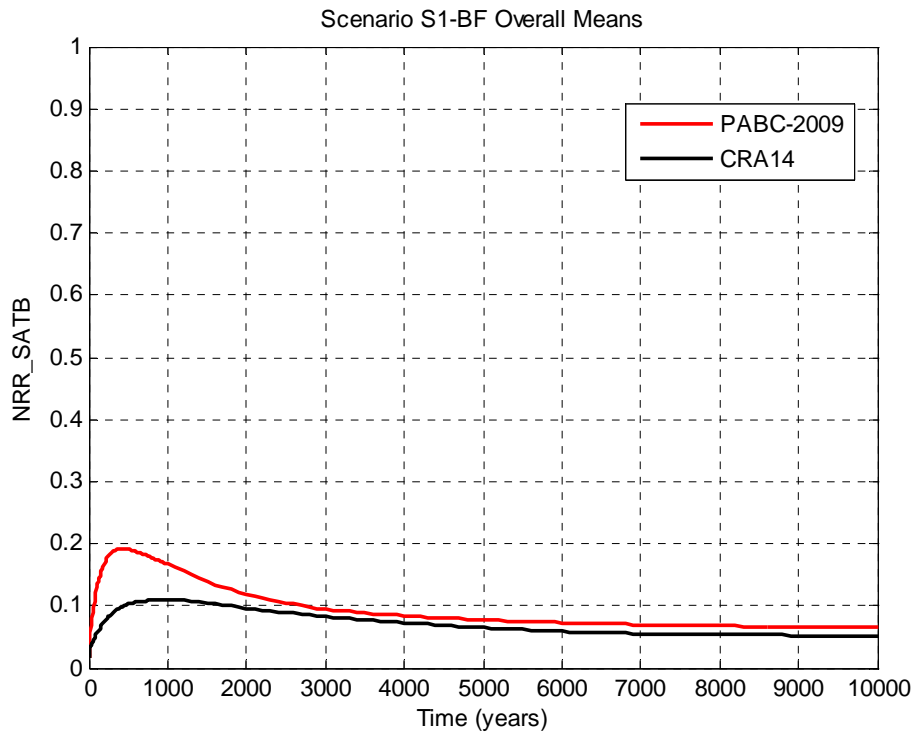


Figure 6-24: Overall Means of NRR Saturation, Scenario S1-BF.

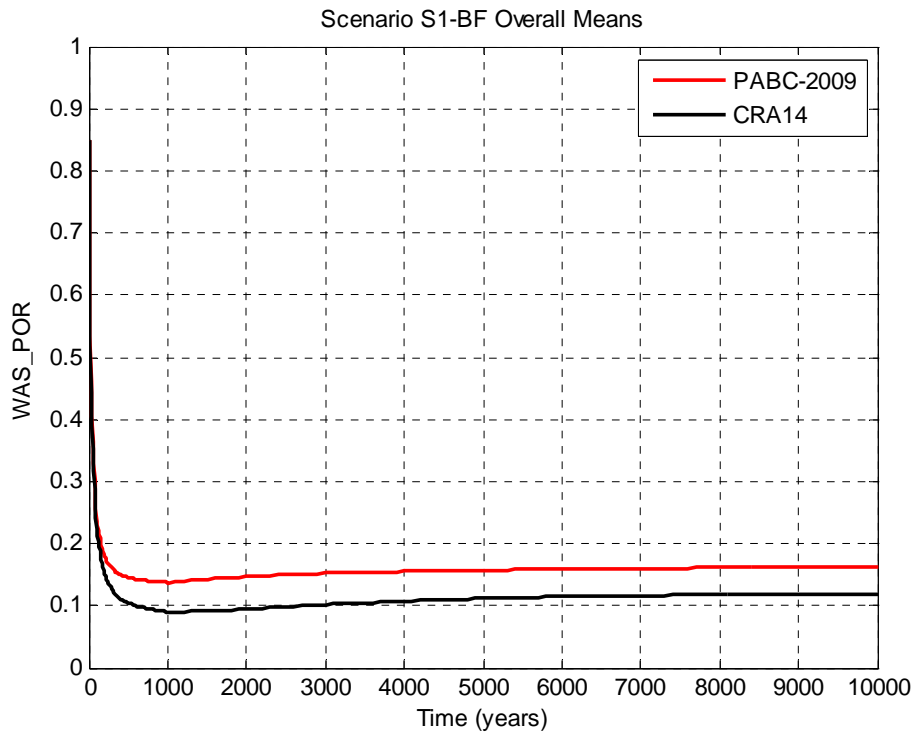


Figure 6-25: Overall Means of Waste Panel Porosity, Scenario S1-BF.

6.3.2 Results for an E1 Intrusion at 350 Years (Scenario S2-BF)

Results are now presented for disturbance scenario S2-BF. Results presented for this scenario are representative of those calculated for E1 intrusion scenarios (scenarios S2-BF and scenario S3-BF), with the only difference being the time of intrusion. In the results that follow, trends discussed for scenario S2-BF also apply to scenario S3-BF. Results presented in this section are limited to those calculated for the intruded waste panel. Quantities calculated for the SRoR, NRoR, and experimental repository regions in scenario S2-BF are very similar to those calculated and previously discussed for undisturbed conditions. Results presented in this section are more fully discussed in Camphouse (2013b).

The overall means of waste panel pressure obtained in the PABC-2009 and Case CRA14-0 are plotted together in Figure 6-26. As seen in that figure, the mean waste panel pressure obtained in the CRA-2014 PA remains higher than that seen in the PABC-2009 for a period of time after the intrusion, but eventually falls below the PABC-2009 result at roughly 6200 years. As discussed in Camphouse (2012c), the “tighter” ROMPCS design results in a period of increased waste panel pressurization after the intrusion as compared to the PABC-2009 results. As discussed in the previous section, the mean waste panel porosity is reduced for undisturbed conditions as compared to the PABC-2009 (see Figure 6-25). As a result, the mean waste panel porosity is lower in the CRA-2014 PA at 350 years when the E1 intrusion occurs, resulting in an additional pressure increase in the waste panel after it is connected to highly pressurized Castile brine during the intrusion. The eventual reduction in mean waste panel pressure is largely due to the revised iron corrosion rate implemented in the CRA-2014 PA. Mean molar gas production due to iron corrosion occurs at a lower rate in the CRA-2014 PA. The reduction (on average) in the

rate of gas production due to iron corrosion yields a corresponding decrease in the rate of mean gas generation in the waste panel after the intrusion, and a corresponding eventual reduction in the mean waste panel pressure (Camhouse 2013b).

The overall means of cumulative brine inflow to the waste panel (quantity BRNWASIC) obtained in the CRA-2014 PA and the PABC-2009 for scenario S2-BF are plotted together in Figure 6-27. Mean waste panel pressure is significantly reduced in the CRA-2014 PA as compared to the PABC-2009 for the undisturbed repository (Figure 6-11). This pressure reduction allows increased brine flow to the waste panel prior to the E1 intrusion at 350 years, as well as increased brine inflow to the panel at the time of intrusion. The result is an overall mean curve for quantity BRNWASIC in the CRA-2014 PA that is greater than that obtained in the PABC-2009. Trends observed for the waste panel also hold for the repository overall. Increased brine inflow to the intruded panel yields an increase in brine inflow to the repository overall for scenario S2-BF in the CRA-2014 PA (Figure 6-28). The increased brine inflow to the waste panel in the CRA-2014 PA, combined with the increase in mean waste panel pressure for a period of time after the intrusion, yields an increase in the overall mean obtained for cumulative brine flow up the intrusion borehole (quantity BNBHUDRZ). Overall means obtained for quantity BNBHUDRZ in the CRA-2014 PA and the PABC-2009 are plotted together in Figure 6-29.

The increased brine inflow to the waste panel in the CRA-2014 PA has a direct impact on waste panel brine saturation. The increased mean waste panel brine inflow seen in the CRA-2014 PA translates to a corresponding increase in the mean waste panel brine saturation following the E1 intrusion (Figure 6-30).

Summary statistics for BRAGFLO scenario S2-BF are shown in Table 6-3. Results presented in that table are calculated over all 300 vector realizations (and all times) of the PABC-2009 and the CRA-2014 PA.

Table 6-3: Summary Statistics for Scenario S2-BF

Quantity (units)	Description	Mean Value		Maximum Value	
		PABC-2009	CRA14-0	PABC-2009	CRA14-0
WAS_PRES (MPa)	Volume-averaged pressure in the waste panel.	7.39	7.36	15.63	16.15
GASMOL_W (x10 ⁶ moles)	Total moles of gas generated in the intruded panel.	54.75	36.66	149.00	92.54
BRNWASIC (x10 ³ m ³)	Cumulative brine inflow to the waste panel.	14.03	16.11	182.15	187.90
BRNREPIC (x10 ³ m ³)	Cumulative brine inflow to the entire repository.	30.26	35.25	204.98	213.42
WAS_SATB (none)	Brine saturation in the waste panel.	0.68	0.73	0.99	0.99
BNBHUDRZ (x10 ³ m ³)	Cumulative brine flow up the intrusion borehole.	3.25	3.62	166.84	173.21

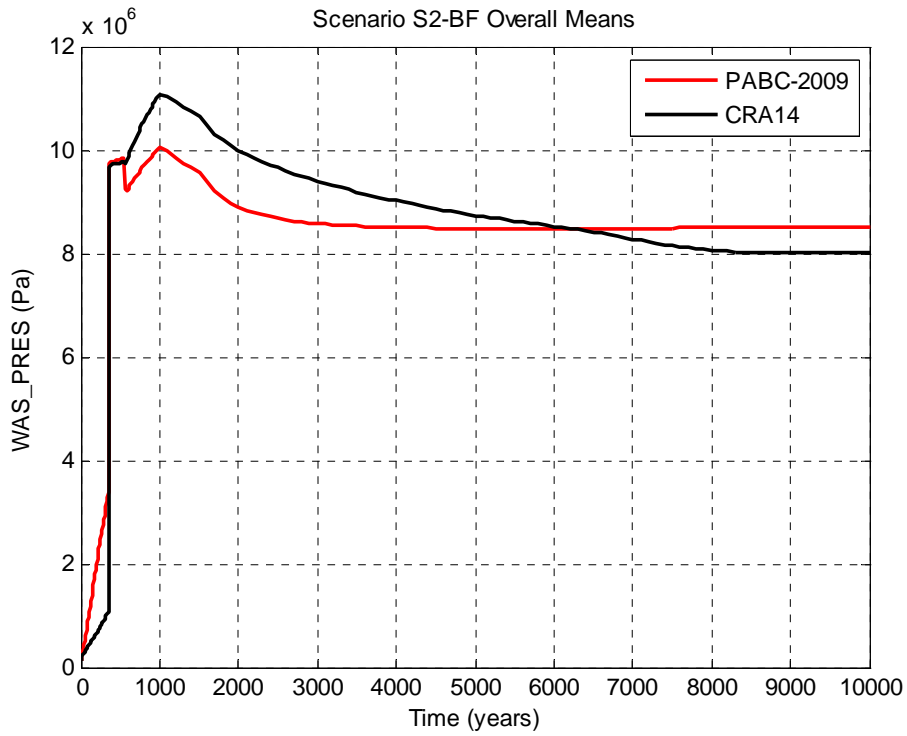


Figure 6-26: Overall Means of Waste Panel Pressure, Scenario S2-BF

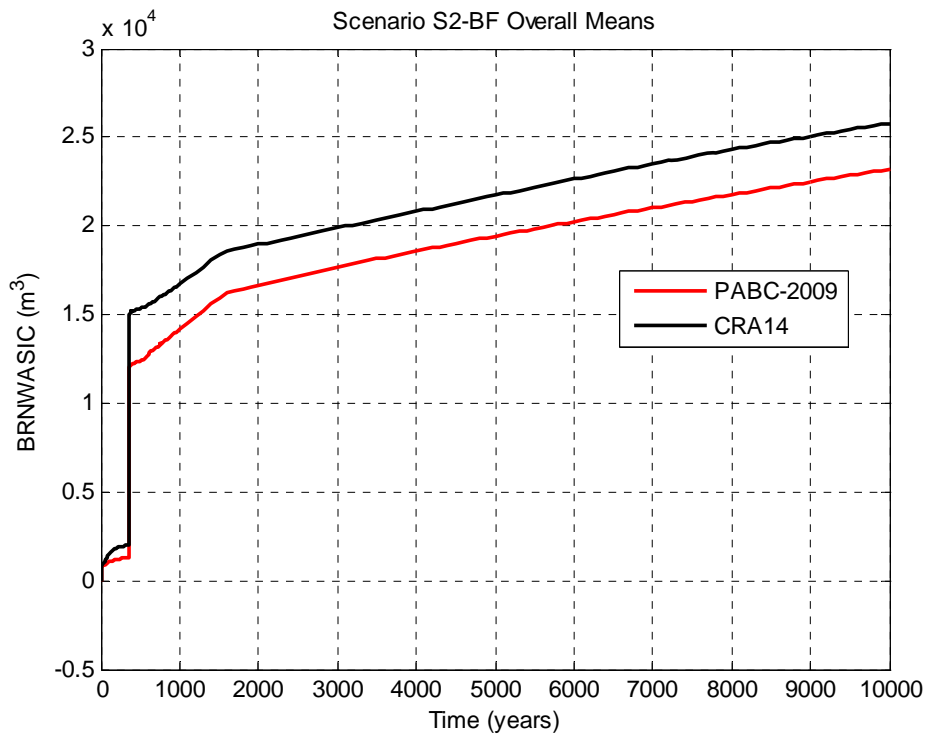


Figure 6-27: Overall Means of Cumulative Brine Inflow to the Waste Panel, Scenario S2-BF.

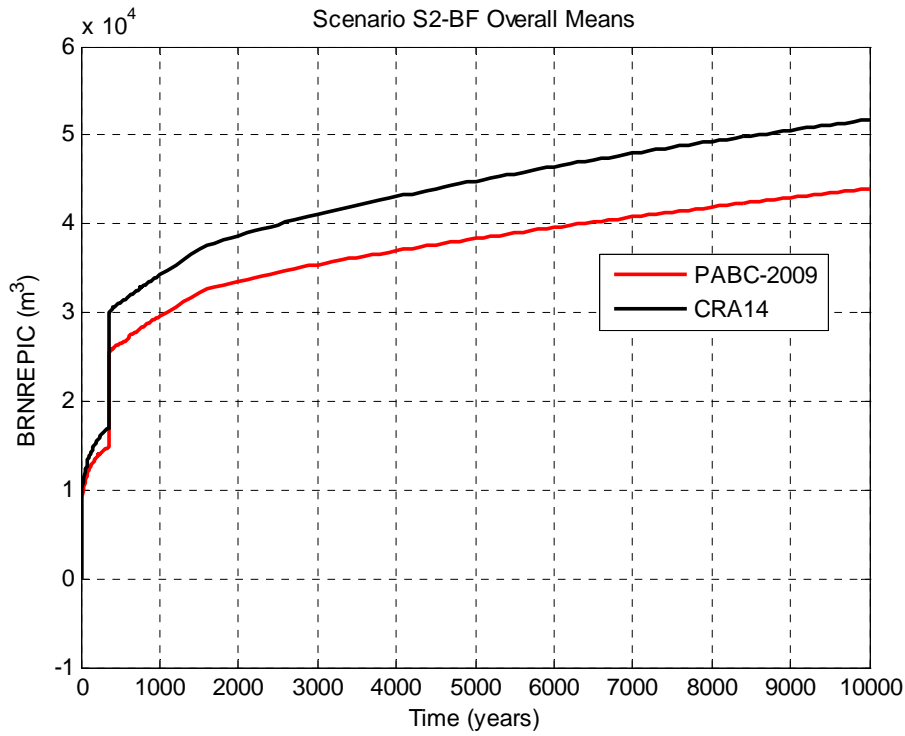


Figure 6-28: Overall Means of Cumulative Brine Inflow to the Repository, Scenario S2-BF.

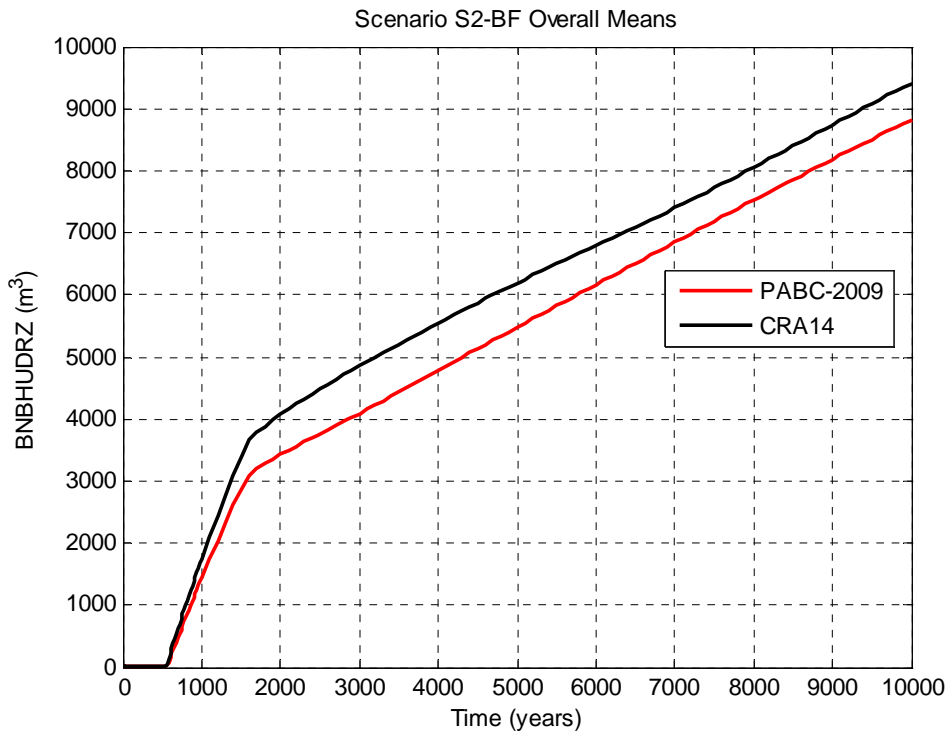


Figure 6-29: Overall Means of Brine Flow up the Borehole, Scenario S2-BF.

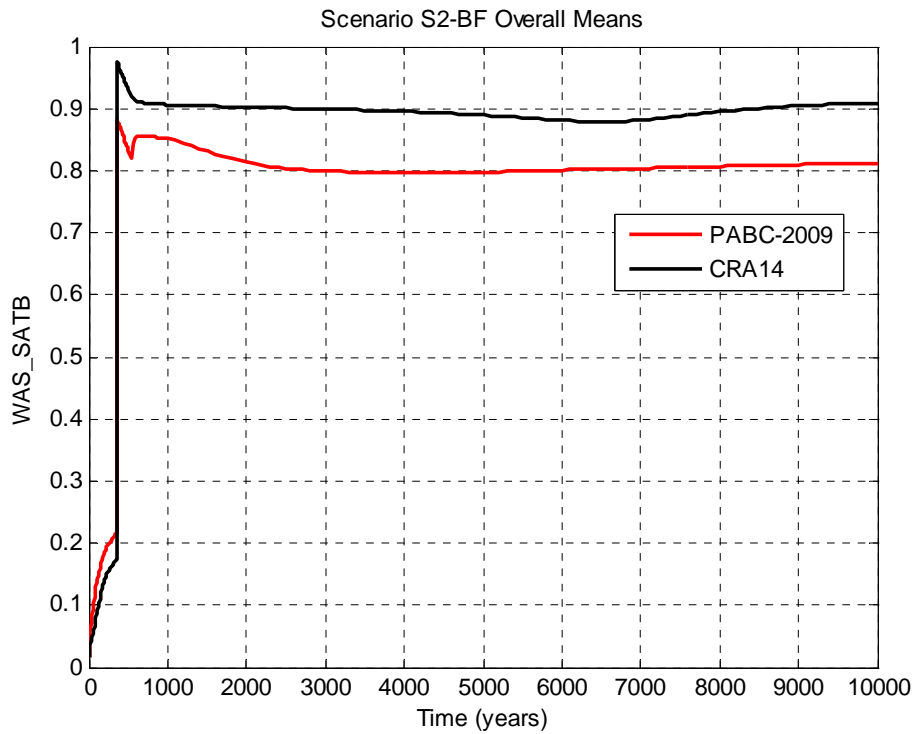


Figure 6-30: Overall Means of Waste Panel Brine Saturation, Scenario S2-BF.

6.3.3 Results for an E2 Intrusion at 350 Years (Scenario S4-BF)

Results are now presented for disturbance scenario S4-BF. Results presented for this scenario are representative of those calculated for E2 intrusion scenarios (scenarios S4-BF and scenario S5-BF), with the only difference being the time of intrusion. In the results that follow, trends discussed for scenario S4-BF also apply to scenario S5-BF. Results presented in this section are limited to those calculated for the intruded waste panel. Quantities calculated for the SRoR, NRoR, and experimental repository regions in scenario S4-BF are very similar to those calculated and previously discussed for undisturbed conditions. Results presented in this section are more fully discussed in Camphouse (2013b).

The overall means of waste panel pressure obtained in the PABC-2009 and the CRA-2014 PA for scenario S4-BF are plotted together in Figure 6-31. As already discussed, the overall mean waste panel pressure is reduced in the CRA-2014 PA for undisturbed conditions as compared to the PABC-2009. Consequently, at the time of the E2 intrusion, the mean waste panel pressure is lower in the CRA-2014 PA than in the PABC-2009, and is also lower 200 years later when the borehole plugs fail. The result is a lower scenario S4-BF mean pressure curve in the CRA-2014 PA than was seen in the PABC-2009. As was the case for the undisturbed results, the reduction in mean waste panel pressure in the CRA-2014 PA is largely due to the revised iron corrosion rate. Mean molar gas production due to iron corrosion occurs at a lower rate in the CRA-2014 PA. The reduction (on average) in the rate of gas production due to iron corrosion yields a corresponding decrease in the rate of mean gas generation in the waste panel, translating to a reduction in mean waste panel pressure (Camphouse 2013b).

The reduction in mean waste panel pressure seen in the CRA-2014 PA allows for increased brine flow to the waste panel prior to the E2 intrusion at 350 years, as well as increased brine inflow to the panel after the borehole plugs fail at 550 years. The result is an overall mean curve for quantity BRNWASIC in the CRA-2014 PA that is greater than that obtained in the PABC-2009 (Figure 6-32). Trends observed for the waste panel also hold for the repository overall. Increased brine inflow to the intruded panel yields an increase to brine inflow to the repository overall for scenario S4-BF. Results for cumulative brine inflow to the repository, quantity BRNREPIC, are shown in Figure 6-33. The mean cumulative brine flow up the intrusion borehole is slightly increased in the CRA-2014 PA scenario S4-BF results (Figure 6-34). This increase is most likely due to the increased brine volume in the waste panel following the E2 intrusion in the CRA-2014 PA.

The increased brine inflow to the waste panel in the CRA-2014 PA has a direct impact on waste panel brine saturation. The increased brine inflow yields a corresponding increase in the CRA-2014 PA mean waste panel brine saturation following the failure of the borehole plugs at 550 years (Figure 6-35).

Summary statistics for BRAGFLO scenario S4-BF are shown in Table 6-4. Results presented in that table are calculated over all 300 vector realizations (and all times) of the PABC-2009 and the CRA-2014 PA.

Table 6-4: Summary Statistics for Scenario S4-BF

Quantity (units)	Description	Mean Value		Maximum Value	
		PABC-2009	CRA14-0	PABC-2009	CRA14-0
WAS_PRES (MPa)	Volume-averaged pressure in the waste panel.	4.64	2.86	14.92	14.85
GASMOL_W (x10 ⁶ moles)	Total moles of gas generated in the intruded panel.	36.40	21.58	149.00	92.54
BRNWASIC (x10 ³ m ³)	Cumulative brine inflow to the waste panel.	2.73	3.81	23.81	21.04
BRNREPIC (x10 ³ m ³)	Cumulative brine inflow to the entire repository.	19.11	22.79	117.40	139.90
WAS_SATB (none)	Brine saturation in the waste panel.	0.28	0.33	0.99	0.99
BNBHURZ (m ³)	Cumulative brine flow up the intrusion borehole.	34.76	52.36	4876.89	5390.83

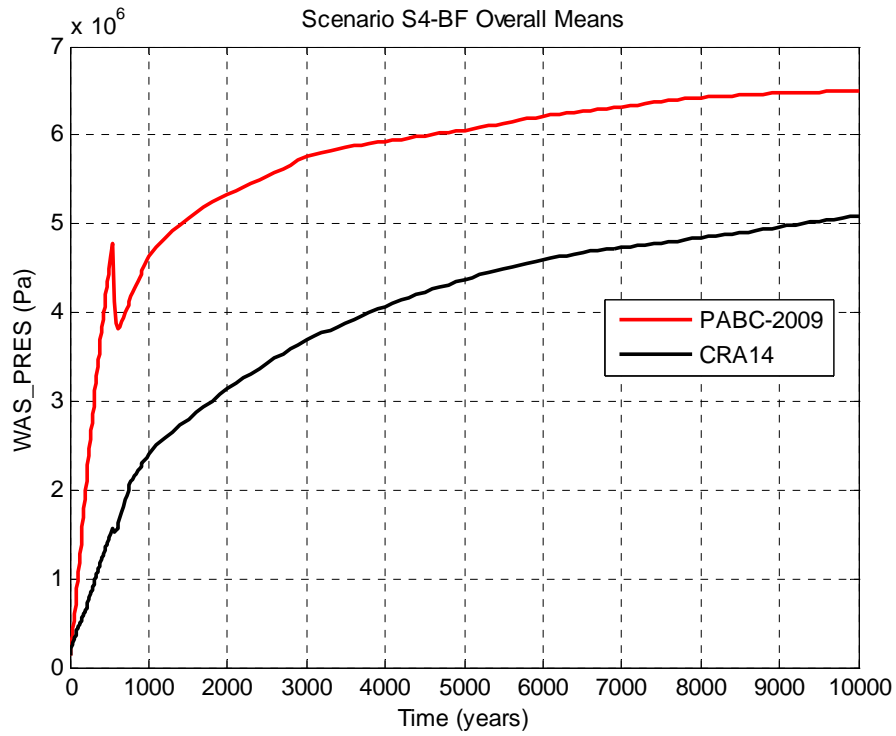


Figure 6-31: Overall Means of Waste Panel Pressure, Scenario S4-BF

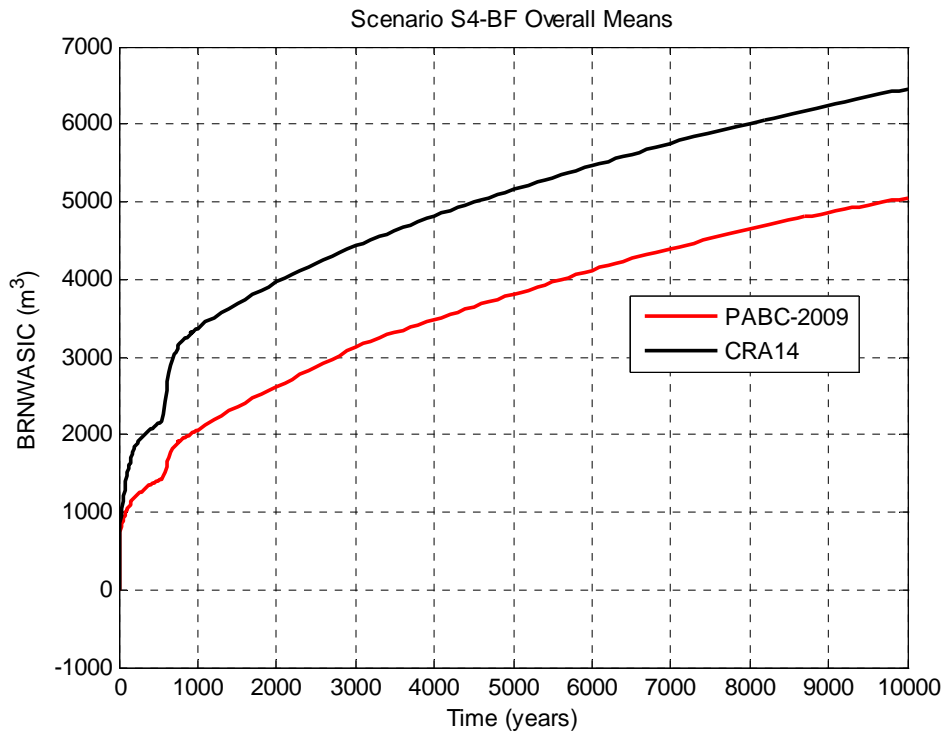


Figure 6-32: Overall Means of Cumulative Brine Inflow to the Waste Panel, Scenario S4-BF.

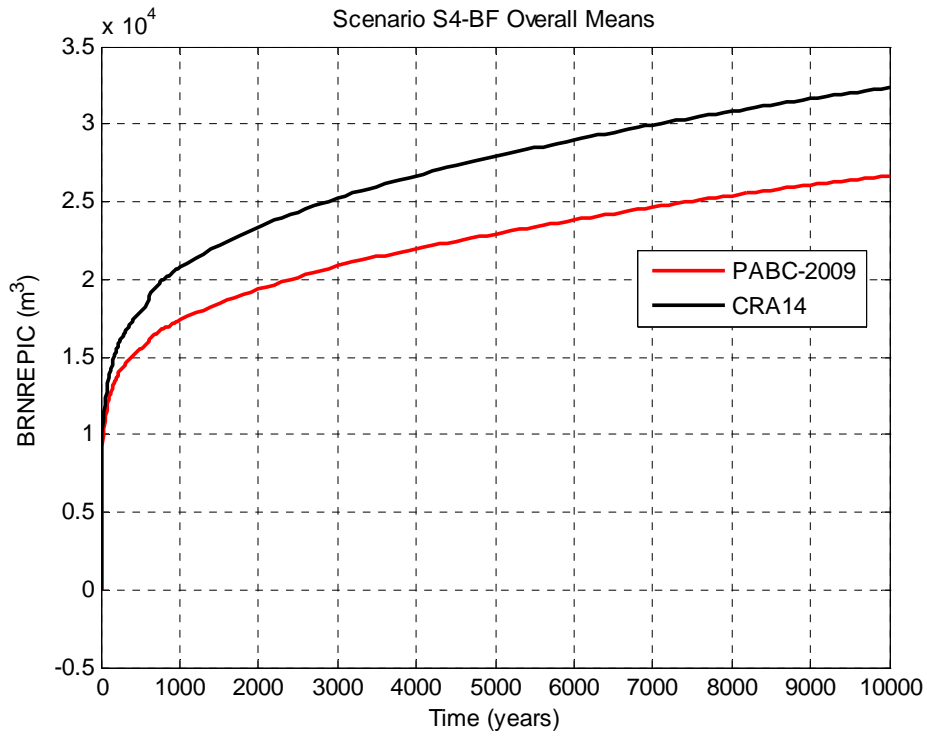


Figure 6-33: Overall Means of Cumulative Brine Inflow to the Repository, Scenario S4-BF.

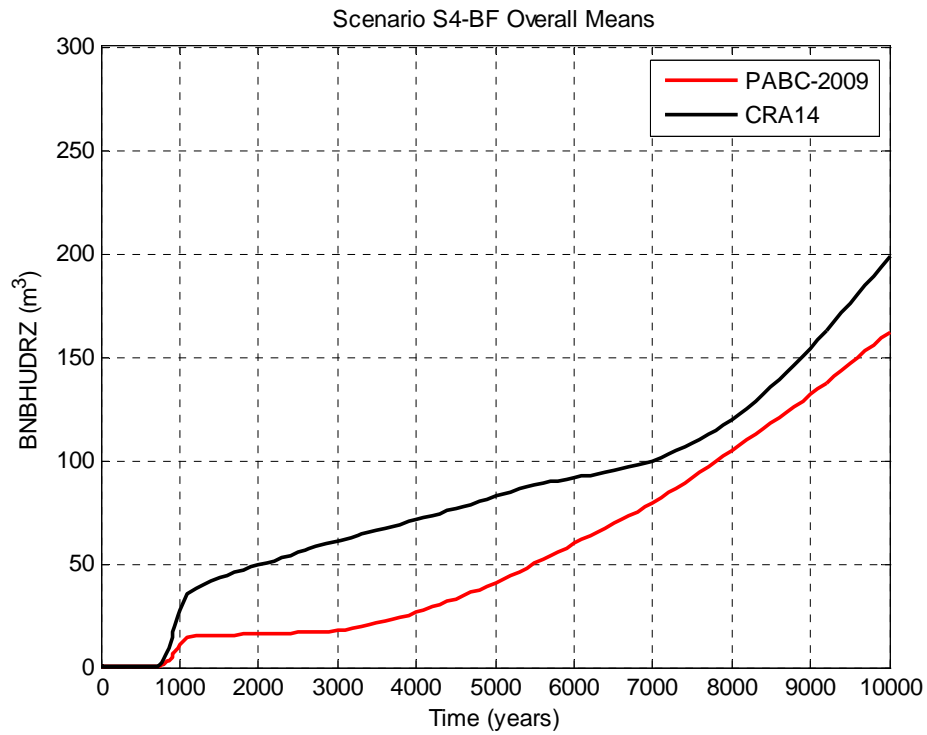


Figure 6-34: Overall Means of Brine Flow up the Borehole, Scenario S4-BF.

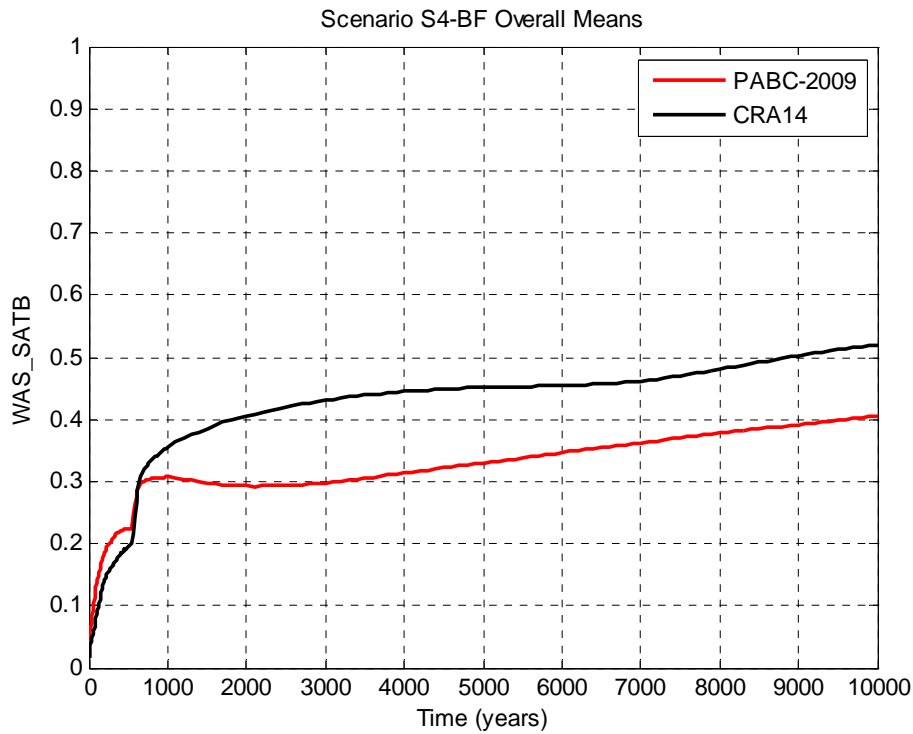


Figure 6-35: Overall Means of Waste Panel Brine Saturation, Scenario S4-BF.

6.3.4 Results for an E2 Intrusion at 1000 Years Followed by a E1 Intrusion at 2000 Years (Scenario S6-BF)

BRAGFLO scenario S6-BF models an E2 intrusion occurring at 1000 years, followed by an E1 intrusion into the same panel at 2000 years. Calculated brine flows up the intrusion borehole obtained in scenario S6-BF are used in PA code PANEL to determine the radionuclide source term to the Culebra. The overall mean of cumulative brine flow up the intrusion borehole is increased in the CRA-2014 PA as compared to the PABC-2009 (Figure 6-36), with the increase similar to that seen for the E1 intrusion results (Figure 6-29).

Summary statistics for quantity BNBHUDRZ obtained in scenario S6-BF are shown in Table 6-5. Results presented in that table are calculated over all 300 vector realizations (and all times) of the PABC-2009 and the CRA-2014 PA.

Table 6-5: Summary Statistics for Scenario S6-BF

Quantity (units)	Description	Mean Value		Maximum Value	
		PABC-2009	CRA14-0	PABC-2009	CRA14-0
BNBHUDRZ (x 10 ³ m ³)	Cumulative brine flow up the intrusion borehole.	2.92	3.10	169.03	173.36

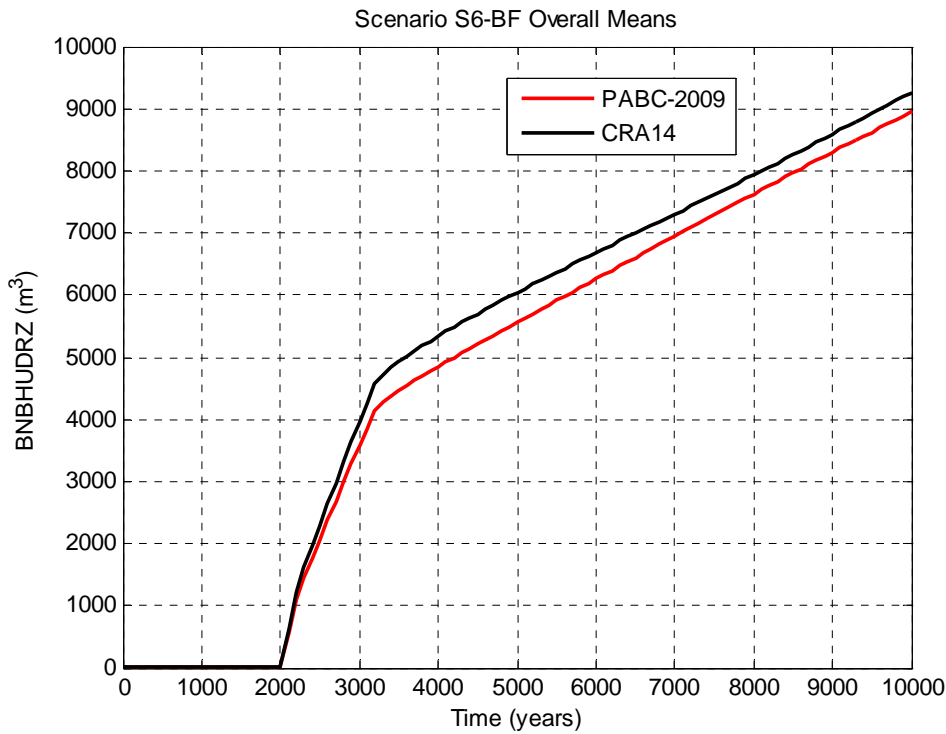


Figure 6-36: Overall Means of Brine Flow up the Borehole, Scenario S6-BF.

6.4 Radionuclide Transport Results

Radionuclide transport results obtained in the CRA-2014 PA are now summarized. Radionuclide transport in the Salado is calculated by the code NUTS. Radionuclide transport from the Salado to the Culebra is calculated by codes NUTS and PANEL. Radionuclide transport through the Culebra is calculated using code SECOTP2D. None of the changes incorporated in the CRA-2014 PA impact SECOTP2D results obtained in the PABC-2009, and so SECOTP2D results obtained in the PABC-2009 are also used in the CRA-2014 PA. Culebra flow and transport results obtained in the PABC-2009 are fully discussed in Kuhlman (2010). The total release of radionuclides across the LWB at the Culebra for given futures is calculated with the code CCDFGF by convolving SECOTP2D results with results calculated by NUTS and PANEL for radionuclide transport to the Culebra. Radionuclide transport results obtained with codes NUTS and PANEL in the CRA-2014 PA are fully discussed in Kim (2013b).

Flow field results obtained with BRAGFLO for scenarios S1-BF to S6-BF (see Table 6-1) are used as inputs to the calculation of radionuclide transport. There are no vectors in the CRA-2014 PA that result in transport releases at the shaft-Culebra interface in any scenario. Similarly, there are no vectors that result in radionuclide transport through the markerbeds and across the LWB in any scenario.

Radionuclide transport to the Culebra via a single intrusion borehole (disturbance scenarios S2-BF, S3-BF, S4-BF, and S5-BF) is modeled with the code NUTS. Transport to the Culebra in the multiple intrusion scenario (S6-BF) is modeled with the code PANEL. Figure 6-37 to Figure 6-41 show cumulative radioactivity transported up the borehole to the Culebra for the intrusion

scenarios modeled with BRAGFLO. Transport to the Culebra is larger and occurs for more vectors in the S2-BF, S3-BF and S6-BF scenarios (with E1 intrusions) than in the S4-BF or S5-BF scenarios (E2 intrusions only). Most transport to the Culebra occurs over a relatively short period of time immediately after the borehole intrusion. For the multiple intrusion scenario (S6-BF), only 5 vectors show radionuclide transport resulting from the E2 intrusion at 1,000 years; most radionuclide transport occurs immediately after the E1 intrusion at 2,000 years.

Radionuclide transport releases to the Culebra obtained in the CRA-2014 PA exhibit larger maximum and average values than were obtained in the PABC-2009 (Kim 2013b). As seen in the Salado flow results of Section 6.3, brine flows up the intrusion borehole are larger (on average) in the CRA-2014 PA than in the PABC-2009. Only the baseline radionuclide solubilities corresponding to the minimum brine volume necessary for a DBR are used in the CRA-2014 PA Salado transport calculation to keep the computational expense associated with NUTS calculations at a feasible level. Baseline solubilities corresponding to this volume of brine in the PABC-2009 and the CRA-2014 PA are similar. However, the mean and maximum values of the solubility uncertainty distribution for +IV actinides increased in the CRA-2014 PA. This, combined with the overall trend toward increased brine flow up the intrusion borehole, results in a trend toward increased radionuclide transport releases to the Culebra for CRA-2014 PA disturbance scenarios.

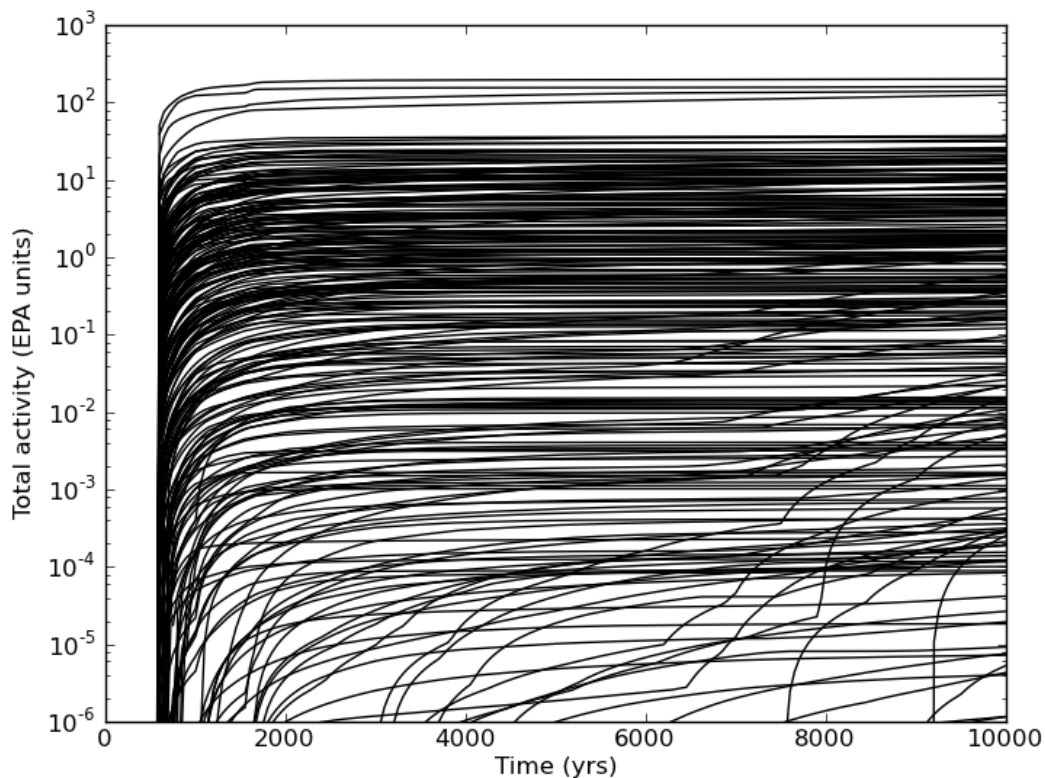


Figure 6-37: CRA-2014 PA Cumulative Transport Release to the Culebra, Scenario S2-BF.

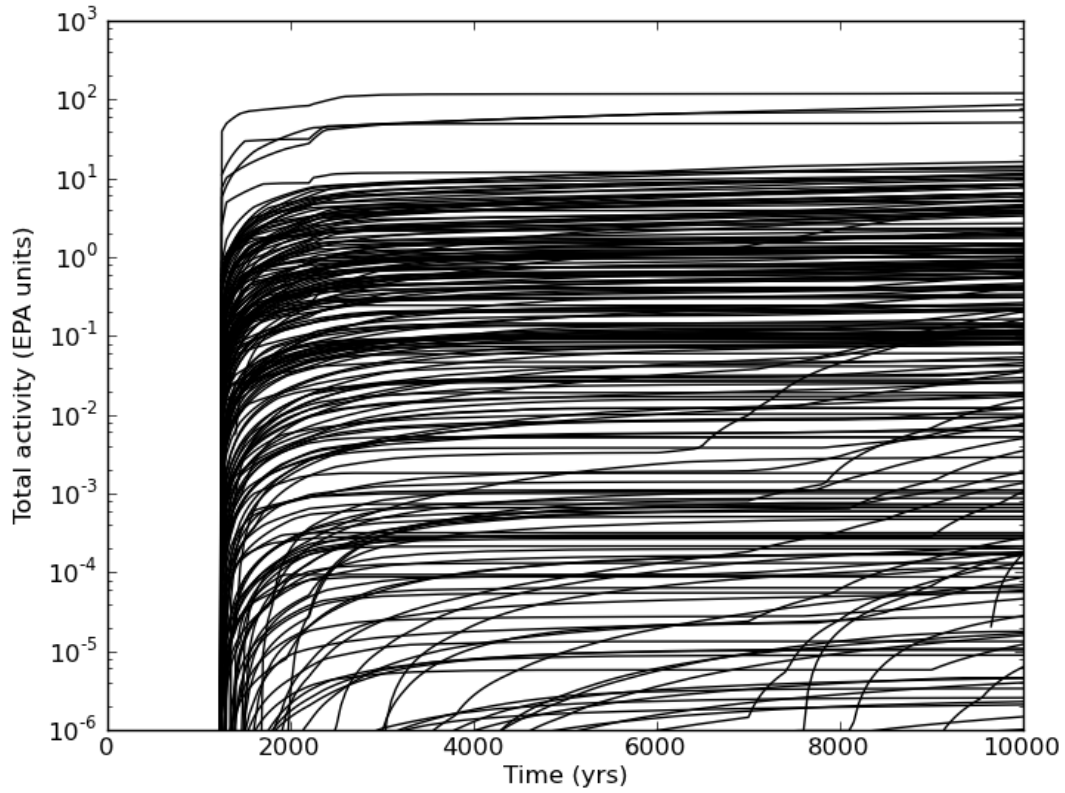


Figure 6-38: CRA-2014 PA Cumulative Transport Release to the Culebra, Scenario S3-BF.

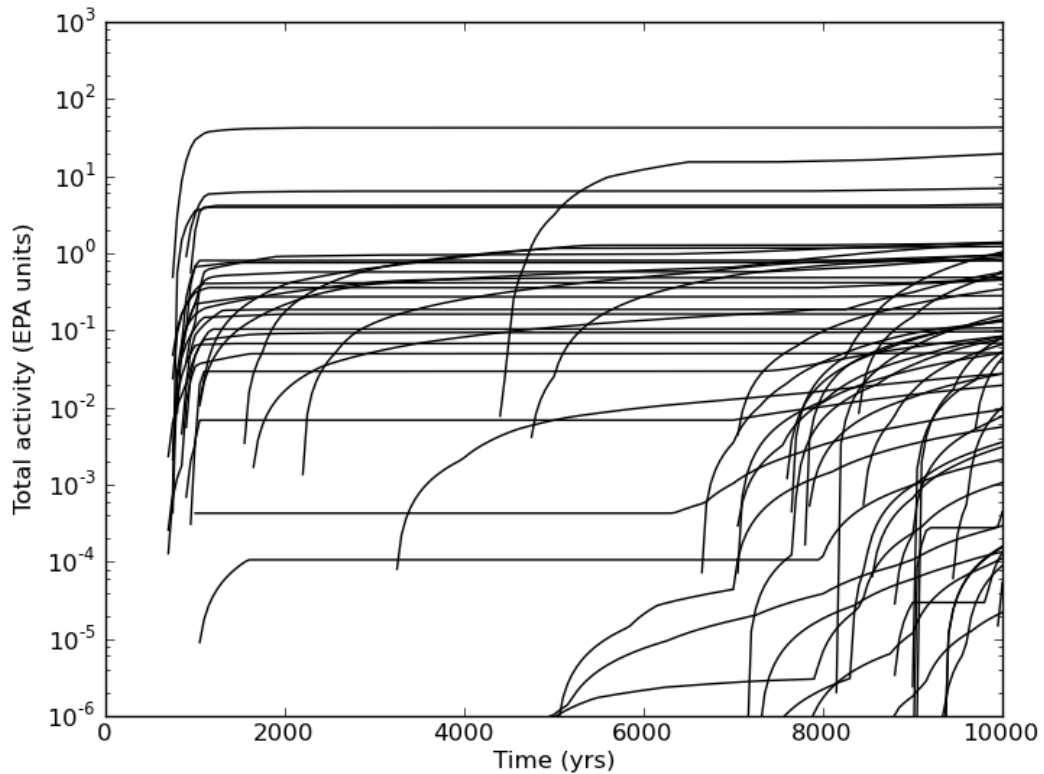


Figure 6-39: CRA-2014 PA Cumulative Transport Release to the Culebra, Scenario S4-BF.

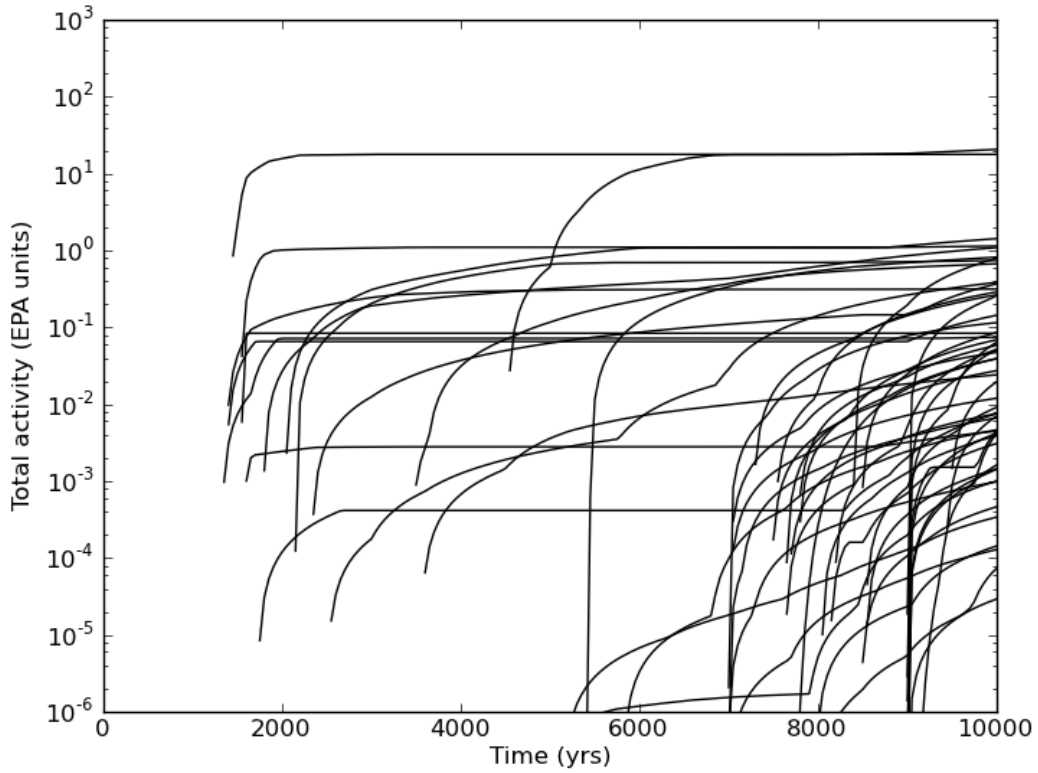


Figure 6-40: CRA-2014 PA Cumulative Transport Release to the Culebra, Scenario S5-BF.

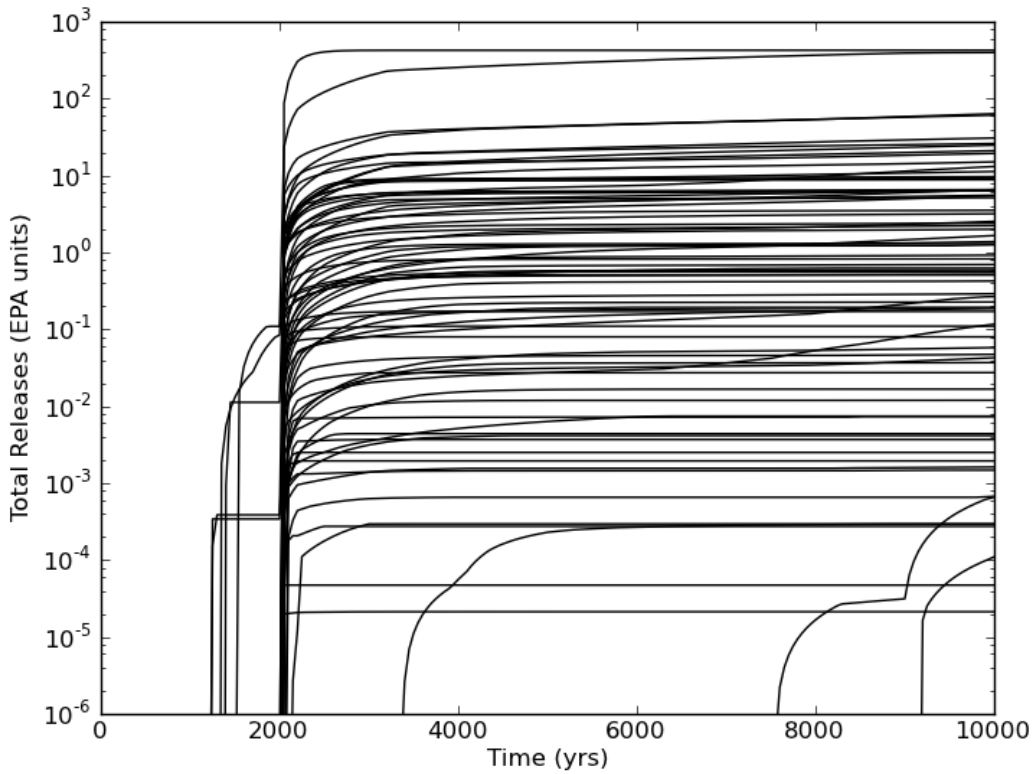


Figure 6-41: CRA-2014 PA Cumulative Transport Release to the Culebra, Scenario S6-BF.

6.5 Direct Brine Release Results

DBRs refer to flow of contaminated brine, from the repository, to the land surface through an intrusion borehole during the period of drilling. In order for a DBR to occur, two criteria must be satisfied (Stoelzel and O'Brien 1996), namely

1. Brine pressure in the repository in the vicinity of the intrusion must exceed the drilling fluid hydrostatic pressure (estimated to be 8 MPa).
2. Brine saturation in the repository must exceed the residual brine saturation of the waste material. The residual brine saturation is sampled from a uniform distribution ranging from 0.0 to 0.552.

Both of these conditions being satisfied results in a DBR for a given drilling intrusion. If one (or both) of these conditions is not satisfied for a given drilling intrusion, then no DBR occurs.

PA code BRAGFLO is used in two ways in WIPP PA calculations. First, it is used to calculate the flow of brine and gas in and around the repository for undisturbed and disturbed conditions. CRA-2014 PA results from this application of BRAGFLO are shown in Section 6.3. Second, it is used in the calculation of DBRs. These two uses of BRAGFLO require different computational grids. Results obtained from the brine and gas flow calculation are used to initialize conditions in the DBR calculation. The representation of the waste area by three regions in the CRA-2014 PA and the PABC-2009 BRAGFLO grids (see Figure 6-9 and Figure 6-10) yields initial conditions to waste regions comprising the Waste Panel (panel 5), the South Rest of Repository or SROR (panels 3,4,6, and 9), and the North Rest of Repository or NROR (panels 1,2,7,8, and 10) in the DBR calculation, with drilling intrusions considered in each of these regions. The types of intrusions considered in the DBR calculation and the times at which they occur are listed in Table 6-6. Scenario S1-DBR corresponds to an initial intrusion into the repository, with repository flow conditions at the time of intrusion transferred from BRAGFLO scenario S1-BF results. Scenarios S2-DBR through S5-DBR are used to model an intrusion into a repository that has already been penetrated. The times at which intrusions are assumed to occur for each scenario are outlined in the last column of Table 6-6; six intrusion times are modeled for scenario S1-DBR, while five times are modeled for each of scenarios S2-DBR through S5-DBR. The scenarios, intrusion locations, and timings used for the CRA-2014 PA are the same as those used for the PABC-2009.

Table 6-6: PA Intrusion Scenarios Used in Calculating Direct Brine Releases

Scenario	Conditioning (or 1 st) Intrusion Time (year) and Type	Intrusion Times – Subsequent (year)
S1-DBR	None	100, 350, 1000, 3000, 5000, 10000
S2-DBR	350, E1	550, 750, 2000, 4000, 10000
S3-DBR	1000, E1	1200, 1400, 3000, 5000, 10000
S4-DBR	350, E2	550, 750, 2000, 4000, 10000
S5-DBR	1000, E2	1200, 1400, 3000, 5000, 10000

The DBR numerical grid and material map used in the CRA-2014 PA calculations are shown in Figure 6-42, and are described in Malama (2013). The color scheme in Figure 6-42 has been chosen so as to correspond to the color scheme used in the CRA-2014 PA BRAGFLO grid and material map shown in Figure 6-10. The computational grid and material map used in the PABC-2009 DBR calculations are shown in Figure 6-43.

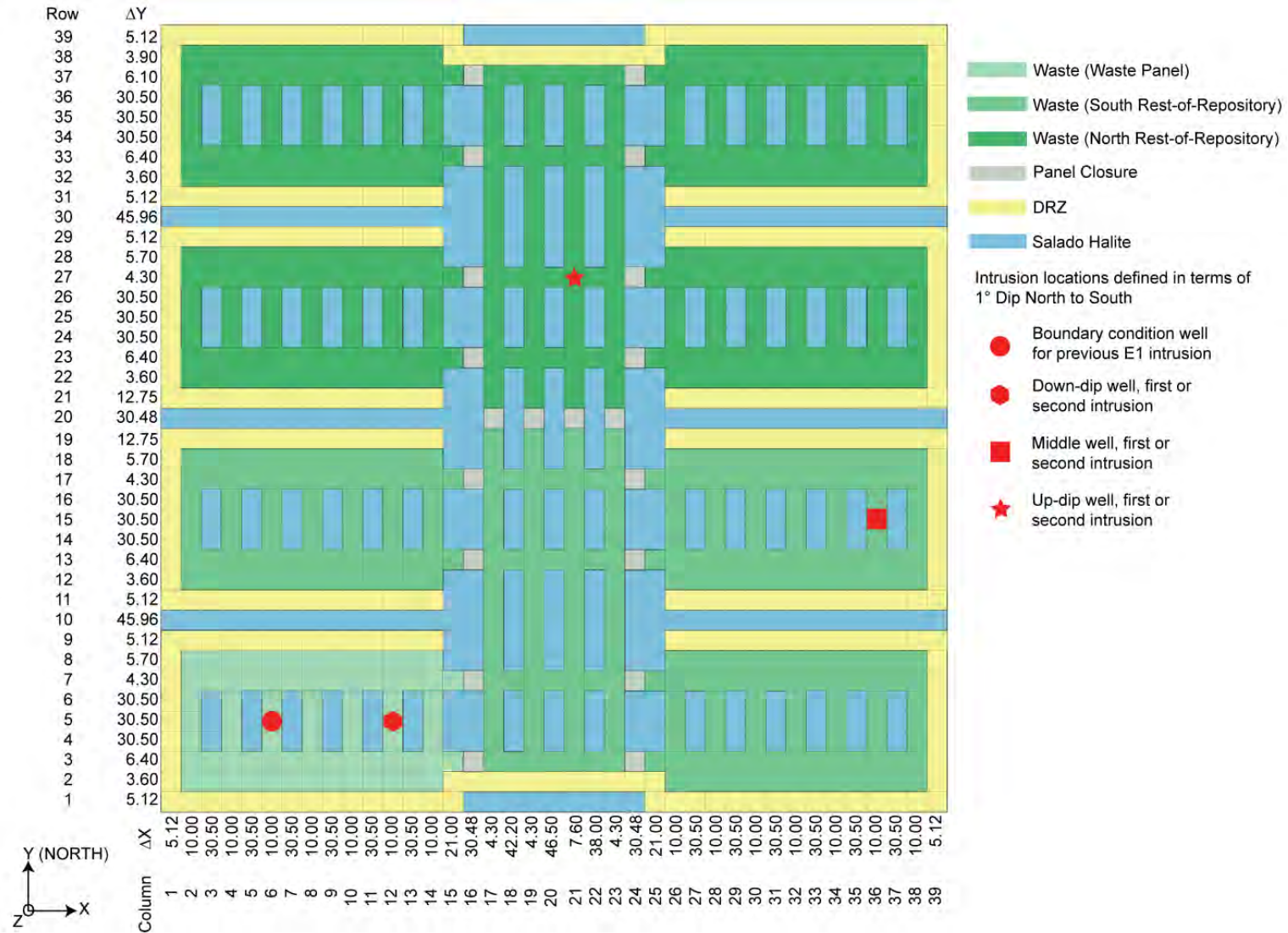
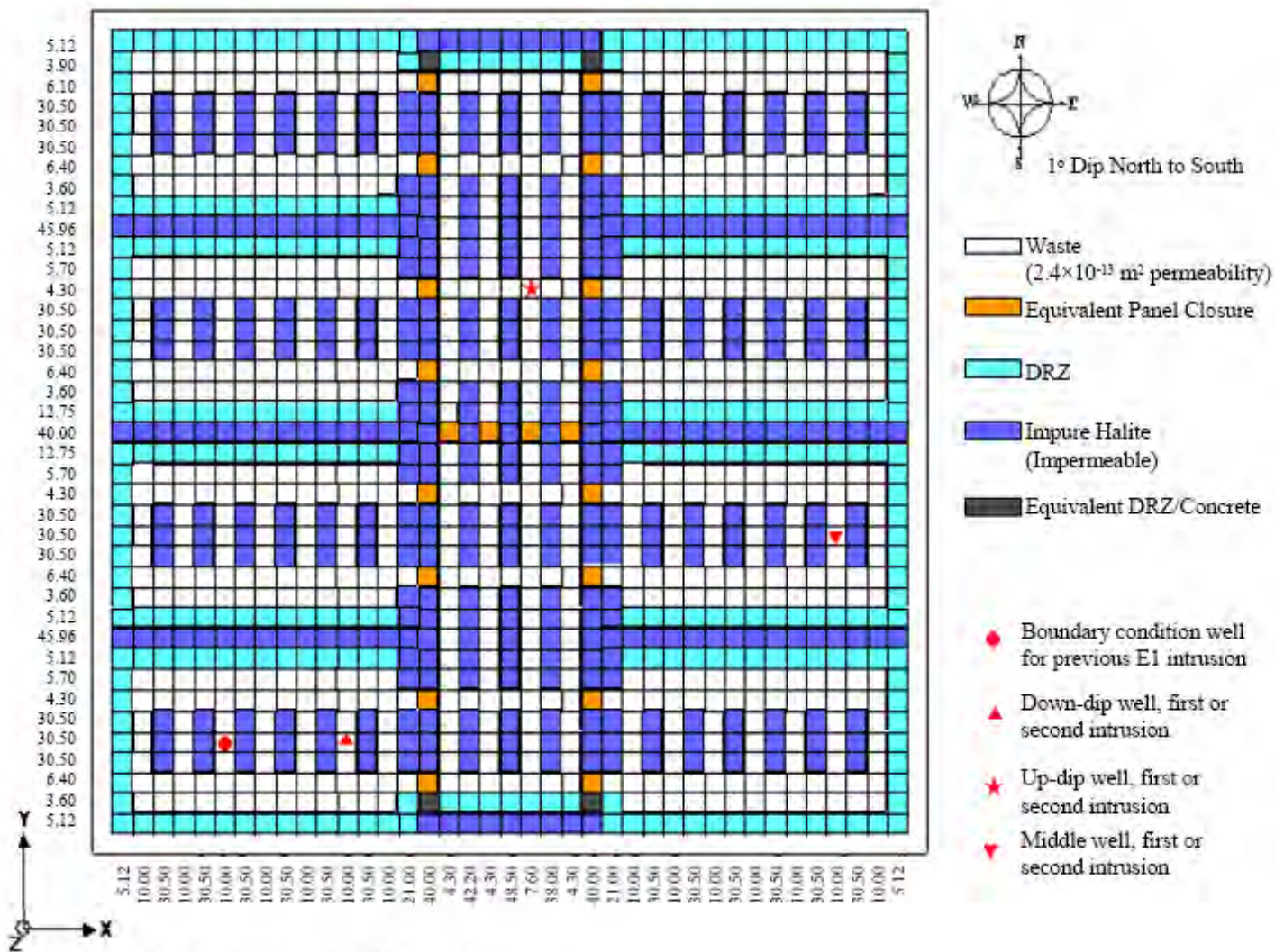


Figure 6-42: CRA-2014 PA DBR Computational Grid and Material Map (logical grid).



Note: Model cells are not to scale. The actual dimensions of the grid blocks are indicated along the edge of the diagram.

Figure 6-43: PABC-2009 DBR Computational Grid and Material Map (logical grid).

With the DBR computational grid and intrusion locations in hand, DBR results from the CRA-2014 PA can now be summarized. DBR results obtained in the CRA-2014 PA are further discussed in Malama (2013). Summary statistics of the calculated DBR volumes for replicates 1-3 and scenarios S1-DBR to S5-DBR are provided in Table 6-7. The maximum DBR volumes shown in that table are assessed over all three replicates, times, vectors, and drilling locations. As was also the case in the PABC-2009, release volumes that are less than $1 \times 10^{-7} \text{ m}^3$ are considered to be inconsequential and are not included in the tally of vectors that result in DBR release volumes in the CRA-2014 PA calculations.

Table 6-7: DBR Summary Statistics for the CRA-2014 PA and PABC-2009 DBR Calculations

Scenario	Number of Vectors		Maximum volume (m ³)		Average volume (m ³)	
	PABC-2009	CRA-2014 PA	PABC-2009	CRA-2014 PA	PABC-2009	CRA-2014 PA
S1-DBR	369	220	27.60	47.31	0.10	0.22
S2-DBR	1179	1140	48.20	58.02	2.80	3.78
S3-DBR	926	988	40.60	55.09	1.50	2.65
S4-DBR	211	104	20.40	36.77	0.10	0.15
S5-DBR	314	133	21.10	36.60	0.10	0.17
Overall	2999	2585	48.20	58.02	0.92	1.39

As seen in Table 6-7, there is a reduction in the overall number of vectors that result in a DBR release volume in the CRA-2014 PA. From the Salado flow results of Section 6.3, changes included in the CRA-2014 PA result in most of the repository being drier (on average) and under lower pressure (on average) than was the case in the PABC-2009. Mean brine saturations and pressures are lower in the south and north rest-of-repository in the CRA-2014 PA as compared to the PABC-2009. The result is an overall reduction in the number of vectors that satisfy the two necessary conditions for a nonzero DBR volume.

There is a consistent increase in the maximum DBR volumes from the PABC-2009 to the CRA-2014 PA. For undisturbed conditions, as well as all intrusion scenarios, increases are seen in the mean brine saturation of the southernmost waste panel in the CRA-2014 PA Salado flow results. For undisturbed and E2 intrusions scenarios, increases in the mean waste panel brine saturation are accompanied by decreases in the mean waste panel pressure. However, increased brine saturation can result in larger maximum DBR volumes for vectors that also satisfy the DBR pressure necessary condition. For E1 intrusion scenarios, the increase in the mean brine saturation of the southernmost waste panel is accompanied by increased mean pressure for a period of time after the intrusion. The result is larger maximum DBR volumes for E1 intrusion scenarios.

DBR volume trends observed in the CRA-2014 PA are consistent with those found in prior analyses with regard to drilling location. DBRs are less likely to occur in intrusions situated in the up-dip (upper) drilling locations than in the down-dip (lower) drilling location. Of all the intrusions that had a non-zero DBR volume in the CRA-2014 PA, 82.4% occurred in the lower location, compared to 66.6% in PABC-2009, a significant increase. As seen in the Salado flow results of the previous section, repository waste regions at higher elevation tend to be drier (on average) in the CRA-2014 PA than in the PABC-2009. Of all the intrusions that have a non-zero DBR volume and occur during a down-dip (lower) drilling intrusion, 89.9% are found in

scenarios S2-DBR and S3-DBR, a modest increase from 82.9% for PABC-2009 (Clayton et al., 2010). DBR results obtained in the CRA-2014 PA continue to demonstrate that the majority of non-zero DBR volumes occur when there is a previous E1 intrusion within the same panel.

In addition to DBRs being less likely to occur for drilling intrusions in the up-dip (upper) locations, DBR volumes from such intrusions tend to be much smaller than those from lower drilling intrusions. For all three replicates of the CRA-2014 PA, the maximum DBR volume for the upper drilling location is 5.1 m³ compared to 58.0 m³ for the lower drilling location. These observations support the conclusion that lower drilling intrusions are the primary source for significant DBRs.

The combination of relatively high pressure and brine saturation in the intruded panel is required for direct brine release to the surface. Figure 6-44 shows a scatter plot of DBR volume versus pressure in the intruded panel at different intrusion times for scenario S2-DBR, replicate 1, lower drilling intrusion for the CRA-2014 PA. In that figure, symbols indicate the value of the mobile brine saturation, defined as brine saturation minus residual brine saturation in the waste. As prescribed by the conceptual model, there are no DBRs until pressures exceed the 8 MPa vertical line in the figure. Figure 6-44 shows a clustering of the data about a linear trend (dashed line in the figure), and indicates that linearity of the correlation between pressure and DBR volumes increases with increasing mobile brine saturation.

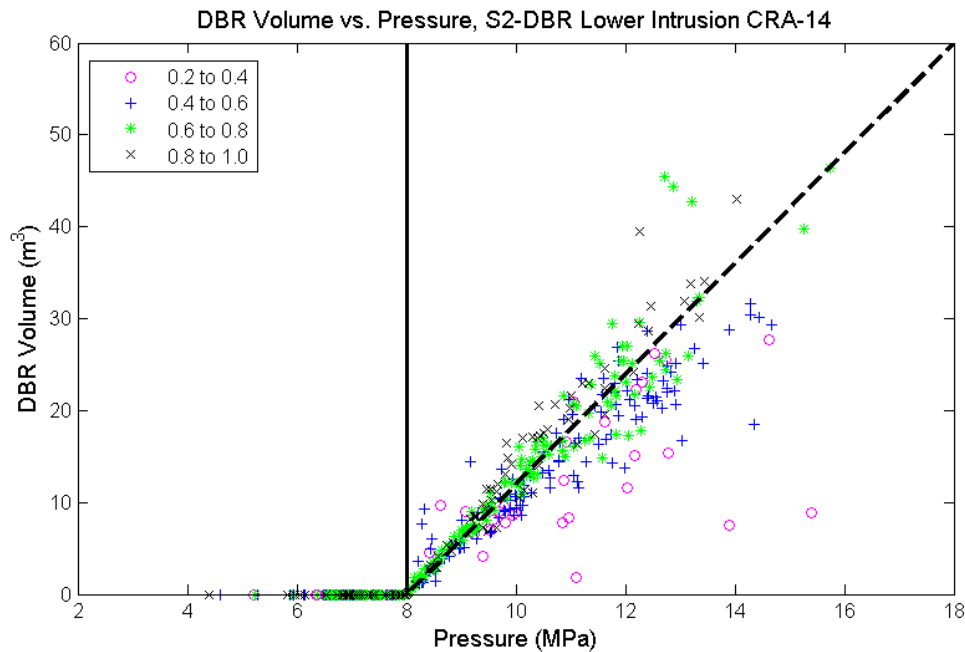


Figure 6-44: DBR Volume vs. Pressure, Scenario S2-DBR, Replicate 1, Lower Intrusion, CRA-2014 PA

6.6 Spallings Release Results

Calculation of the volume of solid waste material released to the surface from a single drilling intrusion into the repository due to spallings is a two-part procedure. First, PA code DRSPALL calculates the spallings volumes from a single drilling intrusion at four values of repository pressure (10, 12, 14, and 14.8 MPa). The second step in calculating spallings volumes from a single intrusion consists of using the code CUTTINGS_S to interpolate between DRSPALL volumes. The spallings volume for a given vector is determined in CUTTINGS_S by linearly interpolating between volumes calculated by DRSPALL based on the pressure calculated in each realization by BRAGFLO. DRSPALL volumes used in the PABC-2009 are also used in the CRA-2014 PA. Intrusion scenarios and times used in the calculation of spallings release volumes correspond to those used in the calculation of DBRs, and are shown in Table 6-6.

Utilizing the spallings volumes calculated by DRSPALL and the repository pressures calculated by BRAGFLO, the impact of changes included in the CRA-2014 PA in regard to spallings volumes can be determined. CRA-2014 PA spallings release results are fully discussed in Kicker (2013). Summary statistics of spallings volumes for the intrusion scenarios considered by CUTTINGS_S are shown in Table 6-8 for both the CRA-2014 PA and the PABC-2009. Results presented in that table are assessed over all three replicates, times, vectors, and drilling locations. As seen in Table 6-8, the maximum spallings volumes obtained for scenarios S1-DBR, S4-DBR, and S5-DBR are reduced in the CRA-2014 PA as compared to the PABC-2009. The same is also true of the average release volumes obtained for these scenarios. Scenario S1-DBR corresponds to an intrusion into a theretofore undisturbed repository. Scenarios S4-DBR and S5-DBR correspond to a subsequent intrusion into a repository that has already undergone an earlier E2 intrusion. From the Salado flow results discussed in Section 6.3, repository waste regions trend toward lower pressure in the CRA-2014 PA for undisturbed conditions and E2 intrusion scenarios. This translates directly to reductions in spallings release volumes for scenarios S1-DBR, S4-DBR, and S5-DBR. For E1 intrusion scenarios, the mean pressure in the intruded panel is increased in the CRA-2014 PA for a period of time after the intrusion, but eventually falls below that seen in the PABC-2009. Scenarios S2-DBR and S3-DBR correspond to a subsequent intrusion into a repository that has already undergone a previous E1 intrusion. The trend toward higher waste panel pressure for a period of time after the initial E1 intrusion results in greater maximum spallings release volumes for scenarios S2-DBR and S3-DBR. The overall trend in the CRA-2014 PA is toward lower waste region pressure as compared to the PABC-2009. The result is a reduction in the number of realizations that result in a nonzero spallings release volume in all scenarios as compared to the PABC-2009.

Spallings results as a function of intrusion location are shown in Table 6-9. From the Salado flow results of Section 6.3, the trend is toward reduced pressure in the south and north rest-of-repository regions in the CRA-2014 PA. This corresponds to reductions in spallings releases in those regions. The trend toward lower pressure is also evident for the intruded southernmost panel, except for E1 intrusion scenarios. For E1 scenarios, the mean pressure in the intruded panel is increased in the CRA-2014 PA for a period of time after the intrusion, but eventually falls below that seen in the PABC-2009. The result is a larger maximum spallings release for intrusions into the lower region in the CRA-2014 PA. The overall trend toward lower waste region pressure yields a reduction in the number of nonzero spallings volumes at all intrusion locations.

Table 6-8: CRA-2014 PA Summary Spallings Results by Intrusion Scenario

Scenario	Maximum Volume (m ³)		Average Nonzero Volume (m ³)		Number of Nonzero Volumes (Percentage of Realizations that Result in a Nonzero Spallings Volume)	
	PABC-2009	CRA-2014 PA	PABC-2009	CRA-2014 PA	PABC-2009	CRA-2014 PA
S1-DBR	4.91	1.67	0.40	0.32	466 (8.6%)	112 (2.1%)
S2-DBR	8.29	9.69	0.44	0.43	352 (7.8%)	278 (6.2%)
S3-DBR	7.97	9.13	0.38	0.45	351 (7.8%)	170 (3.8%)
S4-DBR	2.26	1.67	0.37	0.26	161 (3.6%)	55 (1.2%)
S5-DBR	1.93	1.67	0.38	0.28	233 (5.2%)	66 (1.5%)

Table 6-9: CRA-2014 PA Summary Spallings Results by Intrusion Location

Intrusion Location	Maximum Volume (m ³)		Average Nonzero Volume (m ³)		Number of Nonzero Volumes (Percentage of Realizations that Result in a Nonzero Spallings Volume)	
	PABC-2009	CRA-2014 PA	PABC-2009	CRA-2014 PA	PABC-2009	CRA-2014 PA
Lower Region (Waste Panel)	8.29	9.69	0.43	0.44	591 (7.6%)	428 (5.5%)
Middle Region (South RoR)	4.89	1.67	0.40	0.31	504 (6.5%)	140 (1.8%)
Upper Region (North RoR)	4.85	1.67	0.37	0.31	468 (6.0%)	113 (1.4%)

6.7 Cuttings and Cavings Results

Cuttings and cavings release results obtained in the CRA-2014 PA are fully discussed in Kicker (2013), and are now summarized. Cuttings and cavings are the solid waste material removed from the repository and carried to the surface by the drilling fluid during the process of drilling a borehole. Cuttings are the materials removed directly by the drill bit, and cavings are the material eroded from the walls of the borehole by shear stresses from the circulating drill fluid. The volume of cuttings and cavings material removed from a single drilling intrusion into the repository is assumed to be in the shape of a cylinder. The code CUTTINGS_S calculates the area of the base of this cylinder, and cuttings and cavings results in this section are reported in terms of these areas. The volumes of cuttings and cavings removed can be calculated by multiplying these areas with the initial repository height, 3.96 m (WIPP PA parameter BLOWOUT:HREPO).

The drill bit diameter is specified to be 3.11150E-01 meters in both the PABC-2009 and the CRA-2014 PA. A cuttings area of 0.0760 m² is obtained for all vectors in both the PABC-2009 and the CRA-2014 PA as both analyses use the same constant drill bit diameter value. As discussed in Section 2.5, a refined distribution for parameter BOREHOLE:TAUFAIL is implemented in the CRA-2014 PA. Parameter BOREHOLE:TAUFAIL is used to represent the effective shear strength for erosion of WIPP waste, and so changes to it potentially impact cavings release areas. Cavings area statistics obtained in the PABC-2009 and the CRA-2014 PA are shown in Table 6-10. The distributions of cavings area obtained in the PABC-2009 and the CRA-2014 PA are shown together in Figure 6-45. Table 6-10 and Figure 6-45 both show that the refinement to parameter BOREHOLE:TAUFAIL used in the CRA-2014 PA results in a shift toward a lower mean cavings area as well as a decrease in the overall number of vectors with nonzero cavings area in the CRA-2014 PA as compared to the PABC-2009.

Table 6-10: Cavings Area Statistics for the PABC-2009 and the CRA-2014 PA

Replicate	Mean Cavings Area		Max Cavings Area		Number of Vectors w/o Cavings	
	PABC-2009	CRA-2014 PA	PABC-2009	CRA-2014 PA	PABC-2009	CRA-2014 PA
1	0.177	0.010	0.748	0.090	9	50
2	0.175	0.010	0.785	0.090	10	44
3	0.178	0.010	0.753	0.075	11	50

The uncertainty in cavings area arises primarily from the uncertainty in the shear strength of the waste (Kicker 2013). Lower shear strengths tend to result in larger cavings releases, and hence larger cuttings and cavings releases (Figure 6-46). In Figure 6-46, the lowest attainable cuttings and cavings release area is 0.0760 m², which corresponds to a release due only to cuttings (i.e. a release with zero cavings area).

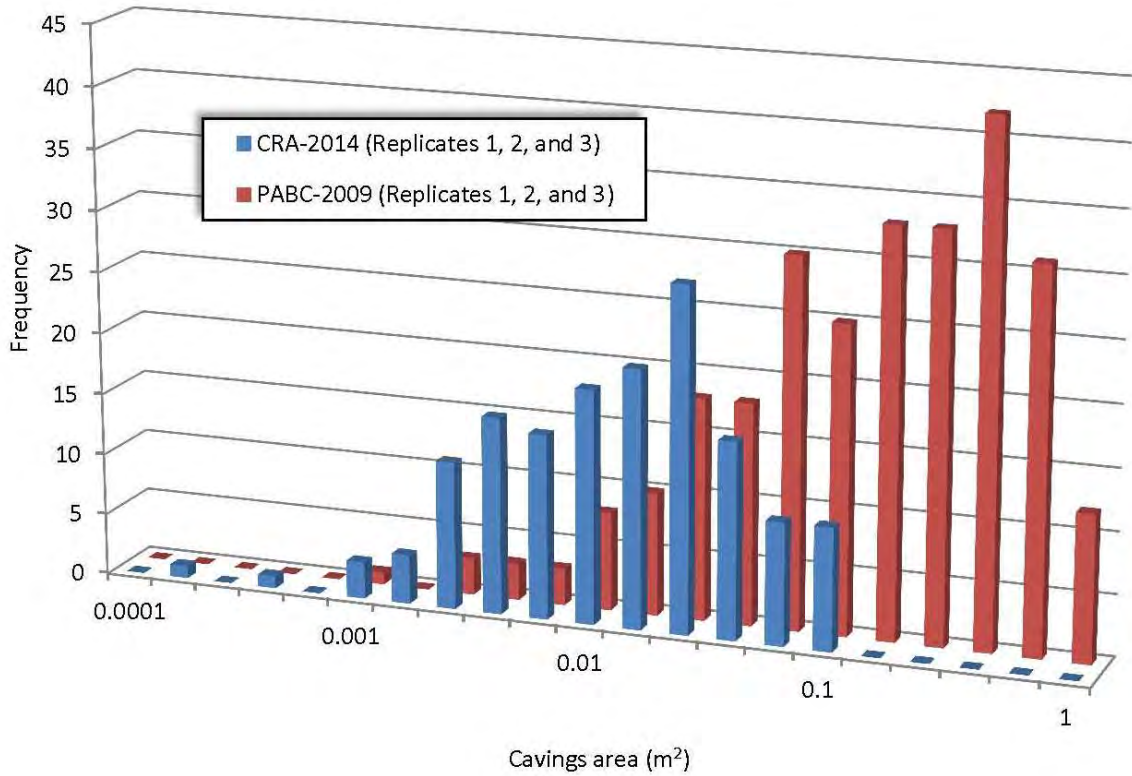


Figure 6-45: Frequency of Cavings Area in the CRA-2014 PA and the PABC-2009.

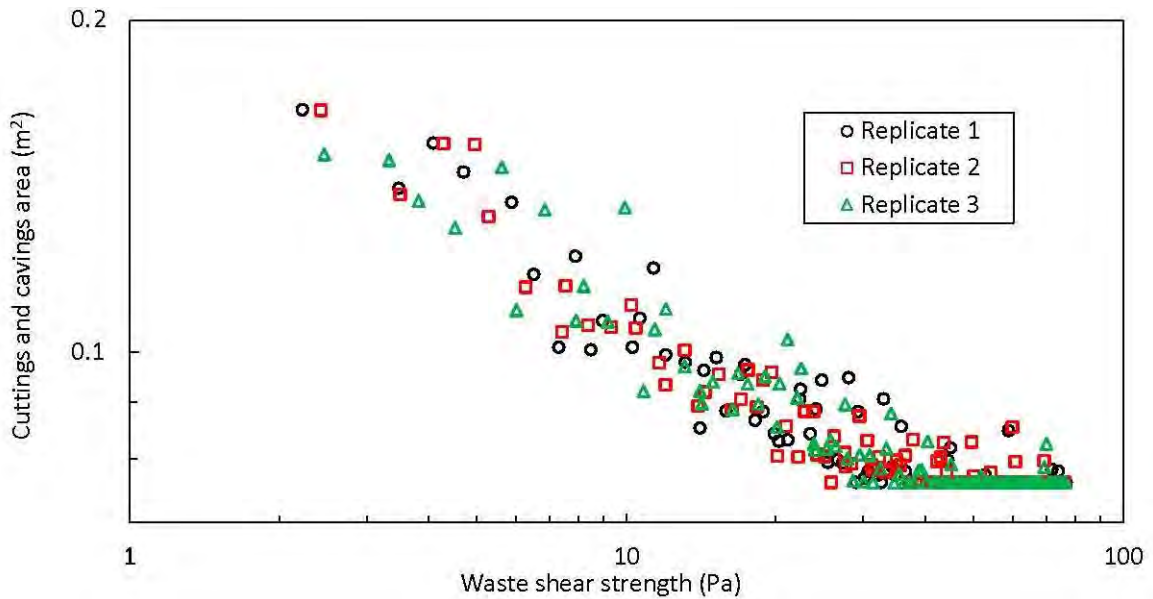


Figure 6-46: CRA-2014 PA Cuttings and Cavings Areas as a Function of Shear Strength

6.8 Normalized Releases

This section presents a discussion of normalized releases for each of the four release mechanisms (cuttings and cavings, spillings, DBRs, and transport releases) that contribute to total normalized releases, followed by a discussion of total normalized releases obtained in the CRA-2014 PA. Normalized releases are calculated with code CCDFGF. In the results that follow, the overall mean CCDF is computed as the arithmetic mean of the mean CCDFs from each replicate. Normalized releases calculated in the CRA-2014 PA are fully discussed in Zeitler (2013). Sensitivities of normalized releases to uncertain parameters used in WIPP PA are documented in a separate report (see Kirchner 2013b).

6.9.1 Cuttings and Cavings Normalized Releases

The overall mean CCDFs for cuttings and cavings releases obtained in the PABC-2009 and the CRA-2014 PA are plotted together in Figure 6-47. Overall, cuttings and cavings normalized releases calculated for the CRA-2014 PA are smaller than those for the CRA-2009 PA. The activity of the CRA-2014 waste inventory is greater over time than that implemented in the PABC-2009 (see Figure 6-1). The drilling rate per unit area is also increased in the CRA-2014 PA, which increases the number of drilling events into repository waste areas. Although the changes in waste inventory and drilling rate both serve to increase cuttings and cavings releases, the effect of the CRA-2014 PA waste shear strength refinement is to reduce cavings release volumes, and hence cuttings and cavings volumes overall, enough so that normalized releases due to cuttings and cavings in the CRA-2014 PA fall below those seen in the PABC-2009.

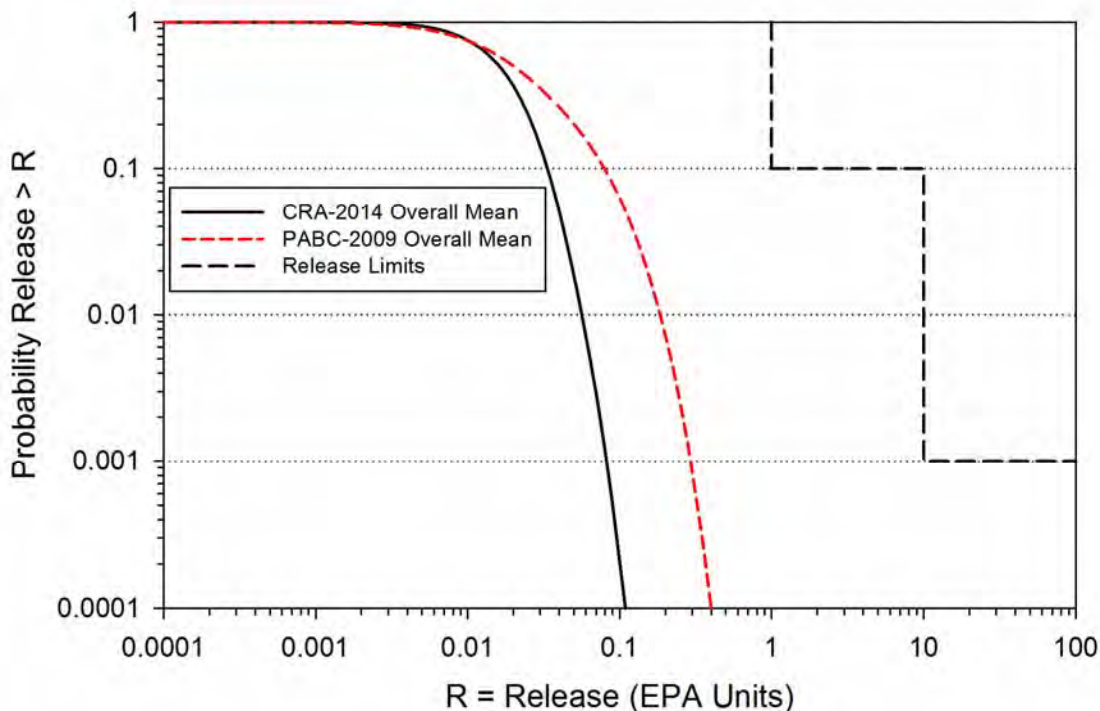


Figure 6-47: CRA-2014 PA and CRA-2009 PABC Overall Mean CCDFs for Normalized Cuttings and Cavings Releases

6.9.2 Spallings Normalized Releases

The overall mean CCDFs for spallings normalized releases obtained in the PABC-2009 and the CRA-2014 PA are plotted together in Figure 6-48. Spallings release volumes directly depend on repository pressure at the time of intrusion. Despite the modified panel closure system, which serves to increase waste panel pressures (on average), the updated steel corrosion rate, additional excavation in the WIPP experimental area, and the updated repository water balance implementation each contribute to a trend toward decreased waste panel pressures in the CRA-2014 PA. This trend toward lower waste panel pressure directly translates to a trend toward decreased spallings release volumes from the PABC-2009 to the CRA-2014 PA. The result is an overall reduction in spallings normalized releases, despite an increase in waste inventory activity, due to a decrease in the number of nonzero spallings volumes.

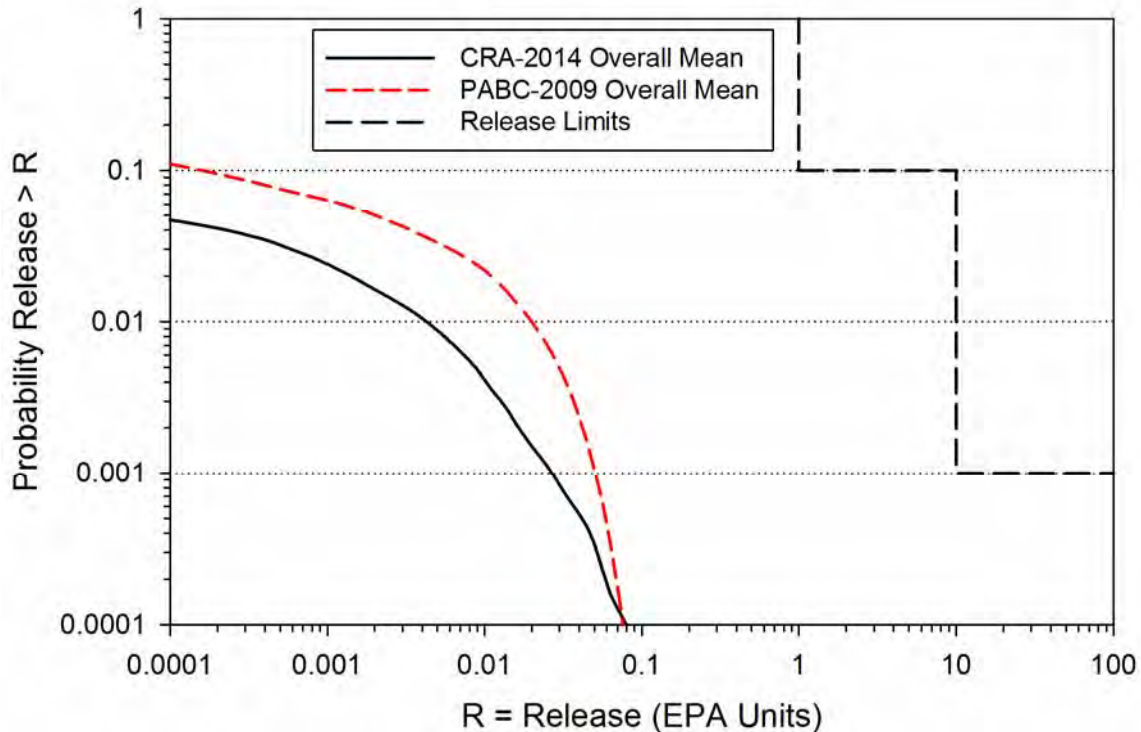


Figure 6-48: CRA-2014 PA and PABC-2009 Overall Mean CCDFs for Normalized Spallings Releases

6.9.3 Normalized Direct Brine Releases

The overall mean CCDFs for normalized direct brine releases obtained in the PABC-2009 and the CRA-2014 PA are plotted together in Figure 6-49. Overall, there is a decrease in normalized DBRs from the PABC-2009 to the CRA-2014 PA. Several changes included in the CRA-2014 PA contribute to this reduction. The refinement to the probability that a drilling intrusion results in a pressurized brine pocket encounter (parameter GLOBAL:PBRINE) yields an overall reduction to DBR volumes in the CRA-2014 PA CCDFGF results. The variable brine volume implementation maps radionuclide mobilized concentrations in brine to volumes of brine

released. Radionuclide mobilized concentrations in brine decrease as brine volume increases in the CRA-2014 PA (see Section 6.2), whereas mobilized concentrations in brine remained fixed (for each vector) in the PABC-2009, regardless of the actual brine volume being released. There is a consistent increase in maximum DBR volumes from the PABC-2009 to the CRA-2014 PA (see Section 6.5). However, the variable brine volume implementation results in lower mobilized radionuclide concentrations in these larger brine volumes. The revised steel corrosion rate and water balance implementation used in the CRA-2014 PA also lead to an overall reduction in the number of vectors that satisfy the two necessary conditions for a DBR. In total, the combined impact of changes included in the CRA-2014 PA is an overall net reduction to normalized direct brine releases as compared to the PABC-2009.

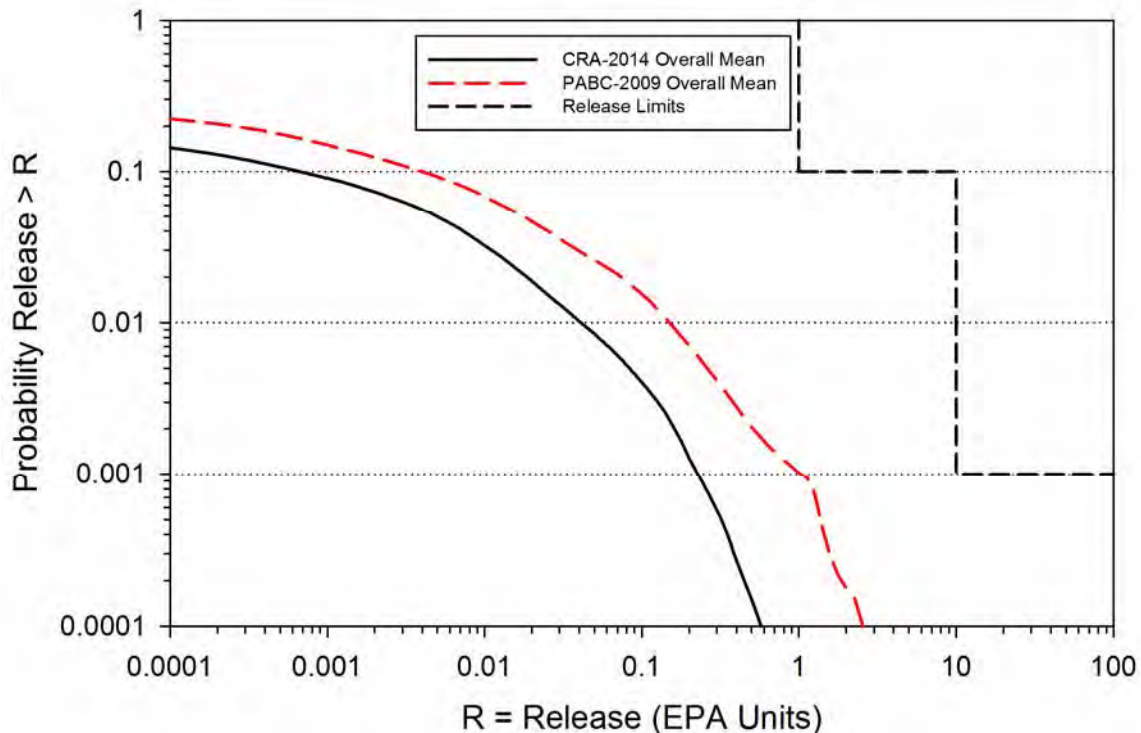


Figure 6-49: CRA-2014 PA and PABC-2009 Overall Mean CCDFs for Normalized Direct Brine Releases

6.9.4 Normalized Culebra Transport Releases

The overall mean CCDFs for normalized Culebra transport releases obtained in the PABC-2009 and the CRA-2014 PA are plotted together in Figure 6-50. As seen in that figure, mean releases from the Culebra decrease from the CRA-2009 PABC to the CRA-2014 PA. Relatively few vectors (roughly 10%) contribute to nonzero Culebra transport releases (Zeitler 2013). The upper limit of the PBRINE parameter distribution has decreased from the CRA-2009 PABC to the CRA-2014 PA while the lower limit has increased. As discussed for the radionuclide transport results of Section 6.4, radionuclide transport releases to the Culebra are most likely to occur during an E1 intrusion. The refinement of the PBRINE distribution, which sets the probability that an E1 drilling intrusion occurs in a given future, results in increased Culebra

transport releases for some vectors (as the PBRINE lower limit as increased) and decreases in others (as the PBRINE upper limit has decreased). The net effect is a reduction in the mean CCDF for normalized Culebra transport releases in the CRA-2014 PA as compared to the PABC-2009

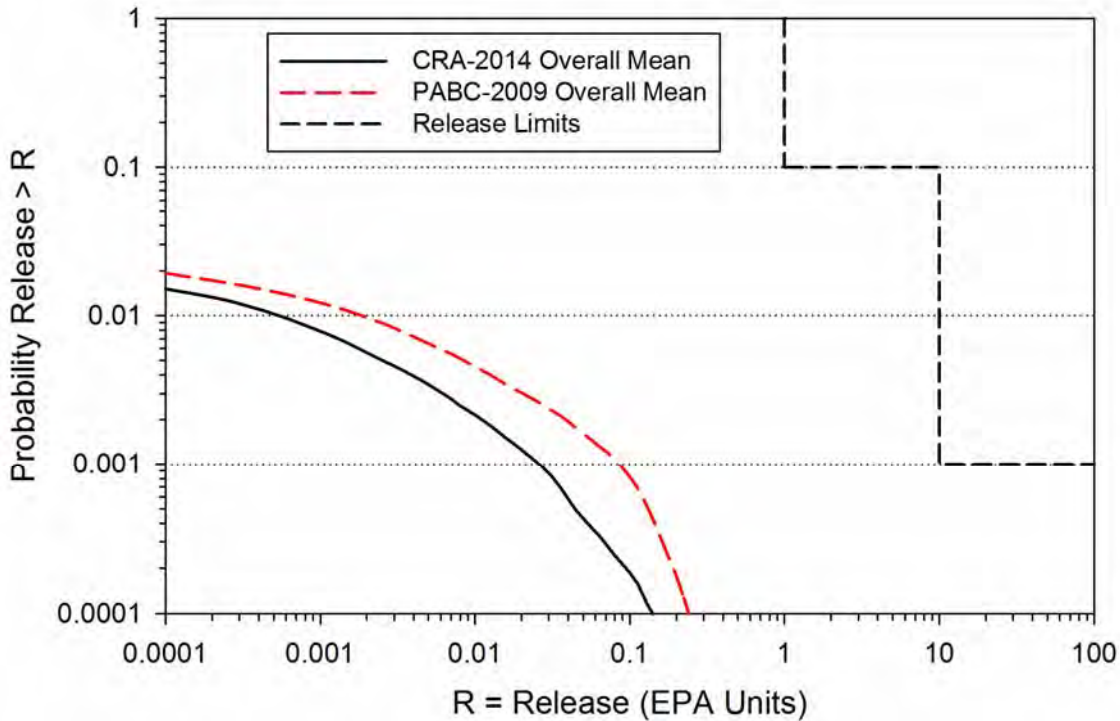


Figure 6-50: CRA-2014 PA and CRA-2009 PABC Overall Mean CCDFs for Normalized Culebra Transport Releases

6.9.5 Total Normalized Releases

Total normalized releases for the CRA-2014 PA are presented in this section and subsequently compared to results obtained in the PABC-2009. Total releases are calculated by forming the summation of releases across each potential release pathway, namely cuttings and cavings releases, spallings releases, direct brine releases, and Culebra transport releases. CRA-2014 PA CCDFs for total releases obtained in replicates 1, 2, and 3 are plotted together in Figure 6-51. Figure 6-52 shows the 95 percent confidence limits about the overall mean of total releases. As seen in that figure, the overall mean for normalized total releases and its lower/upper 95% confidence limits are well below acceptable release limits. As a result, the CRA-2014 PA demonstrates that the WIPP remains in compliance with the containment requirements of 40 CFR Part 191.

Mean CCDFs of the individual release mechanisms that comprise total normalized releases are plotted together in Figure 6-53, as well as the CRA-2014 PA total release overall mean. As seen in that figure, total normalized releases obtained in the CRA-2014 PA are dominated by cuttings and cavings releases and DBRs. Contributions to total releases from spallings and Culebra

transport are much less significant. The rank regression analysis shows that the waste shear strength is the leading uncertain parameter associated with cuttings and cavings releases, and controls about 65% of mean cuttings and cavings releases in the CRA-2014 PA (Kirchner 2013b). For DBRs, the rank regression analysis shows that the solubility multiplier that represents uncertainty in solubility limits for all actinides in the III oxidation state (parameter SOLMOD3:SOLVAR) is ranked first in importance (Kirchner 2013b). The dominant releases mechanisms of the CRA-2014 PA are consistent with those found in the PABC-2009, as are the leading uncertain parameters associated with those mechanisms.

Overall means for total normalized releases obtained in the PABC-2009 and the CRA-2014 PA are plotted together in Figure 6-54. Overall, total normalized releases decrease from the CRA-2009 PABC to the CRA-2014 PA as each contributing component is reduced in the CRA-2014 PA.

A comparison of the statistics on the overall mean for total normalized releases obtained in the PABC-2009 and the CRA-2014 PA can be seen in Table 6-11. At probabilities of 0.1 and 0.001, values obtained for the mean total release are lower for the CRA-2014 PA.

Table 6-11: CRA-2014 PA and CRA-2009 PABC Statistics on the Overall Mean for Total Normalized Releases in EPA Units at Probabilities of 0.1 and 0.001

Probability	Analysis	Mean Total Release	Lower 95% CL	Upper 95% CL	Release Limit
0.1	CRA-2014 PA	0.0367	0.0352	0.0384	1
	CRA-2009 PABC	0.0937	0.0908	0.0959	1
0.001	CRA-2014 PA	0.261	0.109	0.384	10
	CRA-2009 PABC	1.10	0.372	1.77	10

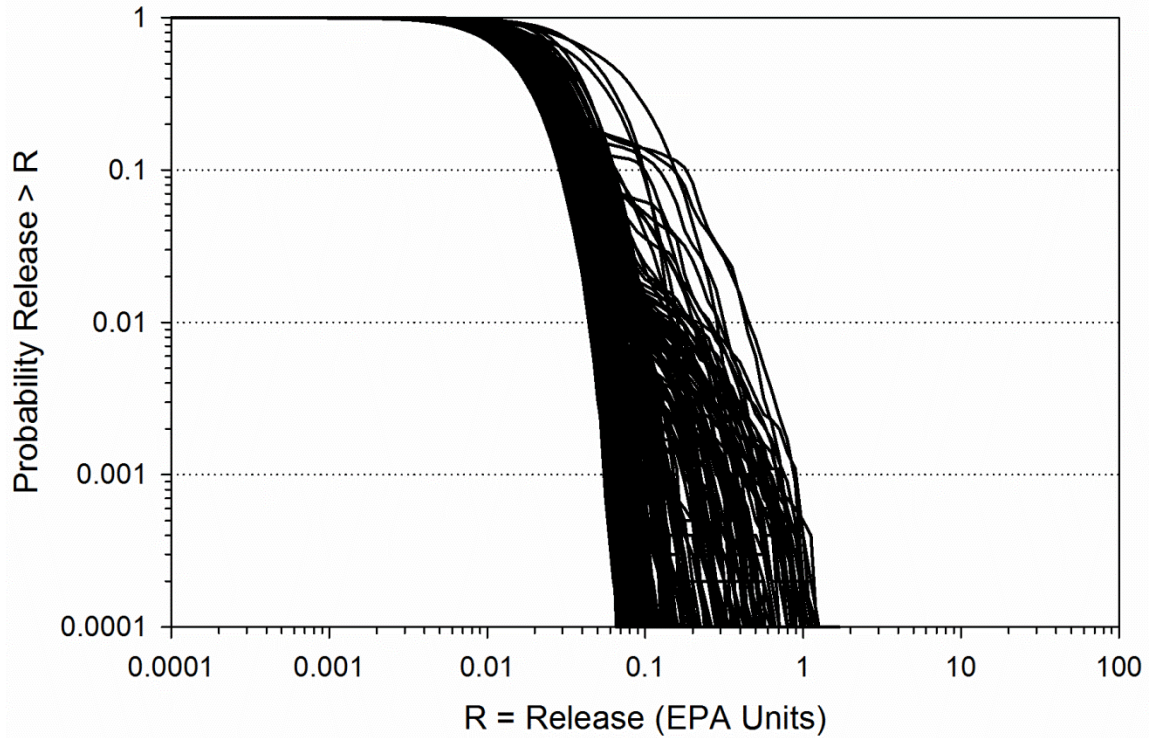


Figure 6-51: CRA-2014 PA Total Normalized Release CCDFs for Replicates 1, 2, and 3

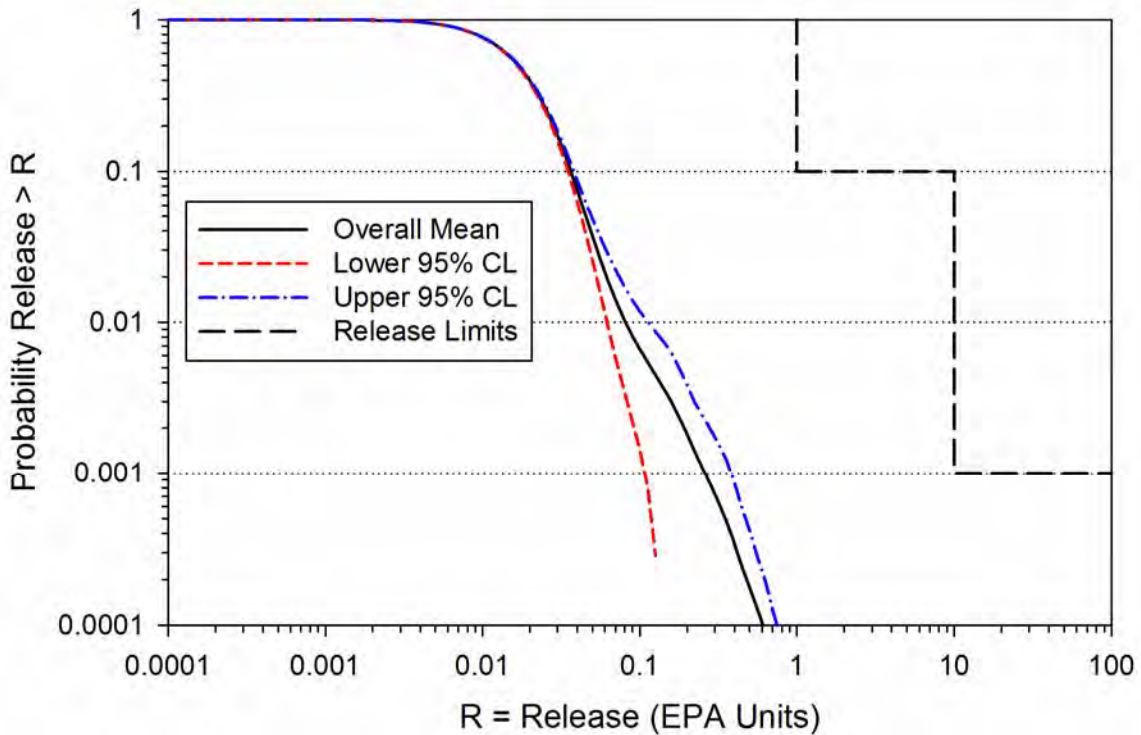


Figure 6-52: CRA-2014 PA Confidence Limits on Overall Mean for Total Normalized Releases

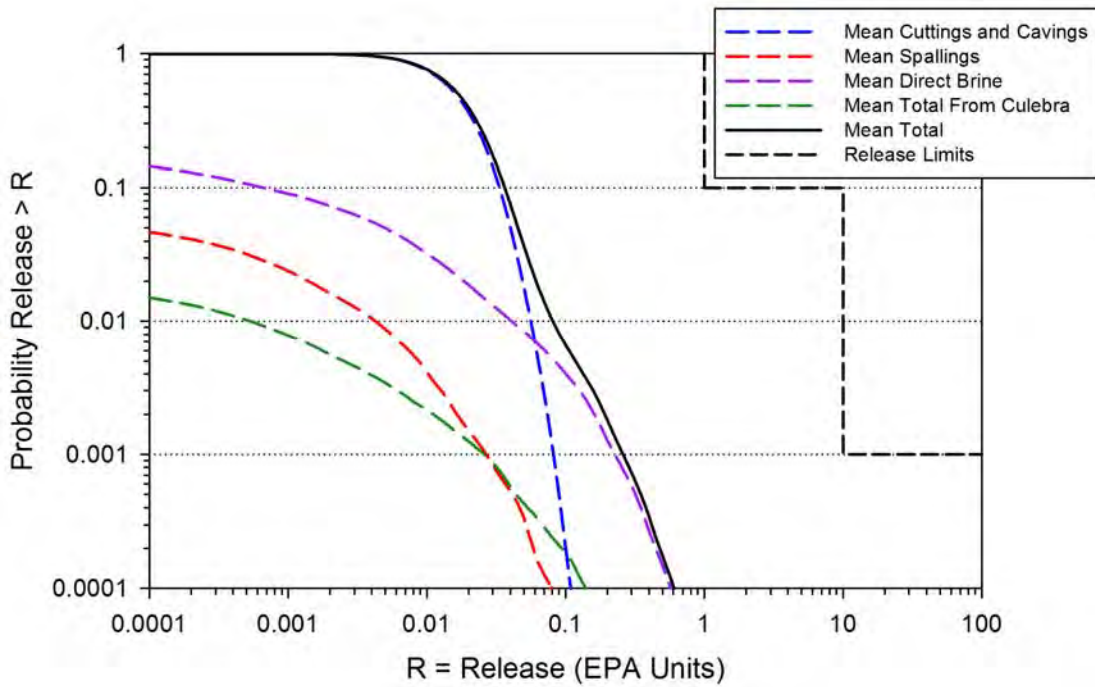


Figure 6-53: Comparison of Overall Means for Release Components of the CRA-2014 PA

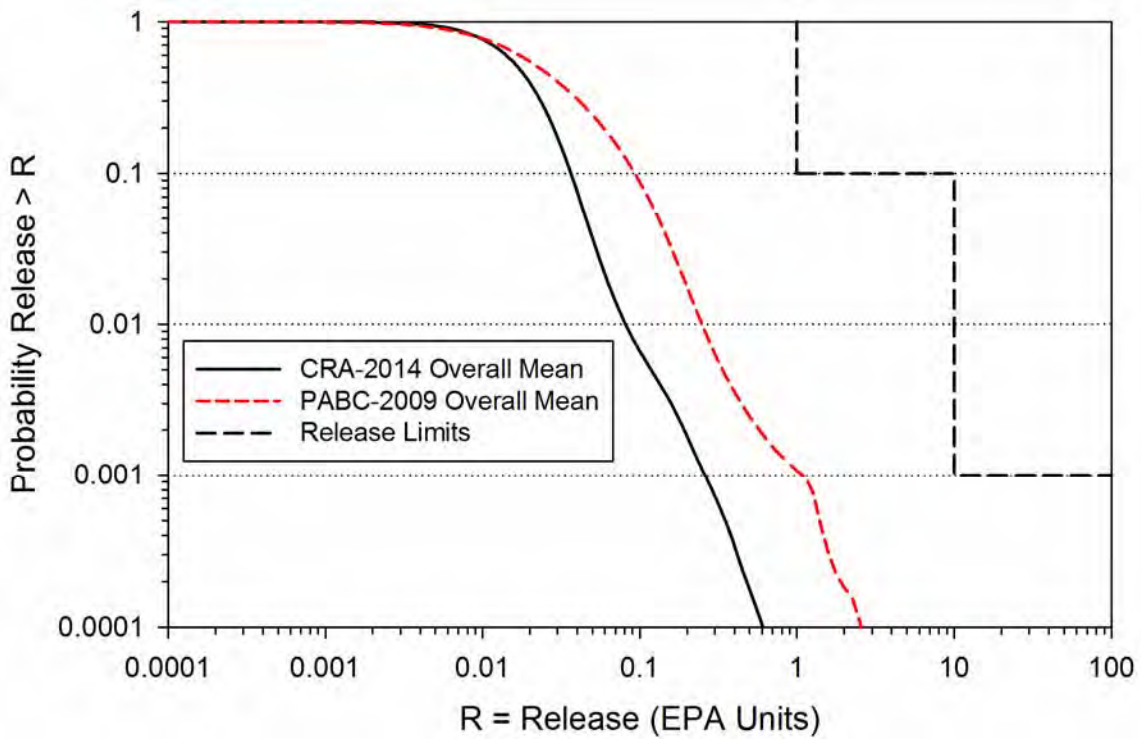


Figure 6-54: CRA-2014 PA and CRA-2009 PABC Overall Mean CCDFs for Total Normalized Releases

7 SUMMARY

Several changes are incorporated into the CRA-2014 PA relative to the PABC-2009. These modifications are comprised of planned repository changes, parameter updates, refinements to PA implementation, and include the following:

- Replacement of the “Option D” WIPP panel closure with a newly designed Run-of-Mine Panel Closure System (ROMPCS).
- Inclusion of additional mined volume in the repository north end.
- An update to the probability that a drilling intrusion into a repository excavated region will result in a pressurized brine encounter.
- Refinement to the corrosion rate of steel.
- Refinement to the effective shear strength of WIPP waste.
- Updates to drilling rate and plugging pattern parameters.
- Updates to WIPP waste inventory parameters.
- Calculation of radionuclide concentration in brine as a function of the actual brine volume present in the waste panel.
- Updates to radionuclide solubilities and their associated uncertainty.
- Implementation of a more detailed repository water balance that includes MgO hydration.
- Updated colloid parameters.
- Parameter corrections.

Total normalized releases obtained in the CRA-2014 PA are lower than those found in the PABC-2009, and continue to remain below regulatory limits. As a result, the CRA-2014 PA demonstrates that the WIPP remains in compliance with the containment requirements of 40 CFR Part 191. Cuttings and cavings releases and DBRs were the two primary release components contributing to total releases in the PABC-2009, and continue to be so in the CRA-2014 PA. Reductions are seen in the contributing mechanisms to total releases in the CRA-2014 PA as compared to the PABC-2009.

8 REFERENCES

Brush, L. 2013. Th(IV), Np(V), and Am(III) Baseline Solubilities and Th(IV) and Am(III) Solubility Uncertainties for the CRA-2014 PA. Memo to Chris Camphouse dated February 22, 2013. Sandia National Laboratories, Carlsbad, NM. ERMS 559279.

Brush, L. and P. Domski. 2013. Uncertainty Analysis of Actinide Solubilities for the WIPP CRA-2014 PA, Rev. 1. Sandia National Laboratories, Carlsbad, NM. ERMS 559712.

Camphouse, R.C. 2012a. A summary of parameters to be implemented in the PCS-2012 PA. Memo to Janis Trone dated July 10, 2012. Sandia National Laboratories, Carlsbad, NM. ERMS 557721.

Camphouse, R.C. 2012b. An overview of the BRAGFLO two-phase flow parameters used to model the run-of-mine salt panel closures implemented in the PCS-2012 PA. Memo to Paul Shoemaker dated June 7, 2012. Sandia National Laboratories, Carlsbad, NM. ERMS 557653.

Camphouse, R.C. 2012c. Analysis Package for Salado Flow Modeling Done in the AP-161 (PCS-2012) Performance Assessment. Sandia National Laboratories, Carlsbad, NM. ERMS 558204.

Camphouse, R.C. 2013a. Analysis Plan for the 2014 WIPP Compliance Recertification Application Performance Assessment. Sandia National Laboratories, Carlsbad, NM. ERMS 559198.

Camphouse, R.C. 2013b. Analysis Package for Salado Flow Modeling Done in the 2014 Compliance Recertification Application Performance Assessment (CRA-2014 PA). Sandia National Laboratories, Carlsbad, NM. ERMS 559980.

Camphouse, R.C., Kicker, D.C., Kirchner, T.B., Long, J.J., and Pasch, J.J. 2011. Impact Assessment of SDI Excavation on Long-Term WIPP Performance. Sandia National Laboratories, Carlsbad, NM. ERMS 555824.

Camphouse, R.C., Kicker, D.C., Kirchner, T.B., Long, J.J., Malama, B., and Zeitler, T.R. 2012a. Summary Report and Run Control for the 2012 WIPP Panel Closure System Performance Assessment. Sandia National Laboratories, Carlsbad, NM. ERMS 558365.

Camphouse, R.C., Gross, M., Herrick, C.G., Kicker, D.C., and Thompson, B. 2012b. Recommendations and Justifications of Parameter Values for the Run-of-Mine Salt Panel Closure System Design Modeled in the PCS-2012 PA. Memo to WIPP Records Center dated May 3, 2012. Sandia National Laboratories, Carlsbad, NM. ERMS 557396.

Clayton, D.J. 2008. Update to the Calculation of the Minimum Brine Volume for a Direct Brine Release. Memorandum to Larry Brush dated April 2, 2008. Sandia National Laboratories, Carlsbad, NM. ERMS 548522.

Clayton, D.J. 2013. Justification of Chemistry Parameters for Use in BRAGFLO for AP-164, Revision 1. Memorandum to SNL Records Center dated March 13, 2013. Sandia National Laboratories, Carlsbad, NM. ERMS 559466.

Clayton, D.J., S. Dunagan, J.W. Garner, A.E. Ismail, T.B. Kirchner, G.R. Kirkes, M.B. Nemer. 2008. Summary Report of the 2009 Compliance Recertification Application Performance Assessment. Sandia National Laboratories, Carlsbad, NM. ERMS 548862.

Clayton, D.J., R.C. Camphouse, J.W. Garner, A.E. Ismail, T.B. Kirchner, K.L. Kuhlman, M.B. Nemer. 2010. Summary Report of the CRA-2009 Performance Assessment Baseline Calculation. Sandia National Laboratories, Carlsbad, NM. ERMS 553039.

Cotsworth, E. 2005. EPA Letter on Conducting the Performance Assessment Baseline Change (PABC) Verification Test. U.S. EPA, Office of Radiation and Indoor Air, Washington, D.C. ERMS 538858.

Cotsworth, E. 2009. EPA Letter on CRA-2009 First Set of Completeness Comments. U.S. EPA, Office of Radiation and Indoor Air, Washington, D.C. ERMS 551444.

Fox, B. and D. Clayton 2010. Analysis Package for EPA Unit Loading Calculations: CRA-2009 Performance Assessment Baseline Calculation. Sandia National Laboratories. Carlsbad, NM. ERMS 552912.

Hansen, C. 2002. A Reconciliation of the CCA and PAVT Parameter Baselines, Revision 1. Sandia National Laboratories, Carlsbad, NM. ERMS 522337.

Herrick, C.G., M.D. Schuhen, D.M. Chapin, and D.C. Kicker. 2012. Determining the Hydrodynamic Shear Strength of Surrogate Degraded TRU Waste Materials as an Estimate for the Lower Limit of the Performance Assessment Parameter TAUFAIL. Sandia National Laboratories, Carlsbad, NM. ERMS 558479.

Herrick, C.G. 2013. Follow-up to Questions Concerning TAUFAIL Flume Testing Raised during the November 14-15, 2012 Technical Exchange Between the DOE and EPA. Memorandum to Chris Camphouse dated January 23, 2013. Sandia National Laboratories, Carlsbad, NM. ERMS 559081.

Ismail, A. 2007a. Revised Porosity Estimates for the DRZ. Sandia National Laboratories, Carlsbad, NM. ERMS 545755.

Ismail, A. 2007b. Update to DRZ_PCS:POROSITY. Sandia National Laboratories, Carlsbad, NM. ERMS 547486.

Kicker, D. 2013. Analysis Package for Cuttings, Cavings, and Spallings: 2014 Compliance Recertification Application Performance Assessment (CRA-2014 PA), Revision 0. Sandia National Laboratories, Carlsbad, NM. ERMS 560060.

Kicker, D. and T. Zeitler. 2013a. Analysis Package for EPA Unit Loading Calculations for the 2014 Compliance Recertification Application Performance Assessment (CRA-2014 PA), Revision 0. Sandia National Laboratories, Carlsbad, NM. ERMS 560065.

Kicker, D. and T. Zeitler. 2013b. Radionuclide Inventory Screening Analysis for the 2014 Compliance Recertification Application Performance Assessment (CRA-2014 PA). Sandia National Laboratories, Carlsbad, NM. ERMS 559257.

Kim, S. 2013a. Analysis Package for PANEL: CRA-2014 Performance Assessment. Sandia National Laboratories, Carlsbad, NM. ERMS 560056.

Kim, S. 2013b. Analysis Package for Salado Transport Calculations: CRA-2014 Performance Assessment. Sandia National Laboratories, Carlsbad, NM. ERMS 560174.

Kirchner, T. 2013a. Generation of the LHS Samples for the CRA-2014 (AP-164) PA Calculations, Revision 0. Sandia National Laboratories, Carlsbad, NM. ERMS 559950.

Kirchner, T. 2013b. Sensitivity of the CRA-2014 Performance Assessment Releases to Parameters. Sandia National Laboratories, Carlsbad, NM. ERMS 560043.

Kirchner, T., T. Zeitler, and R. Kirkes. 2012. Evaluating the Data in Order to Derive a Value for GLOBAL:PBRINE. Memorandum to Sean Dunagan dated December 11, 2012. Sandia National Laboratories, Carlsbad, NM. ERMS 558724.

Kirkes, R. 2013. Features, Events and Processes Assessment for the Compliance Recertification Application – 2013, Revision 0. Sandia National Laboratories, Carlsbad, NM.

Kuhlman, K. 2010. Analysis Report for the CRA-2009 PABC Culebra Flow and Transport Calculations. Sandia National Laboratories, Carlsbad, NM. ERMS 552951.

Leigh, C.D., J.F. Kanney, L.H. Brush, J.W. Garner, G.R. Kirkes, T. Lowry, M.B. Nemer, J.S. Stein, E.D. Vugrin, S. Wagner, and T.B. Kirchner. 2005. 2004 Compliance Recertification Application Performance Assessment Baseline Calculation, Revision 0. Sandia National Laboratories, Carlsbad, NM. ERMS 541521.

Long, J. 2010. Execution of Performance Assessment Codes for the CRA-2009 Performance Assessment Baseline Calculation. Sandia National Laboratories, Carlsbad, NM. ERMS 552947.

Long, J. 2013. Execution of Performance Assessment Codes for the CRA-2014 Performance Assessment. Sandia National Laboratories, Carlsbad, NM. ERMS 560016.

MacKinnon, R.J., and G. Freeze. 1997a. Summary of EPA-Mandated Performance Assessment Verification Test (Replicate 1) and Comparison With the Compliance Certification Application Calculations, Revision 1. Sandia National Laboratories, Carlsbad, NM. ERMS 422595.

MacKinnon, R.J., and G. Freeze. 1997b. Summary of Uncertainty and Sensitivity Analysis Results for the EPA-Mandated Performance Assessment Verification Test, Rev. 1. Sandia National Laboratories, Carlsbad, NM. ERMS 420669.

MacKinnon, R.J., and G. Freeze. 1997c. Supplemental Summary of EPA-Mandated Performance Assessment Verification Test (All Replicates) and Comparison With the Compliance Certification Application Calculations, Revision 1. Sandia National Laboratories, Carlsbad, NM. ERMS 414880.

Malama, B. 2013. Analysis Package for Direct Brine Releases: CRA-2014 Performance Assessment (CRA-2014 PA), Revision 0. Sandia National Laboratories. Carlsbad, NM. ERMS 560069.

Nemer, M.B. 2010. Analysis Package for Salado Flow Modeling: CRA-2009 Performance Assessment Baseline Calculation. Sandia National Laboratories. Carlsbad, NM. ERMS 552956.

Peake, Thomas. 1998. Technical Report Review of TDEM Analysis of WIPP Brine Pockets. Prepared for U. S. Environmental Protection Agency, Office of Radiation and Indoor Air, 401 M. Street, S. W., Washington, DC.

Rechard, R. P., A. C. Peterson, J. D. Schreiber, H. J. Iuzzolino, M. S. Tierney and J. S. Sandha. 1991. Preliminary comparison with 40 CFR Part 191, Subpart B for the Waste Isolation Pilot Plant, December 1991; Volume 3: Reference Data. Sandia National Laboratories, Albuquerque, NM.

Reed, D.J., J. Swanson, J-F Lucchini and M. Richman. 2013. Intrinsic, Mineral and Microbial Colloid Enhancement Parameters for the WIPP Actinide Source Term. Los Alamos Laboratory, Carlsbad, NM. LCO-ACP-18. ERMS 559200.

Roselle, G.T. 2013a. Determination of Corrosion Rates from Iron/Lead Corrosion Experiments to be used for Gas Generation Calculations. Sandia National Laboratories, Carlsbad, NM. ERMS 559077.

Roselle, G.T. 2013b. Summary of Colloid Parameters to be Implemented in the CRA-2014 PA. Memo to Sean Dunagan dated February 15, 2013. Sandia National Laboratories, Carlsbad, NM. ERMS 559205.

Stein, J. 2002. Parameter Values for New Materials CONC_PCS and DRZ_PCS. Sandia National Laboratories, Carlsbad, NM. ERMS 520524.

Stoelzel, D.M. and D.G. O'Brien. 1996. Conceptual Model Description of BRAGFLO Direct Brine Release Calculations to Support the Compliance Certification Application (CCA MASS Attachment 16-2). U.S. Department of Energy, Carlsbad, NM. ERMS 239090.

U.S. Congress. 1992. WIPP Land Withdrawal Act, Public Law 102-579, 106 Stat. 4777, 1992; as amended by Public Law 104-201, 110 Stat. 2422, 1996.

U.S. Department of Energy (DOE) 1996. Title 40 CFR Part 191 Compliance Certification Application for the Waste Isolation Pilot. U.S. Department of Energy Waste Isolation Pilot Plant, Carlsbad Area Office, Carlsbad, NM. DOE/CAO-1996-2184.

U.S. Department of Energy (DOE) 2004. Title 40 CFR Part 191 Compliance Recertification Application for the Waste Isolation Pilot Plant, , 10 vols., U.S. Department of Energy Waste Isolation Pilot Plant, Carlsbad Area Office, Carlsbad, NM. DOE/WIPP 2004-3231.

U.S. Department of Energy (DOE), 2011a. Panel Closure System Design, Planned Change Request to the EPA 40 CFR Part 194 Certification of the Waste Isolation Pilot Plant. U.S. Department of Energy, Carlsbad Field Office. Carlsbad, New Mexico.

U.S. Department of Energy (DOE), 2011b. Notification of Intent to Begin the Salt Disposal Investigations. Letter from Edward Ziemanski to Jonathan Edwards dated August 11, 2011. U.S. Department of Energy, Carlsbad Field Office. Carlsbad, New Mexico.

U.S. Department of Energy (DOE). 2012. Delaware Basin Monitoring Annual Report. DOE/WIPP-12-2308.

U.S. Environmental Protection Agency (EPA). 1996. 40 CFR Part 194: Criteria for the Certification and Recertification of the Waste Isolation Pilot Plant's Compliance with the 40 CFR Part 191 Disposal Regulations; Final Rule. Federal Register, Vol. 61, 5223-5245.

U.S. Environmental Protection Agency (EPA). 1998. 40 CFR 194, Criteria for the Certification and Recertification of the Waste Isolation Pilot Plant's Compliance with the Disposal Regulations: Certification Decision: Final Rule, Federal Register. Vol. 63, 27354-27406.

U.S. Environmental Protection Agency (EPA). 2006. 40 CFR 194, Criteria for the Certification and Recertification of the Waste Isolation Pilot Plant's Compliance with the Disposal Regulations: Certification Decision: Final Rule, Federal Register. Vol. 71, 18010-18021.

U.S. Environmental Protection Agency (EPA). 2010a. 40 CFR Part 194 Criteria for the Certification and Recertification of the Waste Isolation Pilot Plant's Compliance With the Disposal Regulations: Recertification Decision, Federal Register No. 222, Vol. 75, pp. 70584-70595, November 18, 2010.

U.S. Environmental Protection Agency (EPA). 2010b. Technical Support Document for Section 194.24, Evaluation of the Compliance Recertification Actinide Source Term, Backfill Efficacy and Culebra Dolomite Distribution Coefficient Values (Revision 1), November 2010.

Van Soest, G.D. 2012. Performance Assessment Inventory Report – 2012. Los Alamos National Laboratory Carlsbad Operations. Carlsbad, NM. LA-UR-12-26643.

Wall, N.A. and Enos, D. (2006) Iron and Lead Corrosion in WIPP-Relevant Conditions, TP 06-02, Rev 1. Sandia National Laboratories. Carlsbad, NM. ERMS 543238.

Zeitler, T. 2013. Analysis Package for CCDFGF: 2014 Compliance Recertification Application Performance Assessment (CRA-2014 PA), Revision 0. Sandia National Laboratories. Carlsbad, NM. ERMS 560074.